University College London

Computational studies of phosphate clusters and bioglasses

Thesis submitted for the degree of Doctor of Philosophy (PhD) by

Emilia Tang

Supervised by

Prof. Nora H. de Leeuw

University College London

Department of Chemistry

September 2010

Declaration:

I confirm that this is my own work and the use of all materials from other sources has been properly acknowledged.

_____

Emilia Tang

September 2010

Abstract

The aim of this PhD research project is to investigate the aqueous behaviours of phosphate species and the structure of bioactive phosphate glasses via computational modelling. Density functional theory has been employed as the core methodology throughout the project. The molecular structures of bioactive ternary phosphate-based glasses with compositions $(P_2O_5)_{0.45}(CaO)_x(Na_2O)_{0.55-x}$, where x = 0.30, 0.35 and 0.45, have been explored by a range of Car-Parrinello molecular simulations. Careful structure analysis has been carried out in order to provide an accurate description of the local structure and properties of these important materials for biomedical applications. This is followed by the Car–Parrinello molecular dynamics simulations of the first hydration shell structures. Extensive simulations provide new insights into hydrogen transfer and intermolecular and hydration properties of these important aqueous species. Apart from ab-initio molecular dynamics calculations, first principles density functional theory calculations with a cluster-continuum solvation model have been used to evaluate the relative energetic stabilities of various phosphate oligomers in an aqueous environment. As a result, an illustrative picture of different aspects of phosphate species related to the dissolution behaviour of bioactive phosphate glasses was built up from various angles, which will form a solid foundation for further computational studies of bioactive phosphate glasses in the future.

List of Publications

The work described in this thesis has been published in the following papers:

Tang, E., D. Di Tommaso and N. H. de Leeuw (2009). "Hydrogen transfer and hydration properties of $H_nPO_4^{3-n}$ (n = 0--3) in water studied by first principles molecular dynamics simulations." The Journal of Chemical Physics **130**(23): 234502.

Tang, E., D. Di Tommaso and N. H. de Leeuw (2010). "An Ab Initio Molecular Dynamics Study of Bioactive Phosphate Glasses." Advanced Engineering Materials **12**(7): B331-B338.

Tang, E., D. Di Tommaso and N. H. de Leeuw (2010). "Accuracy of the microsolvation-continuum approach in computing the pKa and the free energies of formation of phosphate species in aqueous solution." Physical chemistry chemical physics **12**(41): 13804-13815.

Acknowledgements

First of all, I would like to say thank you to my supervisor, Professor Nora de Leeuw, for all her understanding and generous support throughout this project.

Thanks to EPSRC for funding this PhD project, without their financial support this project will not exist.

Special acknowledgment should go to Dr. Devis Di Tommaso for his invaluable help, guidance and patience. Credits are definitely shared by the group family. I cannot imagine how could I climb through all the obstacles without all your encouragements, especially Dr. Zhimei Du and Dr. Iman Saadoune.

I am so grateful to my mum for her unconditional love and support.

Finally I would like to thank all my dear friends and my pets, BB, Coco, Dide, Fufu and TT who have always stayed with me through all the highs and lows in life.

This work is dedicated to BB and TT, whom I grew up with. They passed away in Macau while I was completing this PhD project in London.

Table of Contents

ABSTRACT **1**

LIST OF PUBLICATIONS **4**

ACKNOWLEDGEMENTS **5**

TABLE OF CONTENTS **6**

TABLE OF FIGURES **11**

TABLE OF TABLES **14**

TABLE OF SCHEMES **17**

CHAPTER 1 INTRODUCTION **18**

1.1 BIOMATERIALS 19

1.1.1 Bioactive Materials *19*

1.2 BIOACTIVE PHOSPHATE GLASSES 22

1.3 PHOSPHATE GLASS STRUCTURE 25

1.4 DISSOLUTION BEHAVIOUR OF PHOSPHATE GLASS 28

CHAPTER 2 THEORETICAL METHODS **29**

2.1 CHAPTER INTRODUCTION 30

2.2 ELECTRONIC STRUCTURE CALCULATIONS 31

2.2.1 Schrödinger Equation 31

2.2.2 Born-Oppenheimer Approximation 34

2.2.3 Density Functional Theory (DFT) 37

2.2.3.1 General theory 37

2.2.3.2 Local Density Approximation (LDA) 41

2.2.3.3 Generalized-Gradient Approximation (GGA) 41

2.2.4 Basis Sets 43

2.2.4.1 Localised Basis Sets 43

2.2.4.2 Plane-wave Basis Sets 48

2.2.5 The Pseudopotential Approach 51

2.2.5.1 Frozen-Core Approximation 52

2.3 MOLECULAR DYNAMICS 54

2.3.1 Classical Molecular Dynamics 54

2.3.1.1 Verlet Scheme 59

2.3.2 Ab-initio Molecular Dynamics 60

2.3.2.1 Born-Oppenheimer Molecular Dynamics 61

2.3.2.2 Car-Parrinello Molecular Dynamics 62

2.4 SIMULATION CONDITIONS 68

2.4.1 Periodic Boundary Condition *68*

2.4.2 Solvation Modelling *69*

2.4.2.1 Polarisable Continuum Models 70

2.4.2.2 COnductor-like Screening MOdel 72

2.5 PRACTICAL METHODOLOGIES 75

2.5.1 Computational Tools *75*

2.5.1.1 Quantum ESPRESSO 75

2.5.1.2 CP Code (CPMD) 76

2.5.1.3 SIESTA 77

2.5.1.4 Dmol^3 78

2.5.2 Analytical Tools *79*

2.5.2.1 Radial Distribution Function (RDF) 79

2.5.2.2 Solvation Free Energy Scheme 81

CHAPTER 3 STRUCTURES OF PHOSPHATE BIOGLASSES 84

3.1 CHAPTER INTRODUCTION 85

3.2 METHODOLOGY 88

3.2.1 Computational details *88*

3.2.2 Simulation protocol *89*

3.3 Q^n DISTRIBUTION AND NETWORK CONNECTIVITY 92

3.4 STRUCTURE OF THE TETRAHEDRAL NETWORK 95

3.5 COORDINATION ENVIRONMENT OF THE NETWORK MODIFIERS NA AND CA 101

3.6 CHAPTER CONCLUSION 107

CHAPTER 4 HYDRATION STRUCTURES OF ORTHOPHOSPHATES 108

4.1 CHAPTER INTRODUCTION 109

4.2 METHODOLOGY 112

4.3 PROTON TRANSFER OF $H_NPO_4^{3-N}$ (N = 0-3) WITH WATER 115

4.4 INTER-MOLECULAR PROPERTIES AND HYDRATION STRUCTURE OF $H_NPO_4^{3-N}$ (N = 0-2) IN AQUEOUS SOLUTION 122

4.5 CHAPTER CONCLUSION 137

CHAPTER 5 HYDRATION PROPERTIES OF PHOSPHATES 139

5.1 CHAPTER INTRODUCTION 140

5.2 METHODOLOGY 144

5.2.1 Electronic Structure Calculations 144

5.2.2 Solvation Model 145

5.2.3 Condensation Reactions In Aqueous Solution 148

5.3 HYDRATION FREE ENERGIES OF ORTHO- AND PYRO-PHOSPHATES 150

5.4 pK_AS OF ORTHO- AND PYRO-PHOSPHATES IN WATER 158

5.5 FORMATION OF PYRO- AND TRI-PHOSPHATES IN AQUEOUS SOLUTION 166

5.6 CHAPTER CONCLUSION 173

CHAPTER 6 CONCLUSION 175

APPENDIX 180

REFERENCE 188

Table of Figures

FIGURE 1-1 ILLUSTRATIONS OF H_4SiO_4 AND H_3PO_4 25

FIGURE 2-1 SCHEMATIC REPRESENTATION OF THE IMAGINARY SYSTEM. 80

FIGURE 2-2 MONOMER THERMODYNAMIC CYCLE SCHEME. 81

FIGURE 2-3 CLUSTER THERMODYNAMIC CYCLE SCHEME. 82

FIGURE 3-1 SNAPSHOT FROM THE CP-MD TRAJECTORY OF THE P45C40N15 GLASS SHOWING THE OCCURRENCE OF CHAIN-LIKE PHOSPHATE NETWORKS. CA, NA, O AND P ARE PICTURED AS GREEN, PURPLE, RED AND PINK SPHERES, RESPECTIVELY. 84

FIGURE 3-2 RADIAL DISTRIBUTION FUNCTIONS OF THE P-O (A), O-O (B) AND P-P (C) ATOMIC PAIRS OBTAINED FROM THE CP-MD SIMULATIONS OF THE $(P_2O_5)_{0.45}CaO_xNa_2O_{0.55-x}$ (X = 30, 35 AND 40) GLASSES. 96

FIGURE 3-3 RADIAL DISTRIBUTION FUNCTIONS OF THE O-P-O (A) AND P-O-P (B) ANGLES OBTAINED FROM THE CP-MD SIMULATIONS OF THE $(P_2O_5)_{0.45}CaO_xNa_2O_{0.55-x}$ (X = 0.30, 0.35 AND 0.40), GLASSES. ..97

FIGURE 3-4 DECOMPOSITION OF THE P-O RADIAL DISTRIBUTION FUNCTIONS INTO THEIR BO (SOLID LINE) AND NBO (DASHED LINE) COMPONENTS. THE INSET REPORTS THE DECOMPOSITION OF THE P-NBO RADIAL DISTRIBUTION FUNCTION INTO THEIR P^{Q1}-NBO AND P^{Q2}-NBO COMPONENTS OF THE GLASS WITH COMPOSITION P45C30N25. 99

FIGURE 3-5 RADIAL DISTRIBUTION FUNCTION OF THE NA-O (A) AND CA-O (B) PAIRS OBTAINED FROM THE CP-MD SIMULATIONS OF THE $(P_2O_5)_{0.45}CaO_xNa_2O_{0.55-x}$ (X = 0.30, 0.35 AND 0.40) GLASSES..... 102

FIGURE 3-6 DECOMPOSITION OF THE M-O RADIAL DISTRIBUTION FUNCTIONS (M = NA, CA) INTO THEIR BO AND NBO COMPONENTS. 103

FIGURE 3-7 SNAPSHOT FROM THE CP-MD TRAJECTORY OF THE P45C30N25 GLASS SHOWING A TYPICAL CALCIUM COORDINATION SHELL. CA, NA, O AND P ARE PICTURED AS GREEN, PURPLE, RED AND PINK SPHERES, RESPECTIVELY. 105

FIGURE 3-8 THE O–NA-O (A) AND O-CA-O (B) ANGULAR DISTRIBUTION FUNCTIONS FOR THE SIMULATED $(P_2O_5)_{0.45}CaO_xNa_2O_{0.55-x}$ (x = 0.30, 0.35 AND 0.40) GLASSES. 106

FIGURE 4-1 SNAPSHOT OF SIMULATION BOX OF $H_2PO_4^-$ WITH 51 WATER MOLECULES. 108

FIGURE 4-2 TIME EVOLUTION OF THE O_P–H DISTANCE OF THE OXYGEN O1 DURING THE CP-MD SIMULATION OF (A) PO_4^{3-}, (B) HPO_4^{2-}, (C) $H_2PO_4^-$ AND (D) H_3PO_4 IN 51 WATER MOLECULES (TIME STEP: 30.25 FS)..... 116

FIGURE 4-3 TIME EVOLUTION OF THE O_P–H DISTANCE DURING THE CP-MD SIMULATION OF $H_2PO_4^-$ IN 51 WATER MOLECULES (TIME STEP:0.60 FS). ABOVE: O1 OXYGEN; BELOW: O4 OXYGEN..... 118

FIGURE 4-4 TIME EVOLUTION OF THE SCF TOTAL ENERGY (TIME STEP OF 0.60 FS) AND REPRESENTATIVE SNAPSHOTS FROM THE CP-MD SIMULATION OF $H_2PO_4^-$ IN 51 WATER MOLECULES (AT SIMULATION TIME 1-5 TOP DOWN.), SHOWING THE PROTON HOPPING PROCESS INVOLVED IN THE DEHYDROGENATION OF $H_2PO_4^-$. 121

FIGURE 4-5 THE O_W–O_W, H_W–H_W AND O_W–H_W RADIAL DISTRIBUTION FUNCTIONS, $G(R)$, OF THE PO_4^{3-} AQUEOUS SOLUTION AND OF PURE WATER OBTAINED FROM THE CP-MD SIMULATIONS. THE DOTTED LINE CORRESPONDS TO THE EXPERIMENTAL O_W–O_W PARTIAL PAIR CORRELATION FUNCTIONS FOR H_2O AT 298 K (HTTP://WWW.ISIS.RL.AC.UK/DISORDERED/DATABASE)..... 123

FIGURE 4-6 (A) THE P–O_W RADIAL DISTRIBUTION FUNCTIONS, $G(R)$, AND RUNNING COORDINATION NUMBERS, $N(R)$, OBTAINED FROM THE CP-MD SIMULATIONS OF PO_4^{3-}, HPO_4^{2-} AND $H_2PO_4^{2-}$ IN 51 WATER MOLECULES. (B) THE O_W–P–O_W ANGULAR DISTRIBUTION FUNCTIONS, ADF, FOR THE WATER MOLECULES PART OF THE FIRST HYDRATION SHELL OF PO_4^{3-}, HPO_4^{2-} AND $H_2PO_4^{2-}$ OBTAINED FROM THE CP-MD SIMULATIONS OF $H_NPO_4^{3-N}$ IN 51 WATER MOLECULES..... 126

FIGURE 4-7 PROBABILITY DISTRIBUTIONS OF THE COORDINATION NUMBERS OF THE FIRST HYDRATION SHELL OF PO_4^{3-}, HPO_4^{2-} AND $H_2PO_4^-$ IN WATER OBTAINED FROM THE CP-MD SIMULATIONS OF $H_NPO_4^{3-N}$ (N = 0-2) IN 51 WATER MOLECULES. 130

FIGURE 4-8 THE O_P–H_W RADIAL DISTRIBUTION FUNCTIONS, $g(R)$, AND RUNNING COORDINATION NUMBERS, $N(R)$, OF PO_4^{3-}, HPO_4^{2-} AND $H_2PO_4^-$ IN WATER OBTAINED FROM THE CP-MD SIMULATIONS OF $H_NPO_4^{3-N}$ IN 51 WATER MOLECULES. 132

FIGURE 4-9 THE H_P–O_W RADIAL DISTRIBUTION FUNCTIONS, $g(R)$, AND RUNNING COORDINATION NUMBERS, $N(R)$, FOR HPO_4^{2-} AND H_2PO_4 IN WATER OBTAINED FROM THE CP-MD SIMULATIONS OF $H_NPO_4^{3-N}$ IN 51 WATER MOLECULES. 133

FIGURE 5-1 THE AQUEOUS-PHASE pK_A AND FREE ENERGIES OF FORMATION OF SMALL POLYPHOSPHATES IN SOLUTION ARE COMPUTED USING AN OPTIMISED MICROSOLVATION-CONTINUUM APPROACH. 139

FIGURE 5-2 AQUEOUS-PHASE DISSOCIATION STEPS OF THE ORTHOPHOSPHATES AND PYROPHOSPHATES. 163

FIGURE 5-3 OPTIMISED STRUCTURE OF REPRESENTATIVE HYDRATED PYROPHOSPHATE SPECIES OBTAINED AT THE COSMO/PBE/DNP LEVEL. BOND LENGTHS IN Å 170

Table of Tables

TABLE 3-1 DETAILS OF THE SIMULATED GLASSES. 90

TABLE 3-2 COORDINATION STATISTICS OF THE PHOSPHATE NETWORK FROM THE CP-MD SIMULATIONS: Q^N DISTRIBUTION, NETWORK CONNECTIVITY (NC), PHOSPHORUS (P) COORDINATION AND AVERAGE P-O COORDINATION NUMBERS (CN_{AV}). 93

TABLE 3-3 COORDINATION ENVIRONMENTS OF THE NA AND CA IONS; $r_{\max}^{M-O}$ IS THE DISTANCES ARE IN Å. COORDINATION NUMBERS ARE OBTAINED USING NA-O AND CAO CUT-OFFS OF 3.1 Å AND 3.2 Å, RESPECTIVELY. 103

TABLE 4-1 POSITIONS $r_{\max}^{P-O}$, $r_{\min}^{P-O}$ (Å) AND AMPLITUDES $g_{\max}^{P-O}$, $g_{\min}^{P-O}$ OF THE MAXIMA AND MINIMA OF THE SECOND PEAKS OF THE $P-O_W$ RADIAL DISTRIBUTION FUNCTIONS, AND FIRST SHELL HYDRATION NUMBER n_w OBTAINED FROM THE CP-MD SIMULATIONS OF $H_NPO_4^{3-N}$ (N = 0-2) IN 51 WATER MOLECULES. . 128

TABLE 4-2 COORDINATION STATISTICS OF THE PHOSPHATE NETWORK FROM THE CP-MD SIMULATIONS: Q^N DISTRIBUTION, NETWORK CONNECTIVITY (NC), PHOSPHORUS (P) COORDINATION AND AVERAGE P-O COORDINATION NUMBERS (CN_{AV}). 135

TABLE 4-3 POSITIONS $r_{\max}^{Hp-Ow}$, $r_{\min}^{Hp-Ow}$ (Å) AND AMPLITUDES $g_{\max}^{Hp-Ow}$, $g_{\min}^{Hp-Ow}$ OF THE MAXIMA AND MINIMA OF THE SECOND PEAK OF THE H_P-O_W RADIAL DISTRIBUTION FUNCTIONS, AND FIRST SHELL HYDRATION NUMBER n_w OBTAINED FROM THE CP-MD SIMULATIONS OF HPO_4^- AND $H_2PO_4^{2-}$ IN 51 WATER MOLECULES. 136

TABLE 5-1 SOLVATION FREE ENERGIES OF THE ORTHOPHOSPHATE $H_NPO_4^{3-N}$ SPECIES COMPUTED USING THE COSMO MODEL AND AT THE VARIOUS LEVELS OF THEORY. CALCULATIONS PERFORMED ON THE GEOMETRIES OPTIMISED IN THE POLARISABLE CONTINUUM MODEL. VALUES IN KCAL/MOL. 146

TABLE 5-2 SOLVATION FREE ENERGIES OF THE ORTHOPHOSPHATE $H_NPO_4^{3-N}$ SPECIES OBTAINED USING THE *MONOMER* THERMODYNAMIC CYCLE. GAS-PHASE FREE ENERGY CONTRIBUTIONS COMPUTED AT THE

PBE/DNP level and solvation free energies computed at the COSMO/PBE/DNP level. Values in kcal/mol. 151

Table 5-3 Solvation free energies of the hydrated $H_NPO_4^{3-N}$ species obtained using the *CLUSTER* thermodynamic cycle. Gas-phase free energy contributions computed at the PBE/DNP level and solvation free energies computed at the COSMO/PBE/DNP level. Values in kcal mol^{-1}. 153

Table 5-4 Average values of the ratio $g_{\max}^{O_p-H_w} / g_{\min}^{O_p-H_w}$ obtained from CP-MD simulations of the orthophosphate species $H_NPO_4^{3-N}$, and of the molecules H_2O and HCO_3^- in water, together with the solvation free energies of these species computed at the COSMO/PBE/DNP level. 154

Table 5-5 Solvation free energies of the pyrophosphate species obtained using the *MONOMER* thermodynamic cycle. Gas-phase free energy contributions computed at the PBE/DNP level and solvation free energies computed at the COSMO/PBE/DNP level using the COSMO optimised geometry. Values in kcal/mol. 157

Table 5-6 Aqueous-phase acid dissociation constant pK_A for the three protonation states of the phosphoric acid. Solvation free energy contributions computed at the COSMO/PBE/DNP level using the COSMO optimised geometry, the microsolvation-continuum approach and the *MONOMER* cycle (pK_A units) 159

Table 5-7 Incremental water binding free energy ($\Delta G^*_{n\,aq}$) of the orthophosphate clusters. Gas-phase free energy contributions computed at the PBE/DNP level, and solvation free energies computed at the COSMO/PBE/DNP using the gas-phase geometry, the microsolvation-continuum approach and the *MONOMER* cycle. In bold the values lowest value of $\Delta G^*_{n\,aq}$. Values in kcal mol^{-1}. 162

Table 5-8 Aqueous-phase acid dissociation constant pKa for the protonation states of the orthophosphoric and pyrophosphoric acids. Solvation free energies contributions

computed at the COSMO/PBE/DNP level using the COSMO optimised geometry. The solvation free energies of the conjugate species HA/A- have been determined using the optimal number of water molecules reported in Table 5-6 (pKa units)..... 162

Table 5-9 Effect of the water molecules n_{H_2O} used to compute the solvation energy term $\Delta\Delta G^*_{solv}$ on the free energies of condensation reaction ΔG^*_{aq} for the formation of the pyrophosphate species. Approaches used to determine the hydration numbers n_{H_2O}: b) "Incremental" binding free energy approach; c) Effective charge approach; d) "Incremental" binding free energy approach for the orthophosphates and Effective charge approach of pyrophosphates. Values in kcal mol^{-1}..... 168

Table 5-10 Gibbs free energies of condensation reaction ΔG^*_{aq} for the formation of the pyrophosphate and triphosphate species. The hydration number n_{H_2O} has been determined applying approach d (the "incremental" binding free energy approach for the orthophosphates and effective charge approach for pyrophosphates). Values in kcal mol^{-1}. 171

Table of Schemes

SCHEME 3-1 92

SCHEME 4-1 115

SCHEME 5-1 148

SCHEME 5-2 160

SCHEME 5-3 THE CONDENSATION REACTIONS OF THE ORTHOPHOSPHATE SPECIES TO FORM PYROPHOSPHATE PRODUCTS. 167

Chapter 1 Introduction

The aim of this research project is to gain understanding, at the molecular level of the process of bioactive phosphate glass dissolution and the stabilities of the dissolution products in the aqueous solution surrounding this phosphate-based material. This task will be accomplished using atomistic and quantum-mechanical simulations. In this chapter, we will introduce the properties and applications of bioactive phosphate glasses and previous work that is relevant to this project.

1.1 Biomaterials

Biomaterials have attracted significant scientific interest in the past few decades, with scientists around the world exploring reliable replacements for hard and soft tissues. The health care costs for patients suffering from tissue or organ failure, which already amount to billions of dollars, are increasing every year (Langer 2000). Scientists in different disciplines such as chemistry, materials, medicine, biology etc. are constantly working together to develop reliable bio-compatible replacement materials for people suffering from a range of diseases, such as periodontal conditions (Allan, Newman et al. 2001) and cruciate ligament knee injuries (Hayem 2001). Biomaterials can also be used as temporary scaffolds for tissue engineering (Kim and Mooney 1998; Bitar, Salih et al. 2004; Ahmed, Parsons et al. 2008).

1.1.1 Bioactive Materials

A paper published in 1980 already identified more than 40 different biomaterials used in 50 different medical and dental applications (Hench 1998). For most of these materials, strong emphasis was put on their bio-inertness (Hench 1998). However, no material is completely inert after implantation into the body, as there is always some response from the living tissue. According to Hench and co-workers (Hench and Wilson 1984), there are four types of response from the living tissue which we can expect when a material is implanted:

1. The material is not compatible with the surrounding living tissue and the surrounding tissue dies because of the toxic implantation.
2. The material is non-toxic; it is dissolved and absorbed by the surrounding tissue and ends up being replaced by the surrounding tissue.
3. The material is non-toxic and biologically inactive, and it will be encapsulated by fibrous tissue from the surrounding living tissue.
4. The material is non-toxic, biologically active and will form interfacial bonds with the living tissue.

Bioactive phosphate glasses belong to the 4th group and are therefore classified as surface-active materials. The most significant property of this class of materials is the interaction with living tissue to form interfacial bonds. This helps prevent one of the most common causes of implant failure. There are currently four main categories of surface-active biomaterials available:

I. Dense Hydroxyapatite (HA) ceramics
II. Bioactive Glasses
III. Bioactive Glass-Ceramics
IV. Bioactive Composites

The bioactive phosphate glass that is the subject of the present study falls into the second category. Bioactive glasses are also referred to as third generation biomaterials due to their ability to stimulate specific cellular responses at the molecular level (Hench and Polak 2002).

As a bioactive material, phosphate glasses have potential application as an implant material for various tissue and bone replacement. The main advantage of phosphate glasses is their chemical composition, which is close to that of natural bone. Their active degradability with high compatibility with cells is also a desired property. Another advantage of these phosphate glasses is their adjustable solubility, which can be modified by controlling their chemical composition. This means the solubility of the glasses can be tailored to suit the needs of specific implantations, where the dissolution rates of the phosphate glasses can be varied by several orders of magnitude (Franks, Abrahams et al. 2000). This controllable dissolution rate is extremely useful as it can be tailored to match the regeneration rate of the new tissue, which replaces the dissolving implant. As a result, the patients will not need a second operation to remove the device, as is commonly required with metallic implants.

1.2 Bioactive Phosphate Glasses

Phosphate-based glasses have many desirable materials properties, such as low dispersion, high refractive indices, and high transparency of ultraviolet light as compared to silicate-based glasses. However the poor chemical durability of the early phosphate glasses discouraged their usage until it was realised that for certain applications this solubility was not a problem, but rather a desired property for surface bioactive materials (Kreidl and Weyl 1941).

One of their most interesting properties is the ability to completely dissolve in aqueous solution, and, as mentioned, the possibility to tailor the dissolution rate to suit specific applications by altering the chemical composition of the glasses. Another benefit is that bioactive phosphate glasses can be synthesised to include ions commonly found in the human body, e.g. Ca^{2+}, Mg^{2+} etc. (Salih, Franks et al. 2000; Franks, Salih et al. 2002; Ahmed, Collins et al. 2004; Ahmed, Lewis et al. 2004). Therefore, phosphate glasses can be developed into bioactive materials with specific tailored compositions for diverse medical and dental applications.

Bioactive glasses employed in surgical implants, such as Bioglass®, mostly use SiO_4^{4-} as a network former. The biocompatibility of Bioglass® is realised by the formation of a double layer, consisting of a calcium phosphate layer and a silica-rich layer, and this first developed calcium phosphate layer is then transformed into an apatite layer (Cheol Y. Kim 1992). However, the long-term reactions are not clear, especially for the silica (Franks, Abrahams et al. 2000). An ideal replacement material will be chemically related to the surrounding tissue and will be biocompatible and bioactive, which is where phosphate-based glasses are

attractive alternatives, since they have the required solubility and composition. The use of phosphate glasses, however, raises the question of the nature of the dissolution products, which is the main theme of this thesis.

Numerous biocompatibility studies have been carried out on phosphate-based glasses (Navarro, Ginebra et al. 2003). All these studies found that the glasses produced no adverse cell reactions and cell proliferation had even increased in some cases in the presence of the glass extracts (Salih, Franks et al. 2000; Franks, Salih et al. 2002; Bitar, Salih et al. 2004). Franks et al. also found that the extracts from the less degradable glass compositions, i.e. ones with greater calcium content, upregulated the proliferation of the cells (Franks, Salih et al. 2002). On the other hand, Gough et al. inverstigated the short-term biocompatibility of the macrophage cell line and primary human craniofacial osteoblasts, which demonstated minimal macrophage activation with high osteoblast compatibility. They showed that the osteoblasts were able to attach, spread and proliferate on the phosphate-based glasses (Gough, Christian et al. 2002). The common theme found in the above studies was that glasses with high calcium content in their compositions lead to better cell proliferation and attachment rates than those with the low calcium content. Salih et al. have also reported that calcium ions play an important role in cell activation mechanisms, which control many growth-associated processes and functional activities of cells (Salih, Franks et al. 2000). However, it is well known that tissue culture media also contain large amounts of calcium ions, Ahmed et. al proposed that both anions and cations released through the degradation of the glasses would have a positive effect with regard to biocompatibility. Hence we are

interested to investigate further the hydrated properties of the released anions, i.e. phosphates, in this study.

According to research by Driessen et al., rhenanite, calcium sodium phosphate $\left(CaNaPO_4\right)$, will be transformed into apatite within 6 weeks of implantation (Driessens, Ramselaar et al. 1992). Similarly, according to Videau et al. (Videau, Portier et al. 1982), brushite $\left(CaHPO_4 \cdot 2H_2O\right)$, which is related to monetite $\left(CaHPO_4\right)$, octacalcium phosphate $\left(Ca\left(HPO_4\right)_2\left(PO_4\right)_4 \cdot 5H_2O\right)$ and one of the most stable defective hydroxyapatite precipitates, will be transformed into hydroxyapatite as the most stable thermodynamic product at pH7. These findings from the literature on phosphate-based minerals indicate the potential of bio-implantation usage of the phosphate-based glasses to transform into hydroxyapatite.

Franks et al. have investigated the solubility properties of bio-phosphate glasses by measuring the solubility of glass discs in both distilled water and Hanks Buffered Saline Solution (HBSS), (Franks, Abrahams et al. 2000; Franks, Salih et al. 2002) where they found that the solubility of these materials strongly depends on their chemical compositions and on the pH of the solution.

1.3 Phosphate Glass Structure

Although phosphate is one of Zachariasen's four principal network formers (Zachariasen 1932), its chemistry leads to interesting structural differences in glass formation compared to silica. In vitreous P_2O_5, the tetrahedral network is not completely polymerized in the same way as vitreous silica, because of the terminal oxygen atoms (double bonded) found in the v-P_2O_5. Therefore, when using the Q^n terminological description of a glass structure, which represents the number of bridging oxygen in a tetrahedron, v-P_2O_5 consists of Q^3 tetrahedra in contrast to Q^4 found in v-silica. The structural features of simple phosphate glasses have been reviewed by Brow (Brow 2000).

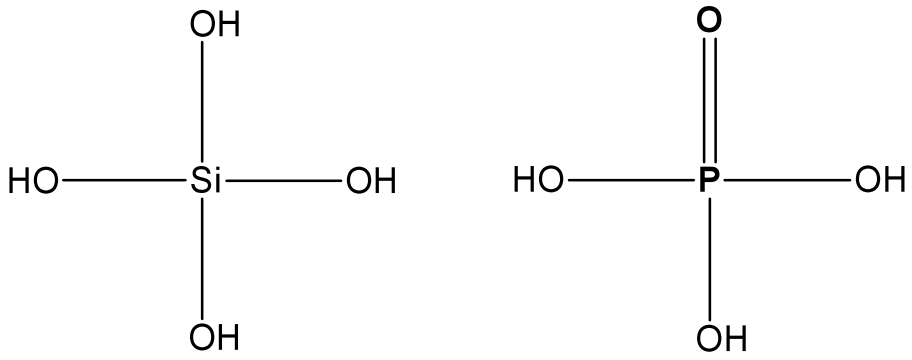

Figure 1-1 Illustrations of H_4SiO_4 and H_3PO_4.

Phosphate glasses can be made with a range of structures, from cross-linked Q^3 tetrahedra to polymer-like metaphosphate chains of Q^2 tetrahedra to glasses based on pyrophosphates Q^1 and orthophosphates Q^0. The structure generally depends on the $[O]/[P]$ ratio of the glass composition. The phosphate glasses being explored for tissue engineering are mainly meta-phosphate compositions, with

around 50 mol% P_2O_5 (Ahmed, Lewis et al. 2004). In principle, the structure of these glasses would be built around Q^2 species and rings and chains would be formed. However, in practice, as the exact stoichiometries of the compositions are difficult to achieve, both Q^2 and Q^1 species are seen, assuming that there may be some sort of distribution of the length of rings and chains. Nevertheless detailed information is not available experimentally, hence one of the goals of this project is to characterise the distributions in the simulated structures.

A number of Molecular Dynamics (MD) studies of phosphate glasses have been carried out that have mainly focused on meta-phosphate compositions. The Capobianco group have modelled Mg, Zn, Pb and Na meta-phosphates glasses (Sourial, Peres et al. 1999; Speghini, Sourial et al. 1999); Tischendorf et al. have studied binary zinc phosphates (Tischendorf, Alam et al. 2003); and Liang et al. have modelled binary lithium phosphates (Liang, Cygan et al. 2000), as have Rao et al., who have also examined binary sodium phosphates (Karthikeyan, Vinatier et al. 1999), whereas Belashchenka has modelled calcium phosphates (Belashchenko and Ostrovskii 2002) as expected. All of these studies have found chains and ring structures in the simulation samples. However, there are no previous computational studies of the mixed Ca-Na-phosphates glasses, which are of interest in this project. Apart from classical MD studies, Car-Parrinello Molecular Dynamics (CPMD) studies are sometimes employed for glass simulations, although again, to our knowledge, there are no previous CPMD simulations of the ternary phosphate based glasses either, with only the CPMD study of phosphosilicate glasses by Tilocca (Tilocca 2007), being comparable, which is a study of silicate-based glasses with a minor fraction of phosphate.

The local structures of binary phosphate glasses have been investigated experimentally in various studies (Brow, Kirkpatrick et al. 1990; Kirkpatrick and Brow 1995; Hoppe 1996), which provided significant insight into the complex structure of these glasses. Hoppe suggested that in addition to the depolymerisation process, there are other structural principles at work. A modified random network will be developed if the metal oxide content keeps increasing when all the terminal oxygen atoms are already occupied (Hoppe 1996). For most of the binary glass system, the metal oxide contents are over 30 mol% due to the high volatility and the hygroscopic nature of a pure P_2O_5 glass (Hudgens, Brow et al. 1998).

For ternary phosphate glasses, a significant proportion of work has centred on the $Na_2O - CaO - P_2O_5$ system (Franks, Abrahams et al. 2000; Salih, Franks et al. 2000), especially the $(Na_2O)_{0.55-x}(CaO)_x(P_2O_5)_{0.45}$ system, which is also the core composition of the phosphate glasses in this study. They have investigated the basic dissolution characteristics of this glass composition and identified an inverse relationship between the CaO content and the dissolution rate (Franks, Abrahams et al. 2000). The dissolution rate appears very linear with time, apart from the glasses with compositions between 32 to 40mol%, where a clear non-linearity was observed after reanalysis of the data and application of a diffusion model. Franks et al. suggested that there is a two-stage degradation process. Structural information of the glasses has been obtained from both FTIR studies and also magic angle spinning nuclear magnetic resonance (MAS-NMR)(Abrahams, E. Hawkes et al. 1997).

1.4 Dissolution Behaviour of Phosphate Glass

There have been a number of experimental studies of the dissolution behaviour of phosphate glasses. The general conclusion is that a large number of dissolution products are formed during the process. However, the compositions of the dissolution products are hard to identify and remain unknown. For this reason, a number of ion chromatography studies have been carried out by Ahmed et al. to investigate the species and the amounts of ions released into the solution during the degradation process of the glasses (Ahmed 2005; Ahmed, Lewis et al. 2005). As a result, a few of the peaks have been identified, but some of the peaks of the chromatograms were quantified with estimations and further verification is needed. Hence, in this study, we aimed to determine the hydration properties of a number of phosphate species at molecular level by cluster calculations based on DFT methods which we hope will help to identify the main dissolution products and to understand more about their stability in aqueous environment.

Chapter 2 Theoretical Methods

In this chapter we describe the computational methods that have been employed in this study. Throughout the research project, we have focused on understanding phosphate clusters and bioactive glasses through the application of a variety of computational applications. All codes employed in this study are based on Density Functional Theory, the description of which will therefore form the bulk of this chapter.

This chapter will be split into three main sections*, namely Electronic Structure Calculations, Ab-initio Molecular Dynamics and Simulation conditions.

* This chapter is an overview of the methods that have been employed in this specific research. For further details please refer to the references or other sources accordingly.

2.1 Chapter Introduction

As in any other methods, there are both advantages and disadvantages to theoretical calculations. Theoretical studies may compensate for insufficiencies in experimental studies, where the calculations offer an alternative way to investigate properties that are otherwise inaccessible to traditional experimental methods. Secondly, the systems studied computationally are generally well defined compared to experimental studies; hence the results are less likely to be "contaminated" by impurities. However, studies of over-idealised systems may lead to results that have little connection with reality. Moreover, some situations may be too complex to be investigated by theoretical methods alone.

2.2 Electronic Structure Calculations

According to the principles of quantum mechanics, all electronic and structural properties of a given material can be calculated by solving the Schrödinger equation. [See Equation (2-1)]

However, the Schrödinger equation cannot be solved exactly for systems with more than one electron. Therefore, various approximations have been developed in order to provide reasonable approximate solutions of the Schrödinger equations for multi-electron systems.

The ideal approximation should be simple enough to be solved, but also accurate enough to represent reality. Two main theories have been developed for this purpose, which are the fundamental theories behind various electonic structure calculations. They are the wavefunction-based Hartree-Fock (HF) approximation (Fock 1930) and the density-based Density Functional Theory (DFT) theory (Hohenberg and Kohn 1964; Kohn and Sham 1965). The calculations in this study are mainly based on electronic structure methods derived from the Density Functional Theory (DFT).

2.2.1 Schrödinger Equation

In principle, all properties of materials can be studied by solving the Schrödinger equation.

$$\hat{H}\Psi = E\Psi \tag{2-1}$$

Ψ is the wavefunction of all participating particles and $\hat{H}$ is the Hamiltonian operator. However, the exact solution to the equation is rarely possible apart from the hydrogen atom and one-electron systems. Appropriate approaches are needed for systems with two or more electrons, such as the variational principle and the Born-Oppenheimer approximation.

$$E = \textit{total energy (kinetic + potential)} \tag{2-2}$$

The variational principle provides a way to approximate the solution to Equation (2-4) by substituting the real wavefunction Ψ_{real} by the approximate wavefunction Φ_{approx}, where $\Phi \approx \Psi$.

If $\Phi \approx \Psi$, (2-1) becomes:

$$\hat{H}\Phi = E\Phi_{approx.} \tag{2-3}$$

then according to the variational principle, $E_{approx.} \geq E_{real}$,

$$E\Phi_{approx.} \geq E_0\Psi_{real} \tag{2-4}$$

Therefore, the variational principle states that no matter what approximate function $\Phi_{approx.}$ we use as substitute to the wavefunction in the Schrödinger equation, the final expected value of the equation will always be higher than or identical to the lowest eigenvalue. So if we imagine we are solving (2-3), assuming the Hamiltonian operator is known and trying to seek the lowest energy of the system, different approximate eigenfunctions Φ will give us different expected values. The eigenfunction that gives the lowest expected value will be the closest to the true eigenfunction of the lowest energy. This enables us to seek an approximate

solution of the lowest eigenvalue to the corresponding eigenfunction for the eigenvalue equation.

We have so far assumed that the Hamiltonian operator $\hat{H}$ is known. Any practical implementation, which attempts to solve the Schrödinger equation, will require the precise form of $\hat{H}$. Here, we consider the non-relativistic case to simplify the problem, which means that the spin dependencies are largely neglected except that each orbital of the fermions, i.e. the electrons, can be occupied by two particles (α spin and β spin). As the non-relativistic Hamiltonian operator can be obtained by writing down the classical total energy of the system of interest,

$$E_{tot} = E_{kin} + E_{pot} \tag{2-5}$$

the total Hamilton operator $\hat{H}$ can be expressed as the sum of kinetic and potential energies of the system: the kinetic energy operator for the nucleus $\hat{H}_{k,n}$, the kinetic energy operator of the electrons $\hat{H}_{k,e}$, the potential energy operator for nucleus-nucleus interactions $\hat{H}_{p,n-n}$, the potential energy operator for electron-electron interactions $\hat{H}_{p,e-e}$, and the potential energy operator for the nucleus-electron interactions $\hat{H}_{p,n-e}$.

$$\hat{H} = \hat{H}_{k,n} + \hat{H}_{k.e} + \hat{H}_{p,n-n} + \hat{H}_{p,e-e} + \hat{H}_{p,n-e} \tag{2-6}$$

Hence the solution of the time-independent Schrödinger equation depends on the spin and position coordinates of all electrons and nuclei. Here we introduce the short-hand notations, where $\vec{x}$ represents the spin and position coordinates of all

electrons, $(\vec{r}_1,\vec{\sigma}_1,\ldots,\vec{r}_N,\vec{\sigma}_N) \equiv (\vec{x}_1,\ldots,\vec{x}_N) \equiv \vec{x}$, and $\vec{X}$ represents the spin and position coordinates of all nuclei, $(\vec{R}_1,\vec{\Sigma}_1,\ldots,\vec{R}_M,\vec{\Sigma}_M) \equiv (\vec{X}_1,\ldots,\vec{X}_N) \equiv \vec{X}$.

$$\Psi = \Psi(\vec{X},\vec{x}) \tag{2-7}$$

The Schrödinger equation can then be written as:

$$\hat{H}\Psi = (\hat{H}_{k,n} + \hat{H}_{k,e} + \hat{H}_{p,n-n} + \hat{H}_{p,e-e} + \hat{H}_{p,n-e})\Psi(\vec{X},\vec{x}) = E \cdot \Psi(\vec{X},\vec{x}) \tag{2-8}$$

If we group the Hamilton operators into two groups, (2-8) becomes,

$$[(\hat{H}_{k,n} + \hat{H}_{p,n-n}) + (\hat{H}_{k,e} + \hat{H}_{p,e-e} + \hat{H}_{p,n-e})\Psi(\vec{X},\vec{x}) = E \cdot \Psi(\vec{X},\vec{x}) \tag{2-9}$$

As (2-9) shows, the first part of the equation solely depends on the nuclear coordinates and the second part mainly depends on electron coordinates. This is where the Born-Oppenheimer approximation becomes useful.

2.2.2 Born-Oppenheimer Approximation

The Born-Oppenheimer (BO) approximation (Born and Oppenheimer 1927) assumes that for a given set of positions of the nuclei as the nuclei move, the electrons adjust their positions ‘immediately’ to the new nuclei positions. This approximation is based on the idea of the electrons moving much faster than the nuclei, given that the nuclei are generally several thousand times heavier than an electron. The question now is how to implement this qualitative consideration into the Schrödinger equation. We can write the solution of (2-9) as a product of two wavefunctions by factorization, one for the nuclear coordinates only and the other

one a wavefunction that depends directly on the electronic coordinates and parametrically on the nuclear coordinates.

$$\Psi(\vec{X},\vec{x}) = \Psi_n(\vec{X}) \cdot \Psi_e(\vec{X};\vec{x}) \tag{2-10}$$

This means the electronic wavefunction changes for different position of the nuclei. If we insert (2-10) into (2-9) we obtain:

$$\begin{aligned}
&[(\hat{H}_{k,n} + \hat{H}_{p,n-n}) + (\hat{H}_{k,e} + \hat{H}_{p,e-e} + \hat{H}_{p,n-e})]\Psi_n(\vec{X}) \cdot \Psi_e(\vec{X};\vec{x}) \\
&= E \cdot \Psi_n(\vec{X}) \cdot \Psi_e(\vec{X};\vec{x})
\end{aligned}$$

$$\begin{aligned}
&[(\hat{H}_{k,n} + \hat{H}_{p,n-n}) + (\hat{H}_{k,e} + \hat{H}_{p,e-e} + \hat{H}_{p,n-e})]\Psi_n(\vec{X}) \cdot \Psi_e(\vec{X};\vec{x}) \\
&= (\hat{H}_{k,n} + \hat{H}_{p,n-n})\Psi_n(\vec{X}) \cdot \Psi_e(\vec{X};\vec{x}) \\
&+(\hat{H}_{k,e} + \hat{H}_{p,e-e} + \hat{H}_{p,n-e})\Psi_n(\vec{X}) \cdot \Psi_e(\vec{X};\vec{x})
\end{aligned} \tag{2-11}$$

If we now apply the BO assumption to (2-11), which assumes that the nuclear part of the kinetic energy that originates from the electronic part of the wavefunctions, is negligible, Equation (2-11) becomes:

$$\begin{aligned}
&\Psi_e(\vec{X};\vec{x})(\hat{H}_{k,n} + \hat{H}_{p,n-n})\Psi_n(\vec{X}) \\
&+\Psi_n(\vec{X})(\hat{H}_{k,e} + \hat{H}_{p,e-e} + \hat{H}_{p,n-e})\Psi_e(\vec{X};\vec{x}) \\
&= E \cdot \Psi_n(\vec{X}) \cdot \Psi_e(\vec{X};\vec{x})
\end{aligned} \tag{2-12}$$

If we now divide (2-12) by the function in (2-10), we obtain:

$$\underbrace{\frac{(\hat{H}_{k,e} + \hat{H}_{p,e-e} + \hat{H}_{p,n-e})\Psi_e(\vec{X};\vec{x})}{\Psi_e(\vec{X};\vec{x})}}_{\textit{e-dependent}} = E - \underbrace{\frac{(\hat{H}_{k,n} + \hat{H}_{p,n-n})\Psi_n(\vec{X})}{\Psi_n(\vec{X})}}_{\textit{n-dependent}} \tag{2-13}$$

Note that the right-hand side of (2-13) does not depend on the electronic coordinates $\vec{x}$ but only on the nuclear coordinates $\vec{X}$ and both sides of the equation are independent of each other. Therefore,

$$\frac{(\hat{H}_{k,e} + \hat{H}_{p,e-e} + \hat{H}_{p,n-e})\Psi_e(\vec{X};\vec{x})}{\Psi_e(\vec{X};\vec{x})} = E_e(\vec{X}) \tag{2-14}$$

leads to the electronic Schrödinger equation,

$$(\hat{H}_{k,e} + \hat{H}_{p,e-e} + \hat{H}_{p,n-e})\Psi_e(\vec{X};\vec{x}) = E_e(\vec{X})\Psi_e(\vec{X};\vec{x}) \tag{2-15}$$

Finally the total energy E of the system can be found from (2-13) and (2-14),

$$E = \frac{(\hat{H}_{k,n} + \hat{H}_{p,n-n})\Psi_n(\vec{X})}{\Psi_n(\vec{X})} + E_e(\vec{X}) \tag{2-16}$$

And if we neglect the kinetic energy component of the nuclei, $\hat{H}_{k,n}$,

$$E = \hat{H}_{p,n-n} + E_e(\vec{X}) \tag{2-17}$$

Therefore the total energy of the system at specific and fixed positions of the nuclei can be calculated by solving the electronic Schrödinger equation. Different sets of nuclear positions will lead to new electronic wavefunctions and hence to a new total energy. Repeating this procedure iteratively with various sets of nuclear positions will define the potential energy surface (PES) of the system. The lowest nuclear energy configuration will represent the most stable configuration of the system.

In view of the above, a number of methods have been developed to solve the electronic Schrödinger equation, including Hartree-Fock methods and Density Functional Theroy (DFT) methods. As we have mostly employed DFT based methods in this study, we will focus on the theory underlying this approach.

2.2.3 Density Functional Theory (DFT)

Even using an approximate electronic Schrödinger equation only, the complete solution of the N-electron wavefunctions $\Psi(\vec{x}_1,\vec{x}_2,\ldots,\vec{x}_N)$ is still difficult to achieve, as the wavefunctions are too complex to solve completely. To overcome this difficulty, more approximations are introduced, reducing the complexity of the calculations but at the expense of accuracy. One approach is to try and avoid determining the N-electron wavefunction which is the approach of the Density Functional Theory (DFT). In DFT, instead of the N-electron wavefunction, the electron density $n(r)$ takes the central role. In this section, we will introduce the basic theory of DFT and consider a few common approximations used in computational materials chemistry.

2.2.3.1 General theory

The fundamental principle of Density Functional Theory states that total energy of a system can be written as a functional of the ground state electronic density $n_0(r)$ (Hohenberg and Kohn 1964). However, the expression of the density functional was difficult to solve and at first remained unknown for any system with more than one electron, until Kohn and Sham in their seminal paper (Kohn and Sham 1965) provided a way to obtain useful approximate ground state functionals

for real systems with many electrons. Kohn and Sham's work remains the basis of many present-day methodologies for treating electrons in atoms, molecules, and condensed matter.

The modern formulation of DFT is based on the approach of Hohenberg and Kohn, who demonstrated that density functional theory is an exact theory of a many-body system, which can be applied to any system of interacting particles under an external potential $V_{ext}(r)$. In the Born-Oppenheimer approximation this concept can be applied to a system composed of N electrons in the field generated by M point charges (nuclei). The Hamiltonian of a molecule can then be written as:

$$\begin{aligned} \hat{H} &= T + E_{\text{int}} + \sum_{i}^{M} V_{ext}(r_i) \\ \hat{H} &= -\frac{h^2}{2m_e}\sum_{i}^{N}\nabla_i^2 + \frac{1}{2}\sum_{i\neq j}\frac{e^2}{|r_i - r_j|} + \sum_{i}^{M} V_{ext}(r_i) \end{aligned} \tag{2-18}$$

which accounts for the kinetic energy, $T = -\frac{h^2}{2m_e}\sum_{i}^{N}\nabla_i^2$, the repulsion interaction between electrons, $E_{\text{int}} = \frac{1}{2}\sum_{i\neq j}\frac{e^2}{|r_i - r_j|}$, and the Coulomb attraction between electrons and nuclei, $\sum_{i}^{M} V_{ext}(r_i)$, which in fact represents the external potential of the N interacting electrons. According to the Hohemberg-Kohn theorems, the total energy of a molecule can be written as a functional E_{HK} of the ground state electronic density $n_0(r)$:

$$\begin{aligned} E_{HK}[n] &= T[n] + E_{\text{int}}[n] + \int d^3 r V_{ext}(r) n(r) \\ &\equiv F_{HK}[n] + \int d^3 r V_{ext}(r) n(r) \end{aligned} \tag{2-19}$$

where $T[n]$ is the kinetic energy functional, $E_{\text{int}}[n]$ is the interaction energy of the electrons, and $\int d^3 r V_{ext}(r) n(r)$ is the interaction energy of the electrons with the nuclei, the source of the external potential. The Hohenbergh-Kohn functional $F_{HK}[n]$ defined in (2-19) includes the entire internal energy, including the kinetic and potential energies of the interacting electron system.

$$F_{HK} = T[n] + E_{\text{int}}[n] \tag{2-20}$$

However, the challenge posed by the Hohenberg-Kohn approach is to write the unknown functionals of the density of a many-electron system. The approach proposed by Kohn and Sham replaces the difficult interacting many-body problem with a different auxiliary system which can be solved more easily. As there is no specific prescription for choosing the simpler auxiliary system, however, they first rephrased the issues.

The Kohn Sham ansatz assumes that the ground state density of the original interacting system is equal to a specifically chosen non-interacting system, which provides a set of independent-particle equations for the non-interacting system that can be solved. All the difficult many-body interacting terms are integrated into an exchange-correlation functional of the density, and it is only this exchange-correlation functional which controls the accuracy of both the ground state density and the energy of the original many-body interacting system. Therefore, the Kohn-Sham approach to treat the full interacting many-body problem allows us to rewrite the Hohenberg-Kohn expression for the ground state energy functional (2-19) as follows (Kohn and Sham 1965):

$$E_{KS} = T_s[n] + \int dr V_{ext}(r) n(r) + E_{Hartree}[n] + E_{XC}[n] \tag{2-21}$$

where $T_s[n]$ is the independent particle kinetic energy, $V_{ext}(r)$ is the external potential due to the nuclei or other external sources, $E_{Hartree}$ is the classic self-interaction Coulomb energy and $E_{XC}[n]$ is the exchange and correlation energy. $E_{XC}[n]$ can be written in terms of the Hohenberg-Kohn functional:

$$\begin{aligned} E_{XC}[n] &= F_{HK}[n] - \left(T_S[n] + E_{Hartree}[n]\right) \\ E_{XC}[n] &= T[n] - T_S[n] + E_{\text{int}}[n] - E_{Hartree}[n] \end{aligned} \tag{2-22}$$

This expression shows that the exchange and correlation energy is just the difference between the kinetic and the internal interaction energies of the true interacting many-body system and the fictitious independent-particle system, with the electron-electron interaction energy replaced by the Hartree self-interaction energy.

If the universal functional $E_{XC}[n]$ were known, the exact ground state energy and density of the many-body electron problem could be found by solving the Kohn Sham equations for independent-particles. Unfortunately there is currently no method to determine the exact exchange-correlation functional. Nevertheless, there are a few very good approximations, e.g. the local density approximation (LDA) and various generalized gradient approximations (GGAs), which give accurate results for condensed matter and molecular systems.

2.2.3.2 Local Density Approximation (LDA)

Solids are often considered to be close to a homogeneous electron gas. Therefore, within certain limits, the effects of exchange and correlation can be approximated to be local in character. The local density approximation is based on this homogeneous electron gas assumption, where the exchange-correlation energy is simply described as an integral over all space with uniform exchange-correlation energy density at each point. In general, for a spin-unpolarized system, a local-density approximation for the exchange-correlation energy is written as

$$E_{XC}^{LDA} = \int E_{XC}[n(r)]dr \tag{2-23}$$

where n is the electronic density and E_{XC} is the exchange-correlation energy density that is a function of the density. The exchange-correlation energy is decomposed into exchange and correlation terms linearly,

$$E_{XC} = E_X + E_C \tag{2-24}$$

Separate expressions for E_X, the exchange energy term and E_C, the correlation term, where the exchange term based on analytic form for the homogeneous electron gas and the correlation term by various approximations since only limited expressions of the correlation density are known exactly.

2.2.3.3 Generalized-Gradient Approximation (GGA)

The success of the LDA has stimulated ideas for constructing improved functionals. Various generalized-gradient approximations (GGAs) have been developed with remarkable improvement over the LDA. The major improvement of

GGA over LDA is the way it accounts for the electron density distribution. LDA assumes the electron density as a homogeneous electron gas, whereas GGA takes into account the inhomogeneity (gradient of the electronic density) of the electron gas, which naturally occurs in any molecular system. The exchange correlation energy is decomposed into exchange and correlation terms in a similar way to the LDA.

$$E_{XC}^{GGA} = \int E_{XC}[n(r),\nabla n(r)]dr \qquad (2\text{-}25)$$

$$E_{XC}^{GGA} = E_{X}^{GGA} + E_{C}^{GGA}$$

In general, GGA approximations provides a considerable improvement in the accuracy of predicted energies and structures compare to LDA approximations. (Mattsson, Armiento et al. 2008)

$$E_{XC}[PBE] = E_{X}[PBE] + E_{C}[PBE] \qquad (2\text{-}26)$$

Among various GGA functionals, Perdew, Burke and Ernzerhof (PBE) functional (Perdew, Burke et al. 1996) (See Equation (2-26)) is employed throughout this study because of its broad range performance compared to the others, for example BLYP (Becke 1988; Lee, Yang et al. 1988) and RPBE (Zhang and Yang 1998) show good performance for molecular systems but not solid-state systems. (Mattsson and Mattsson 2009) As our aim in this study is to study the dissolutions of the phosphate glasses, we need a functional which perform well in both solid and molecular systems. Even though there are more accurate functionals for specific materials, PBE appears to give reasonable accuracy for both molecular and solid-state systems, and it has been tested and used extensively in calculations

for large classes of different materials and properties. However, the water structure modelled by PBE functional tends to be overstructured. This problem is controlled by the increase of simulation temperature to 400K in order to achieve a liquid like behaviour in CP-MD simulations as tested and suggested by previous studies. (Fernandez-Serra and Artacho 2004; Schwegler, Grossman et al. 2004; Sit and Marzari 2005) Hybrid functionals may also be an option in the future, but at present they are relatively new and not as commonly available for ab-initio molecular dynamics like PBE functional.

2.2.4 Basis Sets

In this section, we will introduce one of the cornerstones of all quantum mechanical calculations, which are the basis sets. Quantum calculations for molecules were historically performed as Linear Combinations of Atomic Orbitals, which means that molecular orbitals are constructed from a set of atomic orbitals:

$$\phi_k(\vec{x}) = \sum_{i=1}^{n} c_{ik}\chi_i(\vec{x}) \tag{2-27}$$

where ϕ_k is the k-th molecular orbital, c_{ik} are the coefficients of the linear combination, χ_i is the i-th atomic orbital, and n is the number of atomic orbitals.

2.2.4.1 Localised Basis Sets

The solutions of the Schrödinger equation are based on the atomic orbitals (AO) concept of the atom, which assumes that a wavefunction will be allocated to each single electron in the atom. These atomic orbitals are also called basis functions. At first, Slater Type Orbitals (STO's) (Slater 1930) were used as basis

functions due to their similarity to the atomic orbitals of the hydrogen atom. However, they were soon replaced by other types of orbitals due to their lack of efficiency for integral calculations involving more than one electron. Therefore, Gaussian Type Orbitals (GTOs) were introduced (Boys 1950), which enable an approximation of the shape of the STO functions by summing up a number of GTOs with different exponents and coefficients. The GTOs offer much faster integral calculation speed, where even using a collection of GTOs, the speed of integral calculations will still be more favourable than the original STOs.

2.2.4.1.1 Slater Type Orbitals

Introduced by John C. Slater in 1930, Slater Type Orbitals (STOs) (Slater 1930) are a type of orbital used as atomic functions to construct molecular orbitals in ab-initio calculations. The Slater Type Orbitals are normalised but not orthogonal. This made the calculation of the matrix element for the Fock matrix very complicated. Let χ be an atomic function at the origin,

$$\chi(\vec{r}) = R_{nl}(r)Y_{lm}(\theta,\phi) \tag{2-28}$$

where Y_{lm} is a spherical harmonic function, the angular part of the atomic function and R_{nl} is the radial part of the atomic function. For an atom at another position, r, θ and ϕ are the spherical coordinates with respect to that position. The radial part of the atomic function is given as a polynomial times an exponentially decaying function.

$$R_{nl} = Nr^{n-1}e^{-\zeta r} \tag{2-29}$$

where N is the normalisation constant, $N = \frac{(2\zeta)^{n+1/2}}{(2n!)^{1/2}}$, r is the distance of the electron from the atomic nucleus, n is a the principal quantum number and ζ is a shielding constant related to the effective charge of the nucleus. Hence the STO is represented as:

$$\chi(\vec{r}) = \chi_{\vec{R},\zeta,n,l,m}(\vec{r}) = Nr^{n-1}e^{-\zeta r}Y_{lm}(\theta,\phi) \tag{2-30}$$

2.2.4.1.2 Gaussian Type Orbitals

One solution to the Slater Type Orbitals is to replace the Slater Type Orbitals with some function that resemble the STOs but for which the matrix elements are less complicated to calculate. The standard solution of this problem is the use of Gaussian Type Orbitals (GTOs), (Boys 1950) also called Gaussians, which are defined as:

$$\chi(\vec{r}) = \chi_{\vec{R},\alpha,n,l,m}(\vec{r}) = Nr^{n-1}e^{-\alpha r^2}Y_{lm}(\theta,\phi) \tag{2-31}$$

where the normalisation constant $N = 2^{n+1}\frac{\alpha^{(2n+1)/4}}{\left[(2n-1)!!\right]^{1/2}(2\pi)^{1/4}}$ for the Gaussians and the argument of the exponential function is r^2 dependence compared to r for the STOs. One distinctive character of Gaussian Type Orbitals is its radial part that is given by a Gaussian function $e^{(-ar^2)}$, where r is the length of the electron position vector $\vec{r}$ and α is a parameter that can be taken from tables of atomic

orbital basis sets. The tables of α may have been prepared by energy minimizations or by fitting to other orbitals.

2.2.4.1.3 Basis Set Superposition Error

Basis set superposition errors (BSSE) are usually encountered with interaction energy calculations of systems described by finite basis sets. The problem occurs when two atoms, two molecules or different parts of the same molecule approach each other, when their basis functions overlap. According to the variational principle, the quality of the calculation will improve when the finite basis set is extended to further basis functions in the overlap region and the total electronic energy will be lowered. Therefore, when two particles described by finite basis functions interact, the description of the orbitals of the two particles will be improved through the increase in the number of basis functions in the overlap area. This may cause the total energy of the interacting system to be artificially lower than the sum of the total energies of the two individual systems, and when it comes to energy calculations, the interaction energies may therefore be overestimated.

BSSE can be improved through the Chemical Hamiltonian approach (CHA) (Mayer and VibÛk 1988; Kieninger, Suhai et al. 1994) and counterpoise approach (CP) (Boys and Bernardi 1970). In the Chemical Hamiltonian approach (CHA), the basis set mixing is prevented a priori. Mixing is avoided by removal of the conventional Hamiltonian, which contains projector-containing terms that would allow mixing. In the counterpoise approach (CP), the BSSE is evaluated in a

posteriori way, which all the calculations are re-performed using the mixed basis sets and the error is then subtracted from the uncorrected energy.

2.2.4.1.4 Numerical Basis Functions

Some methods employ basis functions that are represented completely numerically, called numerical basis functions, which are obtained for the isolated atoms and the relevant ions. When constructing the numerical basis functions, all basis functions are represented in the form:

$$\chi(\vec{r}) = R_{nl}(r)Y_{lm}(\theta,\phi) \tag{2-32}$$

where $\chi(\vec{r})$ is the basis function, $Y_{lm}(\theta,\phi)$ is the angular part and $R_{nl}(r)$ is the radial part given numerically. These methods require all integrals to be calculated numerically and efficiently, but they offer good transparency when it comes to interpreting the results. Numerical basis sets are mainly used in density functional theory methods.

Numerical basis sets have been used extensively in this study with Dmol^3 for DFT cluster calculations. In Dmol^3, the values of the numerical basis functions are given on an atomic-centered spherical-polar mesh, rather than as analytical functions like the Gaussian Type Orbitals. The angular part of the function is an appropriate spherical harmonic $Y_{lm}(\theta,\phi)$ and the radial part of the function $R_{nl}(r)$ is obtained by solving the atomic DFT equations numerically. Reasonable accuracy is obtained by using a range of 300 radial points from the nucleus to and outer

distance of 10 Bohrs. The use of the exact DFT spherical atomic orbitals has several advantages, such as the modelled molecule has the ability to be dissociated exactly to its constituent atoms; thanks to the good quality of these orbitals, basis set superposition effects are minimised (Delley 1990; Inada and Orita 2008) and an excellent quality of bond description, even weak bonds, can be acheived. (Benedek, Snook et al. 2005; Inada and Orita 2008) On the other hand, previous studies suggested that numerical basis sets tend to overestimate the binding energy in some cases. (Benedek, Snook et al. 2005; Inada and Orita 2008) However, the results of previous investigations (Benedek, Snook et al. 2005; Henry, Varano et al. 2008; Inada and Orita 2008), have shown that the cost effectiveness in the numerical basis sets in DMol^3 is superior to that in Gaussian basis sets in terms of accuracy per computational cost and the calculations using numerical basis sets offer a definitive advantage where geometry optimization of large systems is required.

2.2.4.2 Plane-wave Basis Sets

In addition to localized basis sets, plane-wave basis are also used in quantum chemical simulations. Different from both the Slater and Gaussian type approach, plane-wave basis functions are completely delocalised and cannot be ascribed to individual atoms.

For periodic systems the potential has the property,

$$V(r + na) = V(r) \tag{2-33}$$

where a is a lattice vector and n is an integer. By applying Bloch's theorem, (Blakemore 1985) the wavefunctions of the plane-wave basis sets can be witten as a product of a cell periodic part and a wavelike part.

$$\chi_i(\vec{r}) = e^{i\vec{k}\cdot\vec{r}} f_i(r) \tag{2-34}$$

where the basis function $\chi_i(\vec{r})$ is written in a plane-wave form $e^{i\vec{k}\vec{r}}$, the wavelike part and a cell periodic part of the wavefunction $f_i(r)$. The cell periodic part $f_i(r)$ can be expanded as a set of plane waves,

$$f_i(r) = \sum_G c_i(G) e^{iG.r} \tag{2-35}$$

where G are the reciprocal lattice vectors. Hence the electronic wave functions can be written as:

$$\chi_{i,k}(\vec{r}) = \sum_G c_{i,k}(G) e^{i(k+G).r} \tag{2-36}$$

As in the localized cases, an infinite number of basis functions are needed to portray the exact wavefunction. This infinite basis functions can be reduced to a finite size by introducing the plane-wave cut-off energy E_{cut}, due to the fact that plane-wave functions with a smaller kinetic energy typically have a more important role than those with high kinetic energy. Only the plane-waves with the lattice vectors, that fit the criteria will be included in the basis set.

$$E_{cut} \geq \frac{\hbar^2 |k+G|^2}{2m_e} \tag{2-37}$$

This kinetic energy cut-off will lead to an error in the total energy of the system as all other basis set truncations, but it should be small if the cut-off energy has been chosen appropriately. The strategy of the plane-wave cut off energy also provides an advantage over many other basis sets that the convergence of the calculation with respect to the basis set may be ensured by variation of a single parameter, E_{cut}.

Plane-wave basis functions are able to provide correct eigenfunctions for free electrons and they are therefore considered to be good basis functions to use for metallic crystalline materials. They are also used in molecular studies, mainly with density-functional theory methods. The main advantages of using plane waves are their orthogonal nature that eliminates BSSE and easy calculation for all kind of matrix elements by Fast-Fourier-Transform techniques and the fact that the size of the basis set can be increased systematically in a simple way. Their main disadvantages are that the basis set can easily become very large and it is less trivial to interpret the results in terms of chemical bonds and other properties. However, the difficulty of a large number of basis functions required for accurate representation of the Kohn-Sham orbitals in a plane-wave can be reduced by the use of pseudopotentials, but several hundreds basis functions per atom must still be used. Despite of this, plane-wave basis sets may actually be more efficient for large systems compared to atomic orbital basis sets, as the number of functions needed to describe the density grows quadratically with the size of the system for atomic orbital basis sets, but has a linear relationship with plane-wave basis sets.

2.2.5 The Pseudopotential Approach

Planewaves have a range of attractive properties: they are simple to use, orthonomal by construction, unbiased because there is no freedom in choosing plane-waves: the basis is fixed by the crystal structure and by the cutoff and simple to check for convergence by increasing the cuttoff. However the extended character of plane-waves makes it impractical to reproduce localized functions such as the charge density around a nucleus. The difficult of describing the core states prevents the use of plane-waves. However, as core states do not contribute in a significant manner to chemical bonding and to solid-state properties, this suggests that one may safely ignore the changes in the core states. (See Section 2.2.5.1 Frozen-Core Approximation) The idea of replacing the full atom with a much simpler pseudoatom with valence electrons first appeared in a paper by Fermi in 1934. (Fermi 1934) Since the 1960s, pseudopotentials have been widely used in solid-state physics. At the beginning, pseudopotentials were devised to reproduce some known experimental solid-state and atomic properties such as energy gaps or ionization potentials. Modern pseudopotentials are called norm-conserving pseudopotentials. These are atomic potentials which are devised to mimic the scattering properties of the full atom. For a given reference atomic configuration, a norm-conserving pseudopotential has the following conditions:

1. Both all-electron and pseudo- wavefunctions must have the same energy.
2. All-electron and pseudo- wavefunctions must also be the same beyond the given core radius r_c.

3. The pseudo –charge and the true charge contained in the region $r < r_c$ must be the same.

The norm-conserving pseudopotentials are relatively smooth functions. Experience has shown that pseudopotentials and all-electron calculations on the same systems yield very similar results.

However, for a number of atoms, the norm-conserving pseudopotentials are still difficult to process as they contain a significant number of Fourier components with large charge, for example N, O, F, and the first row transition metals. These atoms gain little in the pseudization, because there are no orthonomality wiggles that can be removed in the 2p and 3d states. Therefore, more complex Ultrasoft pseudopotentials have been devised to be much softer that the norm-conserving counterparts at the price of considerable additional complexity. It should be remarked that the use of pseudopotentials is not limited to plane-wave basis sets only, pseudopotentials can also be used in conjunction with localized basis sets as well.

2.2.5.1 Frozen-Core Approximation

The frozen-core approximation was developed based on the fact that when describing the electronic orbitals for theoretical calculations, the core electronic orbitals of atoms scarcely change during the transition from isolated atoms to compounds. Hence it is reasonable to assume that for a given system the core orbitials are identical to those of the isolated atoms and only the valence orbitals will be optimized in solving the equations of electronic calculations.

For DFT, as the total electronic energy expression is a functional of the total electron density, which is independent of the electronic orbitals, no explicit expression of wavefunctions is needed. In this case, only the valence electron density is calculated while the core electron density is kept as the isolated atoms in electronic calculations. Consequently, this provides a significant simplification and calculations can be done with similar computational resources regardless the size of the atoms.

2.3 Molecular Dynamics

There are two types of molecular dynamics techniques used in computational simulation studies, Classical Molecular Dynamics and Ab-initio Molecular Dynamics. In contrast to the crucial dependence on accurate potentials in Classical Molecular Dynamics (CMD) simulations, Ab-initio Molecular Dynamics (AIMD) provides a more sophisticated but highly expensive alternative. AIMD offers a way to describe the chemical events involving chemical transformation by combining electronic structure calculations with finite temperature dynamics.

From the available Ab-initio Molecular Dynamics techniques, we have used the Car-Parrinello molecular dynamics (CPMD) method in this research project. In this section, we will start with an introduction to Classical Molecular Dynamics and move on to Ab-initio Molecular Dynamics, which will then be followed by a brief description of the common implementations of AIMD, i.e. Born-Oppenheimer Molecular Dynamics and Car-Parrinello Molecular Dynamics.

2.3.1 Classical Molecular Dynamics

Molecular dynamics (MD) is a computational simulation technique where the time evolution of a set of interacting particles can be followed by integrating the equations of motion of the particles. In MD, the motion of the nuclei is modelled by the laws of classical mechanics, which gives a good approximation for most molecular systems.

Let us consider the case of a particle moving under the influence of a force, $\vec{F}(\vec{r})$:

$$m\frac{d^2\vec{r}}{dt^2} = \vec{F}(\vec{r}) \tag{2-38}$$

where the classical equations of motion are:

$$\frac{d\vec{r}(t)}{dt} = \frac{\vec{p}(t)}{m} \tag{2-39}$$

$$\frac{d\vec{p}(t)}{dt} = F(\vec{r}) \tag{2-40}$$

The integration of the equations of motion can therefore define the trajectory of the particle subject to the external force-field $\vec{F}(\vec{r})$, by the value of the position of $\vec{r}(t)$ and momentum $\vec{p}(t)$ of each time step. For a simple constant force situation, where $\vec{F}(\vec{r}) = F$, the time evolution of the particle's momentum and position are given by:

$$\vec{p}(t) = Ft + \vec{p}_0 \tag{2-41}$$

$$\vec{r}(t) = \frac{1}{2}\frac{F}{m}t^2 + \frac{\vec{p}_0}{m}t + \vec{r}_0 \tag{2-42}$$

where $\vec{p}_0$ and $\vec{r}_0$ are the initial position and momentum of the particle that define the initial trajectory of the particle. This shows that the MD technique is a deterministic approach, i.e. the initial position and momentum determine the whole trajectory of the system. Realistically, the system will consist of more than one particle, and each particle will be interacting with the others. The force acting on each particle will change whenever any particle changes its position in the system: $\vec{F}_i = \vec{F}_i(\vec{r}_1,\vec{r}_2,\cdots,\vec{r}_i,\cdots,\vec{r}_N)$. As a result, a set of N interacting particles will mean solving a set of N coupled Newtonian equations:

$$m_i \frac{d^2\vec{r}_i}{dt^2} = F_i(\vec{r}_1,\vec{r}_2,\cdots,\vec{r}_N),$$
$$M_I\ddot{R} = F_I(\{R_I\}), \quad I = 1,\ldots,N \tag{2-43}$$

Hence the individual equations of motion of each particle become:

$$\frac{d\vec{r}_i}{dt} = \frac{\vec{p}_i}{m} \tag{2-44}$$

$$\frac{d\vec{p}_i}{dt} = \vec{F}_i \tag{2-45}$$

However, the equations of motion are now too complicated to be solved analytically and these differential equations are usually solved via a finite difference approach, e.g. the Verlet scheme. (See Section 2.3.1.1)

In MD simulations, the simulation period is divided into a set of calculations of very short time steps Δt (typically between $10^{-15} - 10^{-14}$ sec). At each step, the forces on each atom are computed and combined with the current positions and velocities to generate a new set of positions and velocities for the next time step. The atoms are then moved to the new position and the new forces for the next time step will be computed and so on. During the time interval Δt, the forces are assumed to be constant.

By going through these calculation steps, the MD simulation generates a dynamical trajectory that describes the time evolution of the dynamic variables $\vec{p}_i$ and $\vec{r}_i$ of each particle in the simulation time period. Therefore MD is a technique, which allows the microscopic dynamical behaviour of the simulated system being followed by a set of trajectories of each particle in the system.

In a MD simulation, the N interacting particles follow Newton's equations of motion and consequently the total energy of the system is conserved. This property of energy conservation is important to establish a link between molecular dynamics and statistical mechanics. Statistical mechanics relate the macroscopic properties of the material to microscopic details of the simulated system and provide microscopic details such as the distribution and motion of the atoms and molecules of the N-body system.

Statistical mechanics is based on the Gibbs' ensemble concept, which defines an ensemble as a collection of all possible systems that have different microscopic states. Common ensembles with various characteristics are:

- Microcanonical ensemble (NVE): ensemble with thermodynamic state characterised by a fixed number of atoms, N, fixed volume, V, and fixed energy, E, (isolated system).
- Canonical ensemble (NVT): ensemble with thermodynamic state characterised by a fixed number of atoms, N, fixed volume, V, and fixed temperature, T.
- Isothermal-isobaric ensemble (NPT): ensemble with thermodynamic state characterised by a fixed number of atoms, N, fixed pressure, P, and fixed temperature, T.
- Grand-canonical ensemble (μVT): ensemble with thermodynamic state characterised by a fixed chemical potential, μ, fixed volume, V, and fixed temperature, T.

Classical molecular dynamics rely on the Born-Oppenheimer approximation, which assumes the nuclei move according to classical mechanics in an effective potential from the electrons. The effective potential is calculated by solving the electronic Schrödinger equation for each set of fixed nuclear coordinates and usually presented in approximated forms, i.e. in terms of truncated expansion of many-body contributions. Hence the electronic degrees of freedom can be replaced by the interaction potentials and are not featured as explicit degrees of freedom in the equation of motion.

Effective potential:

$$V\left(\overline{R}_1,\overline{R}_2,\ldots,\overline{R}_N\right)=\sum_i V\left(\overline{R}_i\right)+\sum_{ij} V\left(\overline{R}_i,\overline{R}_j\right)+\cdots \tag{2-46}$$

As a result, the mixed quantum/classical problem is reduced to pure classical mechanics where two-body and three-body interactions are taken into account typically. This creates a dramatic simplification effect as the electrons are now constructed from a manageable sum of additive few-body contributions. However the down side is that the possibility of chemical transformation is basically eliminated from the classical molecular dynamics simulations. To monitor and study precise bond transformation processes, ab-initio molecular dynamics methods are needed.

2.3.1.1 Verlet Scheme

The Verlet algorithm is probably the most widely used method of integrating the equations of motion. It was initially adopted by Verlet and attributed to Stormer. This method is a direct solution of the second-order equation:

$$m_i \ddot{r}_i = f_i \tag{2-47}$$

where m_i is the mass of the atom i, r_i is the Caetesian coordinates and f_i is the force on atom i. The method is based on positions $r(t)$, accerlations $a(t)$, and the positions $r(t-\delta t)$ from the previous step. The equation for advancing the postions is:

$$r(t+\delta t) = 2r(t) - r(t-\delta t) + \delta t^2 a(t) \tag{2-48}$$

Note that the velocities do not appear at all and have been eliminated by the addition of the equations obtained by Taylor expansion about $r(t)$:

$$\begin{aligned} r(t+\delta t) &= r(t) + \delta t v(t) + (1/2)\delta t^2 a(t) + \ldots \\ r(t-\delta t) &= r(t) - \delta t v(t) + (1/2)\delta t^2 a(t) - \ldots \end{aligned} \tag{2-49}$$

The velocities are not required to compute the trajectories, however they are useful for estimating the kinetic energy and hence the total energy, which can be obtained from:

$$v(t) = \frac{r(t+\delta t) - r(t-\delta t)}{2\delta t} \tag{2-50}$$

where the error of the velocity from Equation (2-50) is of the order of δt^2 and the error of Equation (2-49) is of the order of δt^4. Higher accuracy can be achieved by storing more variables, but this will increase the already implicitly present inconvenience in Equation (2-50), where the velocity $v(t)$ can only be computed once the Cartesian coordinate $r(t+\delta t)$ of next step is known. This problem can be overcome by the velocity Verlet scheme, where positions, velocities and accelerations at the time $t+\delta t$ are computed from the same quantities at the time t.

2.3.2 Ab-initio Molecular Dynamics

Ab-initio Molecular Dynamics (AIMD) is a link between and combination of quantum mechanical electronic structure calculations and classical molecular dynamics calculations. In contrast to the high dependence of Classical Molecular Dynamics on accurate potentials, AIMD provides an expensive but sophisticated alternative to describing the events involved in chemical transformations by combining electronic structure calculations with finite temperature dynamics. Hence AIMD becomes the natural choice of MD approach to use in the present study, where chemical bonding and transformations are of interest, i.e. glass formation, hydration shell structure, and hydrogen bonding.

There are three ab-initio molecular dynamics approaches that rely on the Born-Oppenheimer approximation: Ehrenfest molecular dynamics, Born-Oppenheimer molecular dynamics and Car-Parrinello molecular dynamics. In this study, the latter two have been employed to simulate phosphate clusters and phosphate bioglasses. The theoretical approaches of both are presented below.

2.3.2.1 Born-Oppenheimer Molecular Dynamics

Born-Oppenheimer Molecular Dynamics (BOMD) is based on the Born-Oppenheimer (BO) approximation, where the static electronic calculation is included in the molecular dynamics simulations as if the nuclear positions are fixed at each molecular dynamics step. The electronic structure part can therefore be reduced to a time-independent quantum calculation, by solving the time-independent Schrödinger equation. The nuclei, on the other hand, are treated as chemical particles, and the equation of motion for the nuclear potentials are defined by:

$$M_I \ddot{R}_I(t) = -\nabla_I [E_0(\{R_I\}) + V_{NN}(\{R_I\})] \tag{2-51}$$

where $E_0(\{R_I\})$ is the corresponding ground-state electronic energy at the nuclear configuration $\{R_I\}$ and $V_{NN}(\{R_I\})$ is the constant nuclear repulsion:

$$E_0(\{R_I\}) = \left\langle \Psi_0 \middle| H_e(R_I) \middle| \Psi_0 \right\rangle \tag{2-52}$$

$$V_{NN} = \frac{1}{2} \sum_{IJ} \frac{Z_I Z_J e^2}{|R_I - R_J|} \tag{2-53}$$

For each set of nuclear configurations $\{R_I\}$, the corresponding wavefunctions Ψ_0 are obtained by solving the time-independent Schrödinger equation, from which we can then compute the forces acting on the atoms:

$$F_I = -\nabla_I \left\langle \Psi_0 \middle| H_e(R_I) \middle| \Psi_0 \right\rangle + F_{ion-ion} \tag{2-54}$$

$F_{ion-ion}$ is the force due to the direct core-core repulsion and the first term of (2-54) can be evaluated using the Hellman-Feynman theorem (Hellmann 1937;

Feynman 1939). The forces are then calculated and the ionic positions are updated by the Verlet algorithm. This process is repeated until a sufficient length of MD trajectory is generated. In summary, the steps that involved in a BOMD simulation are:

1. Relax the electronic configuration to its ground state for the present ionic configuration $\{R_I(t)\}$.
2. Calculate the forces on the atoms $\{F_I(t)\}$ using the Hellman-Feynman theorem.
3. Integrate the equations of motion for the ionic system $M_t\ddot{R}_I(t) = F_I$ to give the next set of ionic configuration $\{R_I(t+\Delta t)\}$.
4. Repeat above until a sufficient length of MD trajectory is generated.

The major difficulties about this relatively straightforward method are the costly process of evaluating the electronic structure calculation for each electronic configuration during a MD simulation. Early applications of BOMD relied on the appropriate approximation schemes, such as semiempirical and Hartree-Fock approximations, to solve the electronic problem, i.e. the Schrödinger equation, but the breakthrough of density functional theory to solve the Schrödinger equation has provided a new viable solution to the application of ab-initio molecular dynamics to materials science.

2.3.2.2 Car-Parrinello Molecular Dynamics

Car-Parrinello molecular dynamics (CPMD) (Car and Parrinello 1985) is another ab-initio molecular dynamics method that is based on the Born-

Oppenheimer (BO) approximation and it is often implemented in the framework of the Kohn-Sham Density Functional Theory. The starting point of the CP method is based on the validity of the BO approximation itself.

The electronic energy of a simulated system, E_0, can be evaluated with wavefunction, Ψ_0, that is also a function of the nuclear positions, [R_I]:

$$E_0 = \left\langle \Psi_0 \middle| H_e(R_I) \middle| \Psi_0 \right\rangle = E_0\{(R_I)\} \tag{2-55}$$

At the same time, E_0 can also be considered as a functional of the wavefunction, Ψ_0.

$$E_0 = E_0[\Psi_0(r)] \tag{2-56}$$

In the framework of the density functional theory, E_0 can be written as a functional of the Kohn-Sham one-electron orbitals, $\{\psi_i\}$, that are used to build the wavefunction, Ψ_0. For this reason, we can write:

$$E_0(t) = E_0(\{\psi_i(r)\},\{R_I(t)\}) \tag{2-57}$$

This represents a Born-Oppenheimer system which is characterised by two-components, quantum (electrons) and classical (nuclei). In the Car-Parrinello approach, electrons and nuclei that evolve according to the BO approximation as a two-component system with two different energy scales, where the ions move at the pre-assigned temperature and the electrons have to follow adiabatically at their instantaneous ground states, essentially at zero temperature.

In the Car-Parrinello (CP) method, the BO system is mapped into a system in which nuclei and electrons are treated classically. i.e. they move according to Newton's equation of motion. In order to achieve this, the single-electron orbitals are imbued with a fictitious time dependence, $\psi_i(r) \rightarrow \psi_i(r,t)$, and the orbitals are moved according to the Newtonian equations of motion by defining a particular class of Lagrangians, i.e. $L = T - V$.

The potential energy of the system with respect to specific time in the CP method is given as:

$$E_0(t) = E_0\left(\{\psi_i(r,t)\},\{R_i(t)\}\right) \tag{2-58}$$

note that the orbitals are now dependant on the time t.

The kinetic energy of the system T is now the sum of two terms, the kinetic energy of the nuclei and the kinetic energy of the electrons:

$$T = T_N + T_e = \frac{1}{2}\sum_I M_I \dot{R}_I^2 + \frac{1}{2}\mu\sum_i \int \dot{\psi}_i^*(r,t)\dot{\psi}_i(r,t)dr \tag{2-59}$$

where μ is the fictitious mass ascribed to the orbital degrees of freedom. The Lagrangian in Car Parrinello is defined as:

$$L_{CP} = T_N + T_e - E_0 + \ constraints \tag{2-60}$$

where the $constraints = \sum_{ij} A_{ij}\left(\int \psi_i^*(r)\psi_j(r)dr - \delta_{ij}\right)$.

Hence, the Euler-Lagrange equations can be applied:

$$\frac{d}{dt}\frac{\partial L}{\partial \dot{q}_j} - \frac{\partial L}{\partial q_j} \tag{2-61}$$

Considering the nuclear case, where the variables q_j equal a nuclear coordinate:

$$\frac{d}{dt}\frac{\partial L_{CP}}{\partial \dot{R}_I} = \frac{\partial L}{\partial R_I} \tag{2-62}$$

from which we obtain the equation which defines the classical equation of motion for the nuclei:

$$M_I \ddot{R}_I(t) = \frac{-\partial E_0(t)}{\partial R_I} \tag{2-63}$$

For the electronic case, the simple derivative is substituted by the functional derivative, since our parameters are now functions in a continuous position space:

$$\frac{d}{dt}\frac{\partial L_{CP}}{\partial \psi_i^*(r,t)} = \frac{\partial L_{CP}}{\partial \psi_i^*(r,t)} \tag{2-64}$$

from which we obtain the Newtonian equation of motion for the electron orbitals:

$$\mu \ddot{\psi}_i(r,t) = \frac{-\delta E_0(t)}{\delta \psi_i^*(r,t)} + \frac{\delta}{\delta \psi_i^*(r,t)}\{constraints\} \tag{2-65}$$

Given that the CP method is usually implemented in the framework of the Kohn-Sham Density Functional Theory (KS-DFT), the force acting on the KS orbitals can be defined as:

$$\frac{\delta E_0^{KS}(t)}{\delta \psi_i^*(r,t)} = h_{eff}^{KS}(t)\psi_i(r,t) \tag{2-66}$$

with $h_{eff}^{KS}(t)$ being the time-dependent single particle Kohn-Sham operator.

In CP molecular dynamics the nuclei and the orbitals evolve together, i.e. the equations of motions for nuclear and electronic degrees of freedom are solved simultaneously using a standard time integration algorithm, e.g. Verlet Scheme.

By considering the expansion of the single-electron orbital in terms of a basis set:

$$\psi_i = \sum_\alpha c_\alpha^{(i)} \phi_\alpha(r) \tag{2-67}$$

and introducing the time dependence of the orbitals $\psi_i = \psi_i(r,t)$, we have,

$$\psi_i(r,t) = \sum_\alpha c_\alpha^{(i)}(t) \phi_\alpha(r) \tag{2-68}$$

The CPMD equations of motion are therefore:

$$M_I \ddot{R}_I(t) = \frac{-\delta E_0(t)}{\delta R_I} \tag{2-69}$$

$$\mu \ddot{c}_\alpha^{(i)}(t) = \frac{-\delta E_0(t)}{\delta c_\alpha^{(i)}(t)} + \frac{\delta}{c_\alpha^{(i)}(t)} \{constraints\} \tag{2-70}$$

In the CP method, nuclei and orbitals are treated as part of an extended classical system where the nuclei evolve in time at a certain physical temperature and a “fictitious temperature” associated with the electronic degrees of freedom. The terminology of “low electronic temperature” or “cold electrons” means that the

electronic subsystem is close to its instantaneous minimum energy. Hence a ground state wavefunction optimised for the initial configuration of the nuclei will stay close to its ground state during the time evolution if the wavefunction is kept at a sufficiently low temperature. Therefore, an important check in CP-MD simulation is the time evolution of the "fictitious temperature" of the electrons, which must maintain a constant value close to zero.

2.4 Simulation Conditions

In this session we will introduce a few conditioning assumptions of the simulation systems that have been employed in our study, namely Periodic Boundary Conditions (PBC), Polarisable Continuum solvation Model (PCM) and COnductor-like Screening MOdel (COSMO).

2.4.1 Periodic Boundary Condition

In computational modelling, the simulation system is limited to a finite size that may not be comparable in reality. In order to calculate a representable structure of a material, special treatment for the simulation system is needed. The common solution is to use Periodic Boundary Conditions (PBC).

In a simulation system, if the boundaries of the simulation cell are not treated accordingly, the atoms near the boundary will have fewer neighbours than the atoms in the centre as the simulation cell terminates. This setup is appropriate for cluster simulations but unrealistic for materials simulations, since no matter how large the simulated system is, it will be incomparable to a macroscopic system. The ratio between the number of surface atoms and the total number of atoms would be much larger than in reality, which will cause the surface effects to be overestimated. Periodic boundary conditions (PBC) enable a unit cell replication approach, which allows the simulation box to be replicated in all three Cartesian directions. The PBC approach gives a more realistic presentation of the simulated system. The key idea is that now every particle in the box is interacting not only with other particles in the same box but also their images in the nearby imaginary boxes. Hence the interaction range can be extended and is not limited by the simulation cell

boundaries. Using PBC, surface effect can be virtually eliminate, from the system, with the forces acting on the particles the same regardless of the relative positions of the boundaries of the simulated unit cell.

2.4.2 Solvation Modelling

A molecule in the gas phase, which is isolated from other molecules, has different properties from a molecule in solution. Molecules in solution will experience interactions with the solvent molecules and these interactions will lead to modifications in the properties of the molecule of interest. As many experiments are carried out in the liquid phase, it is desirable to be able to describe such systems by theoretical methods in appropriate ways. Assuming that molecular properties are unchanged from gas phase to liquid phase is clearly a simplification in most cases, and the development of a viable alternative way to model molecules in liquid phase becomes essential.

Treating solvated molecules is similar to treating impurities in infinite crystalline materials. Both are concerned with a small finite segment in a relatively infinite system. However, the solvated molecules usually have much weaker interactions with their surroundings compared to the impurities in the crystal, given that there is no covalent bond formation involved. Hence the effects of the solvated molecules are relatively smaller than the crystalline environment of impurities and are often treated by approximation only. This does not mean treating solvated molecules is any easier; in fact it is more difficult and due to the lack of long-range order, it can only be treated with difficulty by electronic-structure methods.

One of the early approaches of treating solvated molecules was simply to build a finite system, which is large enough to imitate the infinite system, referred to as the supermolecule approach (Dreyfus and Pullman 1970; Kollman and Allen 1970). This approach provides a way to incorporate in the simulation the effects of the solvent molecules on the solutes, but its practicality is often limited by the size of the simulated system. In order to reduce the computational demands, the assumption is made that the electronic structure of the solvent molecules remains frozen, based on the fact that they only change a little in the solution compared with the solute, referred to as the frozen-density-functional-theory (Frozen-DFT) method (Wesolowski and Warshel 1993). However, this method is still relatively expensive and requires a large finite system.

2.4.2.1 Polarisable Continuum Models

In contrast to the Frozen-DFT, some approaches treat the solvent as a dielectric continuum (Duben and Miertus 1981), the so-called Polarisable Continuum Model (PCM). The solvent is assumed to form a continuous medium, a dielectric continuum, and a cavity is formed when a solute is introduced into the solvent. Depending on the polarity of the solute, the dielectric continuum will respond by being polarized. The main effects that should be addressed are the energy costs related to the creation of the cavity that accommodates the solute and the various interactions between the solute and the dielectric continuum. Given that the interactions between the solute and the dielectric continuum are of a dielectric nature, defining a suitable cavity is not straightforward. After defining the shape and size of the cavity, the effects of the charge distribution of the solute on the solvent also need to be accounted for. Since the solvent is treated as a homogenous

dielectric continuum, the effects of the charge distribution of the solute on the solvent can be treated by polarizability, which is independent from positions and directions.

In this study, PCM is our basic approach for solvation modelling. A typical solvation calculation by PCM will consist firstly of the definition of the size and shape of the cavity, followed by the insertion of the solute into the cavity and the calculation of the electronic properties of the solute by either Hartree-Fock or Density Functional Theory methods, where the extra complications of the electrostatic interactions between the solute and its polarized surrounding are to be included. Therefore a self-consistent procedure is required to solve the correlations between the polarization of the dielectric continuum and the electron distribution of the solute. As a result of redistribution of the electrons, the structure of the solute may change. The basic definition of the PCM can be summarised by:

$$\sigma(\bar{s}) = \frac{\varepsilon - 1}{4\pi\varepsilon} \frac{\partial}{\partial \vec{n}} \left(V_{total}\right)_{in}$$
$$\sigma(\bar{s}) = \frac{\varepsilon - 1}{4\pi\varepsilon} \frac{\partial}{\partial \vec{n}} \left(V_M + V_\sigma\right)_{in} \qquad (2\text{-}71)$$

where $\sigma(\bar{s})$ is the apparent surface charge distribution, ε is the permittivity of the dielectric continuum, $\frac{\partial}{\partial \vec{n}}$ is the gradient factor ($\vec{n}$ indicates that the unit vector is perpendicular to the cavity surface and pointing outward.) and V_{total} is the total electrostatic potential of the cavity, $V_{total} = \left(V_M + V_\sigma\right)$, which is the sum of the electrostatic potential generated by the charge distribution and the solvent reaction potential, V_M, and the electrostatic potential generated by the polarisation of the dielectric continuum, V_σ.

Two types of PCMs are popular in ab-initio computations, dielectric PCM (D-PCM), where the continuum is treated as a polarisable dielectric continuum with a specific value of the dielectric constant ε, and the conductor-like PCM (C-PCM), where the continuum is treated as a conductor-like continuum with a dielectric constant equal to infinity, $\varepsilon = \infty$, which corresponds to the conductor, such as the Conductor-like Screening Model (COSMO).

2.4.2.2 COnductor-like Screening MOdel

COSMO, the abbreviation of Conductor-like Screening Model (Klamt and Schuurmann 1993) is the conductor-like continuum solvation models that has been used in the present study to compute solvation free energies. Like other continuum solvation models, the solvent is modelled as a dielectric continuum with a permittivity, ε . The solute molecule forms a cavity within the dielectric continuum. The details of the cavity construction differ in different COSMO implementations. Unlike other continuum solvation models, COSMO derives the polarization charges of the continuum, which are induced by the polarity of the solute, from a scaled-conductor approximation.

In COSMO, the dielectric constant of the continuum equals infinity, instead of a specific value by assuming the continuum is a conductor. In this case, the electrostatic potential will cancel out at the cavity surface. Hence the apparent surface charge can be determined by the local value of the electrostatic potential instead of the normal component of its gradient in equation (2-71).

$$\sigma^*(\bar{s}) = \frac{\varepsilon - 1}{4\pi\varepsilon}\left[V_M(\bar{s}) + V_\sigma(\bar{s})\right]_{in} \tag{2-72}$$

Finally, the ideal unscreened charge density $\sigma^*(\bar{s})$ corresponding to $\varepsilon = \infty$ is scaled by a proper function of ε.

$$\sigma(\bar{s}) = f(\varepsilon)\sigma(\bar{s}) \tag{2-73}$$

where the scaling function is empirically determined by comparing COSMO (unscaled) and correct electrostatic solvent-solute energies.

$$f(\varepsilon) = \frac{\varepsilon - 1}{\varepsilon + k} \tag{2-74}$$

The k value is suggested as 0.5 based on theoretical arguments in the original formulation (Klamt and Schuurmann 1993). However, some re-implementations proposed $k = 0$ and showed that the choice of k has a minimal effect for water but may be important for other solvents (Lozzi, Cossi et al. 2006). Therefore the energy of the interaction between the solvent and the solute molecule can be calculated from the solvent charge $\sigma(\bar{s})$ and the known charge distribution of the molecule. The solute-solvent interaction energy E_{int} is defined by:

$$E_{\text{int}} = \sum_i V_i q_i = \sum_i V_i \sigma(\bar{s}_i) a_i \tag{2-75}$$

where V_i is the solute electrostatic potential and q_i is the surface charge associated with the small region i of the cavity surface with area a_i. The solute energy *in vacuo,* is $E^0 = E\left[\rho^0\right] + V_{NN}$, where ρ^0 is the electonic density for the molecule *in vacuo*, the electrostatic component of the Gibbs free energy of the solute-solvent system, G, at fixed position of the solute nuclei, referred both to non-

interacting electrons, nuclei, and to the unpolarized dielectric, is given by: (Cammi and Tomasi 1995)

$$G = E[\rho] + V_{NN} + \frac{1}{2} E_{\text{int}} \tag{2-76}$$

where $E[\rho]$ is the electronic energy *in vacuo,* ρ is the density perturbed by the solvent and V_{NN} is the nuclear repulsion energy of the solute. This expression applies to all the variational methods for which an "electronic density can be defined. (Cossi, Rega et al. 2003)

The COSMO method can be used in all methods in theoretical chemistry, where the charge distribution of a molecule can be determined, such as Hartree-Fock and Density Functional Theory calculations. Unlike methods based on the multipole expansion charge distribution of a molecule, that are limited to small quasi-spherical or ellipsoidal molecules, the COSMO method has the advantage that it can be applied to large and irregular molecules. The performance of COSMO is also better for solvents with a higher permittivity, such as water ($\varepsilon \approx 80$), due to the theoretical assumption of treating solvent as a conductor ($\varepsilon = \infty$) in the model. Another advantage of COSMO methods compared to other dielectric methods is that COSMO eliminates the outlying charge error, which is caused by small parts of the electron density of the solute lying outside the cavity.

2.5 Practical Methodologies

In this section, we will introduce the specific computational chemistry codes and packages that have been used in this study, followed by descriptions of a selection of analysis methods that have been employed.

2.5.1 Computational Tools

The main code we have used in this project for ab-initio molecular dynamics simulations is the CP code from the Quantum-ESPRESSO package (Car-Parrinello and Born-Oppenheimer, DFT, PW). SIESTA (Born-Oppenheimer, DFT, Numerical Basis Sets) was also employed for annealing structures from ab-initio molecular dynamics simulations in our phosphate oligomers study. For static electronic structure calculations, we have used DMol^3 (DFT, Numerical Basis Sets).

2.5.1.1 Quantum ESPRESSO

Quantum ESPRESSO (QE) (Giannozzi, Baroni et al. 2009) is a simulation suite for electronic calculations and materials modelling, based on density functional theory (DFT), which employs plane waves and pseudopotentials to describe the electronic orbitals. QE is an open source package and freely available to researchers around the world under the terms of the GNU General Public License. It comes with a core package of standard functions with plug-ins for advance functions. In this project, we have employed QE for its CP code – Car-Parrinello Molecular Dynamics function within its ab-initio molecular dynamics package.

Quantum ESPRESSO implements a variety of methods and algorithms aimed at a chemically realistic modelling of materials from the nanoscale upwards. The package is constructed around the use of periodic boundary conditions, which allows for a straightforward treatment of infinite systems. The atomic cores can be described by separable norm-conserving pseudopotentials (Hamann, Schl et al. 1979), ultrasoft pseudopotentials (Vanderbilt 1990) or by projector-augmented wave sets (Blöchl 1994). Different exchange-correlation functionals are available in the framework of the local-density (LDA) or generalized-gradient approximation (GGA) (Perdew, Chevary et al. 1992). Some hybrid functionals are also available (Becke 1993; Stephens, Devlin et al. 1994; Perdew, Ernzerhof et al. 1996). A range of computations/simulations can be performed with QE, such as calculation of Kohn-Sham (KS) orbitals and energies for isolated or extended/periodic systems, and of their ground-state energies; complete structural optimizations of the microscopic (atomic coordinates and macroscopic (unit cell) degrees of freedom and ab-initio molecular dynamics (AIMD) by either the Car-Parrinello or the Born-Oppenheimer approach in a variety of thermodynamical ensembles.

2.5.1.2 CP Code (CPMD)

The Car-Parrinello Molecular Dynamics code of Quantum ESPRESSO is a parallelized ab-initio molecular dynamics code based on Density Functional Theory with plane-waves and pseudopotentials implementation, originally developed by Jurg Hutter at IBM Zurich Research Laboratory. Many people from different backgrounds have contributed to the development of the code and the pseudopotential over the years. Copyright of the CPMD code is owned by IBM

Corp. and by the Max Planck Institute, Stuttgart. It is free for non-profit organizations, such as researchers from universities.

The CP code is the specialized module performing Car-Parrinello ab initio MD in QE. Both norm-conserving pseudopotentials (Hamann, Schl et al. 1979) and ultrasoft pseudopotentials (Vanderbilt 1990) can be used. For the latter case, the implementation is particularly efficient for large-scale calculations. CP implements with the well-established LDA and GGA exchange-correlation functionals in the Quantum ESPRESSO except the hybrid ones. In the Car-Parrinello algorithm, microcanonical (NVE) MD is performed using the Verlet algorithm. Constant-pressure (NPT) MD is performed using the Parrinello-Rahman Lagrangian (Bernasconi, Chiarotti et al.) and additional degrees of freedom for the cell. Nose-Hoover thermostats (Tobias, Martyna et al. 1993) and Nose-Hoover chains (Martyna, Klein et al. 1992) allow simulations to be performed in different canonical ensembles. CP can also be used to directly minimize the electronic energy functional to self-consistency while keeping the nuclei fixed or to perform structural minimizations of nuclear positions by the global minimization approaches (Payne, Teter et al. 1992; Marx and Hutter 2000).

2.5.1.3 SIESTA

SIESTA stands for Spanish Initiative for Electronic Simulations with Thousands of Atoms, which refers to both the method and the implementation of the simulation code (Ordejon, Artacho et al. 1996). SIESTA provides a way to perform electronic structure calculations and ab-initio molecular dynamics calculations in relatively smaller computational expense, and it is therefore

especially suitable for large systems (>100 atoms). Instead of plane-waves like CPMD, SIESTA employs flexible numerical linear combinations of atomic orbitals (LCAO) as basis sets for its calculations. Its main advantage is an essentially perfect order-*N* scaling algorithm (Soler, Artacho et al. 2002), which means that the CPU time used by the calculations scale linearly with the number of atoms in the simulation cell. SIESTA can therefore perform both extremely fast simulations using minimal basis sets and very accurate calculations with complete zeta and polarized bases. For academic users, SIESTA is freely available on a valid academic license.

2.5.1.4 Dmol^3

Dmol^3 is a density functional theory (DFT) quantum mechanical code that can simulate processes in different phases, such as gas, solvent, solid or a surface environment. It is one of the fastest methods available for molecular calculations, especially for large molecules. Dmol^3 is also capable of modelling the solid state in periodic systems by its high-performance internal coordinate optimizer. Dmol^3 uses numerical functions on an atom-centered grid as its atomic basis set (Delley 1990). The atomic basis functions are obtained from solving the DFT equations for the individual atoms. The atomic basis sets are confined within a cut off limit which can be tailored to fit different levels of Dmol^3 calculations, which is an important feature of the numerical basis set as it can speed up the calculation, especially the solid state systems. The high quality of the basis sets minimizes the superposition effect and even weak bonds, e.g. hydrogen bonds, can be described accurately, which allows the calculation of the dissociation of molecules.

In Dmol^3, apart from the minimal basis set (MIN), all other basis sets consist of a second set of basis functions, which allows the basis set size to be bigger. This is called the double-numerical (DN) basis set and its notation is similar to the Gaussian double-zeta (DZ) sets, but the N is used to emphasise the numerical nature of the orbital. Basis set qualities have been analyzed in detail by Delley (Delley 1990). Dmol^3 is a commercial code within the Accelrys Materials Studio software. However, separate standalone licenses for clusters/machines are needed for parallel implementations.

2.5.2 Analytical Tools

Various analysis methods have been employed in this study, two of which that we have used extensively during our investigation of the phosphate species, are the Radial Distribution Function and Solvation Free Energies Calculations.

2.5.2.1 Radial Distribution Function (RDF)

The Radial Distribution Function (RDF), $g_{\alpha\beta}(r)$, can be used to describe the probability of finding particle β within a radiance distance r from particle α. It is a useful tool to describe the structure of a system, especially in liquids and amorphous materials. The RDF of a solid is represented by an infinite number of sharp peaks which correspond to the lattice structure.

In a system that consists of particles α and β, the radial distribution function of the two, $g_{\alpha\beta}(r)$, can be measured by counting the appearances of two atoms at separation r $\begin{pmatrix} r=0 \\ r=\infty \end{pmatrix}$.

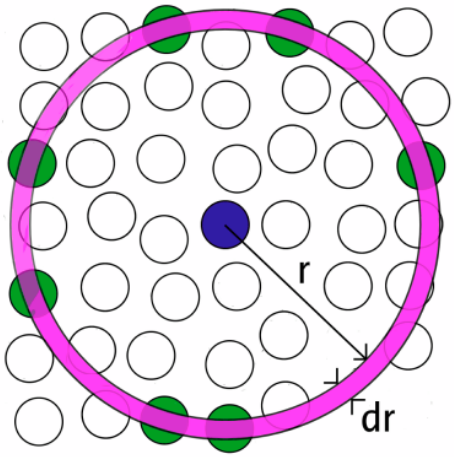

Figure 2-1 Schematic representation of the imaginary system.

If we consider a homogenous distribution of atoms in space, the $g(r)$ represents the probability of finding an atom in a shell with thickness ∂r at the distance r of another atome that is chosen to be the reference point. The volume of the shell is given by:

$$V = \frac{4}{3}\pi(r+\delta r)^3 - \frac{4}{3}\pi r^3 \approx 4\pi r^2 \delta r \tag{2-77}$$

If the density of the atoms in the system is ρ, the total number of the atoms in the volume of the shell is $4\pi\rho r^2\delta r$ and the number of the atoms per volume varies as r^2.

For more complex systems that involve more than one species, partial radial distribution function $g_{\alpha\beta}(r)$ can be used to find out the density probability of an atom of the α species to have a neighbour of the β species at a given distance r.

$$g_{\alpha\beta}(r) = \frac{\delta n_{\alpha\beta}(r)}{4\pi r^2 \delta r \rho_\alpha} \tag{2-78}$$

where $4\pi r^2 \delta r \rho_\alpha$ is the total number of the α atoms in the volume and $\delta n_{\alpha\beta}(r)$ is the number of the neighbour β atoms from the α atoms at distance r.

2.5.2.2 Solvation Free Energy Scheme

To compute the solvation free energies ΔG^*_{solv} of the phosphate species we have used the *monomer* and *cluster* thermodynamic cycles (Bryantsev, Diallo et al. 2008).

2.5.2.2.1 Monomer cycle

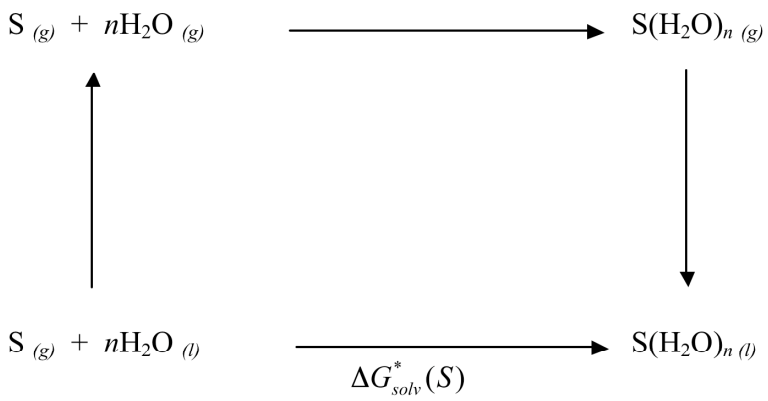

Figure 2-2 Monomer thermodynamic cycle scheme.

In the *monomer* cycle (Pliego and Riveros 2001), which is presented in Figure 2-2, ΔG^*_{solv} of a solute S is computed applying the following expression:

$$\Delta G^*_{solv}(S) = \Delta G^O_{clust}\left(S(H_2O)_n\right) + \Delta G^*_{solv}\left(S(H_2O)_n\right) + n\Delta G_{vap}(H_2O) \qquad (2\text{-}79)$$

In equation (2-79), $\Delta G^O_{clust}\left(S(H_2O)_n\right)$ is the gas-phase free energy of cluster formation at 1 atm, $\Delta G^*_{solv}\left(S(H_2O)_n\right)$ is the solvation free energy of the hydrated cluster corresponding to the 1 mol L^{-1} (gas) → 1 mol L^{-1} (solvent) process, and

$\Delta G_{vap}(H_2O)$ is the vaporization free energy of a single water molecule, which is calculated as (Pliego and Riveros 2001):

$$\Delta G_{vap}(H_2O) = -\Delta G^{*}{}_{solv}(H_2O) - RT\ln[\tilde{R}T] - RT\ln[H_2O] \quad (2\text{-}80)$$

where $\tilde{R} = 0.082053\ \mathrm{K}^{-1}$. Note that the term $RT\ln[\tilde{R}T]$ takes into account the free energy change associated with moving from a standard state that uses a Scheme sconcentration of 1 atm in gas phase and 1 mol L^{-1} in the aqueous phase.

2.5.2.2.2 Cluster cycle

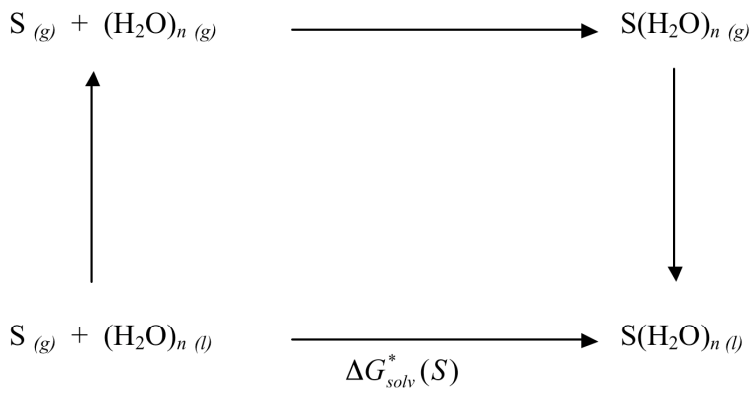

Figure 2-3 Cluster thermodynamic cycle scheme.

In the *cluster* cycle (Zhan and Dixon 2001) (Scheme 2), the solvation free energy is computed using the following expression:

$$\Delta G^{*}_{solv}(S) = \Delta G^{O}_{clust}\left(S(H_2O)_n\right) + \Delta G^{*}_{solv}\left(S(H_2O)_n\right) - \Delta G^{*}_{solv}\left((H_2O)_n\right) - \Delta G^{o\rightarrow *} - RT\ln\left([H_2O]/n\right) \quad (2\text{-}81)$$

In equation (2-81), $\Delta G^{O}_{clust}\left(S(H_2O)_n\right)$ is the gas-phase free energy of cluster formation from the $(H_2O)_n$ water clusters; $\Delta G^{*}{}_{solv}(S(H_2O)_n)$ is the solvation free

energy of the hydrated solute; $\Delta G^{*}_{solv}\left(\left(H_2O\right)_n\right)$ is the solvation free energy of the water cluster $\left(H_2O\right)_n$, which is computed using the following expression (Bryantsev, Diallo et al. 2008):

$$\Delta G^{*}_{solv}\left(\left(H_2O\right)_n\right) = -\Delta G^{O}_{g,bind} + \left(n-1\right)\Delta G^{O\rightarrow *} + n\Delta G^{*}_{solv}\left(H_2O\right) + RT\ln\left(n\left[H_2O\right]^{n-1}\right) \quad (2\text{-}82)$$

In equation (2-82), $\Delta G^{O\rightarrow *}$ = 1.89 kcal/mol (T = 298.15 K) is the free energy change of 1 mol of an ideal gas from 1 atm to 1 M, and taking $\left[H_2O\right]$ = 55.5 M and T = 298.15 K, then $RT\ln\left(\left[H_2O\right]/n\right) = \left(2.378 + 0.592\left(n\right)\right)$ kcal/mol. The structures of the $\left(H_2O\right)_n$ water clusters were generated from *ab-initio* MD simulations.

Chapter 3 Structures of Phosphate Bioglasses

In this chapter, first principles molecular dynamics simulations of ternary phosphate-based glasses P_2O_5−CaO−Na_2O (PBGs) have been carried out in order to provide an accurate description of the local structure and properties of these important materials for biomedical applications. The structures of PBGs with compositions $(P_2O_5)_{0.45}(CaO)_x(Na_2O)_{0.55-x}$ (x = 0.30, 0.35 and 0.40) were generated using a full *ab initio* molecular dynamics melt-and-quench procedure.

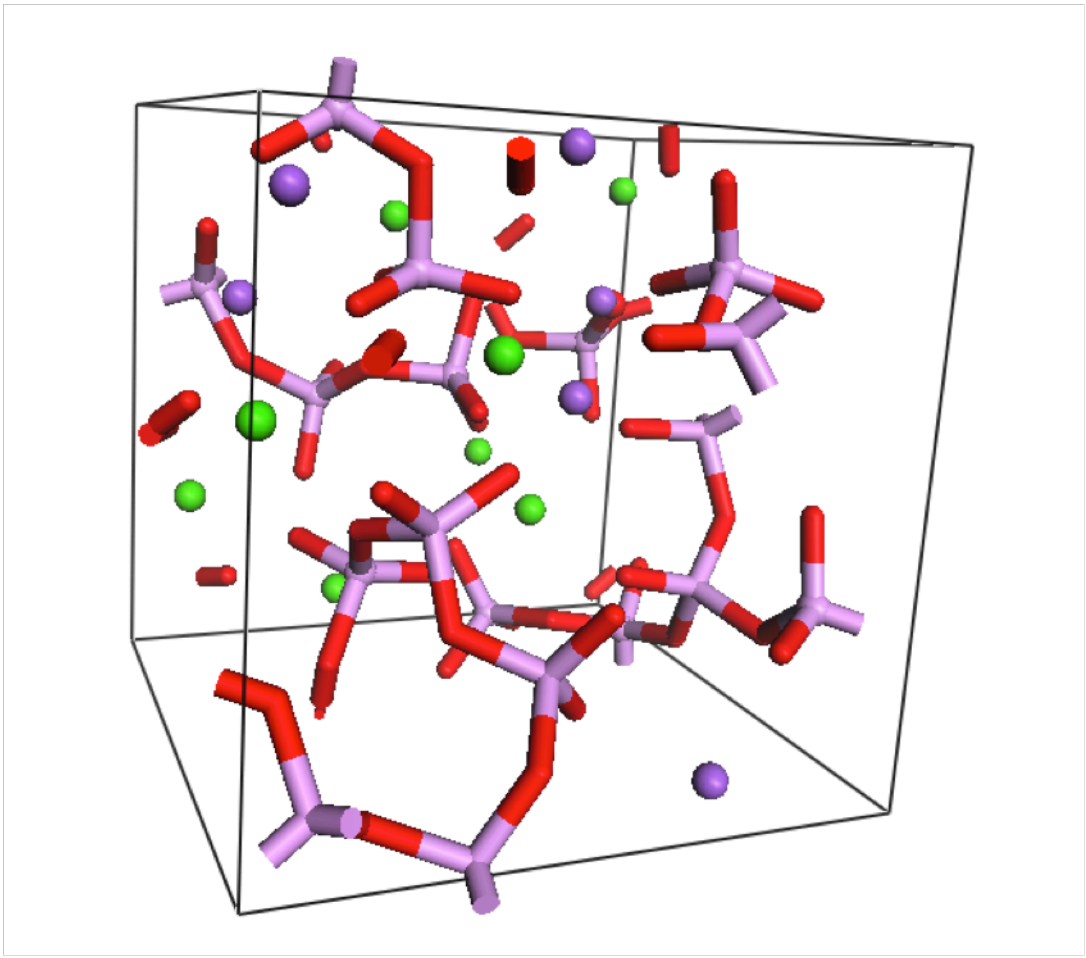

Figure 3-1 Snapshot from the CP-MD trajectory of the P45C40N15 glass showing the occurrence of chain-like phosphate networks. Ca, Na, O and P are pictured as green, purple, red and pink spheres, respectively.

3.1 Chapter Introduction

Biomedical materials for use in the body used to be dominated by implants formed of metals, which are designed to have physical properties close to the replaced hard tissue and a minimal toxic response in the host, i.e. bio-inert materials without significant interactions with the surrounding tissue.(Hench 1980) However, the current trend in biomaterials is the development and use of implants that play an active role in tissue regeneration, rather than passive materials, and which degrade after the tissue has healed. This class of implants has been described as the "Third Generation" of bioactive materials.(Hench and Polak 2002) One commercially available bioactive glass is Bioglass®, composed of 45.0 wt% SiO_2, 24.5 wt% CaO, 24.5 wt% Na_2O and 6.0 wt% P_2O_5(Saravanapavan, Jones et al. 2003; Day and Boccaccini 2005), which has been remarkably successful in many clinical applications, especially in dental and orthopaedic fields. However, questions relating to the long term effect of silica(Salih, Franks et al. 2000), and the slow degradation of these glasses, taking one to two years to disappear from the body,(Tadjoedin, de Lange et al. 2000) have prompted a search for more benign materials.

Among the "third-generation" biomedical materials, phosphate-based bioactive glasses (PBGs) have become topical materials for scientists and engineers working in the field of biomaterials and tissue engineering. (Knowles 2003; Abou Neel, Pickup et al. 2009) These glasses, containing phosphorus pentoxide (P_2O_5) as a network former and sodium oxide (Na_2O) and calcium oxide (CaO) as network modifiers, have many unique properties: (i) their composition is chemically related to the surrounding tissue; (ii) they dissolve completely in aqueous media; (iii) their

dissolution rate can be controlled by changing the composition of the phosphate-sodium-calcium glass (Ahmed, Lewis et al. 2004). Experimental evidence shows, for example, an inverse relation between CaO content and dissolution rate,(Franks, Abrahams et al. 2000) which suggests that the interaction of the Ca^{2+} ions with the glass network controls the glass degradation. The solubility can thus be tailored to suit the end application. As the solubility of a glass is linked to its structure, insights into the effect of calcium and sodium ions on the P_2O_5 network is of fundamental interest to the design of phosphate glass compositions for applications in tissue engineering.

Information on the structural features of PBGs with different composition has been obtained using various experimental techniques, such as X-ray and neutron diffraction methods,(Hoppe, Walter et al. 2000; Hoppe 2005) magic angle spinning nuclear magnetic resonance (MAS-NMR) (Franks, Abrahams et al. 2001) and ^{31}P NMR.(Ahmed, Lewis et al. 2004) A common problem in the investigation of these materials, generally related to their amorphous nature, is the lack of detailed information on the microscopic structure of the glasses and how this structure is affected by the network modifying ions Ca^{2+} and Na^{+}. In this respect, molecular dynamics simulations allow an atomistic resolution of the structure and dynamics of the simulated system, which can thus be extremely useful in complementing and supporting experiment towards a fundamental understanding of the properties of bioactive phosphate glasses. Classical molecular dynamics simulations (MD) have already been applied to model bioactive phospho-silicate glasses,(Tilocca 2009) but modelling the ternary glasses $(P_2O_5)_{0.45}(CaO)_x(Na_2O)_{0.55-x}$ with different compositions, represents a challenge for classical MD, due to the difficulty of

incorporating many-body interactions and complex bonding effects in a reliable force field. Consequently, computational studies of phosphate glasses have been mostly limited to the vitreous P_2O_5 (Suzuki, Takase et al. 2001) and to simple binary systems (Speghini, Sourial et al. 1999; Alam, McLaughlin et al. 2000), and only recently a MD study of a ternary phosphate glass was reported.(Martin, Mountjoy et al. 2009)

An alternative computational approach is the *ab initio* molecular dynamics technique, efficiently implemented in the Car-Parrinello method.(Car and Parrinello 1985) The *ab initio*, parameter-free approach, explicitly taking into account the electronic structure of the system, enables the accurate modelling of many-body and polarization effects, but at the expense of much larger computational requirements compared to classical MD simulations. CP-MD simulations have been used previously to model the structural, electronic and dynamical properties of bioactive silicate(Tilocca and de Leeuw 2006) and phospho-silicate glasses, (Alam, Liang et al. 2000; Martin, Mountjoy et al. 2009) and we now present CP-MD simulations of ternary phosphate-based glasses with composition $(P_2O_5)_{0.45}(CaO)_x(Na_2O)_{0.55-x}$, where x = 0.30, 0.35 and 0.40. PBGs with these compositions have been studied extensively by Knowles and co-workers,(Ahmed, Lewis et al. 2004; Ahmed, Lewis et al. 2004; Ahmed, Lewis et al. 2005) using *in vitro* solubility measurements, X-ray powder diffraction, NMR and ion chromatography techniques. Our study thus should complement their findings with atomic-level insights into the structural properties of these PBGs.

3.2 Methodology

3.2.1 Computational details

CP-MD simulations were carried out using the Car-Parrinello code included in the Quantum-ESPRESSO package, version 4.0.1. (Giannozzi, Baroni et al. 2009) The electronic structure was described by the Perdew-Burke-Ernzerhof (PBE) gradient-corrected functional (Perdew, Burke et al. 1996). Vanderbilt ultrasoft pseudopotentials (Vanderbilt 1990; Laasonen, Car et al. 1991) represented core-valence electron interactions for all atomic species; semicore shells were explicitly included for Na and Ca. The ultra-soft pseudo-potentials (USPP) for O, H and P were generated using the USPP 7.3 pseudopotential program with a scalar-relativistic calculation (Langer 2000), whereas the USPP for Ca and Na were taken from the standard Quantum-ESPRESSO distribution (Hench 1998). The accuracy and transferability of the Na, Ca and O pseudopotentials were tested by comparing the optimized structures of several glass structures containing these atoms with the corresponding experimental values (Tilocca and de Leeuw 2006), whereas for phosphorus the optimized structure and the hydration energies of phosphate species calculated with the USPP-PW approach were compared with the results obtained from an all-electron calculation using the $DMol^3$ code (Delley 1990), the PBE functional and the double-numeric-polarised basis sets on all atoms method (Tang, Di Tommaso et al. 2009). The electronic wavefunctions were expanded in a plane wave (PW) basis set with a kinetic energy cutoff of 40 Ry, and *k*-sampling was restricted to the Γ point of the Brillouin zone. The time step for simulations was set to 0.121 fs and the electronic mass was set to 700 a.u. This computational setup has been used to model bioactive silicate glasses with good accuracy (Tilocca and de

Leeuw 2006). Moreover, previous *ab initio* simulations (Sarnthein, Pasquarello et al. 1997; Benoit, Ispas et al. 2001; Donadio, Bernasconi et al. 2004) have proved the accuracy of the method employed in this work in determining structural, dynamical, and electronic properties of glasses.

3.2.2 Simulation protocol

The phosphate glasses considered in the present study have the chemical formula $(P_2O_5)_{0.45}(CaO)_x(Na_2O)_{0.55-x}$, with x = 0.30, 0.35 and 0.40 (P45C30N25, P45C35N30 and P45C40N35, where P_2O_5=P, CaO=C and Na_2O=N). The size and composition of these simulated glasses are reported in Table 3-1. Previous studies have shown that the local structure and dynamics of silicate glasses could be accurately reproduced using a cubic periodic cell of ~ 10 Å (Ispas, Benoit et al. 2001; Van Ginhoven, Jonsson et al. 2005), and the compositions that we have investigated in this work are therefore built for a similar cell, according to the experimental densities at room temperature, as reported in Table 3-1. Since it is commonly difficult for MD simulations to reproduce both experimental density and pressure of glasses, (Benoit, Ispas et al. 2001; Ispas, Benoit et al. 2001; Benoit 2002; Donadio, Bernasconi et al. 2004; Lammert and Heuer 2005; Van Ginhoven, Jonsson et al. 2005; Du and Corrales 2006; Giacomazzi, Massobrio et al. 2007) in this study we have decided to reproduce the experimental density. The accumulated average pressure of our models is around 2 GPa, but, according to previous MD studies of silica and phosphosilicate glasses, (Liang, Miranda et al. 2007; Tilocca 2007) the structural and dynamical properties of glasses at this level of pressure do not significantly change with respect to 1 atm.

Table 3-1 Details of the simulated glasses.

$(P_2O_5)_{0.45}CaO_xNa_2O_{0.55-x}$	Composition	Density (g/cm^{-3}) *	Cell size (Å)	No. of atoms
x = 0.30	$P_{18}O_{56}Na_{10}Ca_6$	2.56	10.767	90
x = 0.35	$P_{18}O_{56}Na_8Ca_7$	2.57	10.742	89
x = 0.40	$P_{18}O_{56}Na_6Ca_8$	2.59	10.704	88

* Experimental density from Carta et al. is used (Carta, Pickup et al. 2007).

The structures of the phosphate glasses P45C30N25, P45C35N30 and P45C40N35 were generated using a full *ab initio* molecular dynamics melt-and-quench procedure. For each glass, the initial configuration was created by randomly placing the atoms in the simulation box, taking care to avoid significant overlaps by means of appropriate distance cut-offs. This configuration was allowed to relax in the NVE ensemble (constant number of particles, volume and energy), and after an initial quench of all ion velocities, the system spontaneously (i.e. without external thermostatting) heated up to around 1500 K. At this point, we started a series of 10 subsequent NVT (constant number of particles, volume and temperature) runs of 10-15 ps each, whose target temperature was set to 3000 K, 2700 K, 2400 K, ..., 600 K, using a Nosé-Hoover chain thermostat (Martyna, Klein et al. 1992) and with the coefficients of the electronic wavefunction re-optimised at each new temperature. This cooling phase corresponds to a nominal cooling rate of 20 K/ps, which is higher than typical cooling rates accessible in classical MD simulations of glasses (Ispas, Benoit et al. 2001; Van Ginhoven, Jonsson et al. 2005), but comparable or

lower than those used in the generation of silicate (Van Ginhoven, Jonsson et al. 2005) or phosphosilicate (Tilocca 2007) glasses using a full *ab initio* melt and quench glass approach. Finally, at 300 K the production phase was carried out for a 20 ps duration.

3.3 Q^n distribution and network connectivity

The PO_4 tetrahedron represents the basic building block of the structure of phosphate-based glasses. The phosphate tetrahedra are classified in terms of the number of bridging oxygens (BOs) they share with other phosphate tetrahedra in the glass. (Walter, Vogel et al. 2001) The various types of phosphate tetrahedra that result from this classification are labelled using the Q^n terminology, where *n* represents the number of BOs per PO_4 tetrahedron and ranges from 0 to 3 (see Scheme 3-1). For example, Q^3 phosphate species share three covalently bonded BOs with neighbouring PO_4 tetrahedra. The structure of vitreous P_2O_5 consists of only Q^3 species that form a three-dimensional network, but the inclusion of modifying metal oxides, like Ca and Na, leads to the breaking of P−BO−P bonds, and their replacement by P−NBO···M (where NBO stands for non-bridging oxygen and M is calcium or sodium).

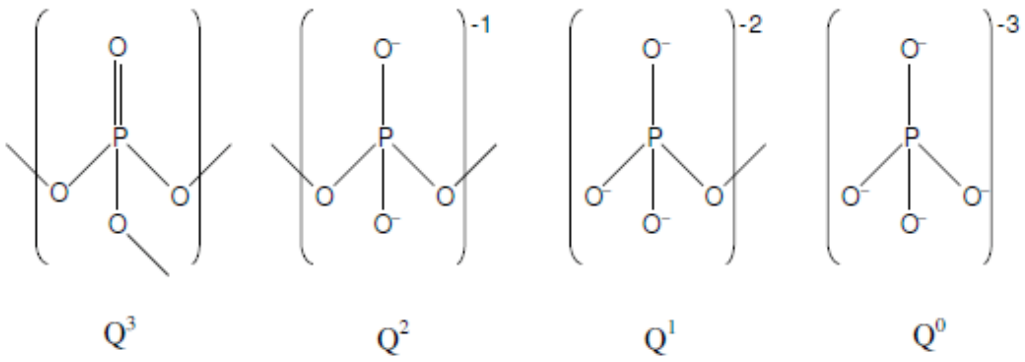

Scheme 3-1

The coordination statistics of the tetrahedral network obtained from the CP-MD calculations, summarised in Table 3-2, denote a shift of the Q^n distribution from 100% Q^3 in vitreous P_2O_5 to lower values of n for the simulated $(P_2O_5)_{0.45}(CaO)_x(Na_2O)_{0.55-x}$ (x = 0.30, 0.35 and 0.40) glasses. The coordination statistics reported in Table 3-2 also denote an ideal tetrahedral (P_4c) environment for phosphorus, with no under- (P_3c) or over-coordinated (P_5c) phosphorus atoms.

Table 3-2 Coordination statistics of the phosphate network from the CP-MD simulations: Q^n distribution, network connectivity (NC), phosphorus (P) coordination and average P-O coordination numbers (CN_{av}).

	Q^n Distribution						**CN_{av}**				
	Q^0	Q^1	Q^2	Q^3	Q^4	NC	P_3c	P_4c	P-O	P-BO	P-NBO
P45C30N25	5.6	22.2	61.1	11.1	0.0	1.8	0	100	4	1.8	2.2
P45C35N20	0.0	22.2	77.8	0.0	0.0	1.8	0	100	4	1.8	2.2
P45C40N15	0.0	27.8	66.7	5.6	0.0	1.8	0	100	4	1.8	2.2

For the three glasses, the calculated Q^n distributions show the prevalence of metaphosphate Q^2, forming chain-like phosphate fragments, and pyrophosphate Q^1 species, in agreement with the experimental ^{31}P NMR analysis of PBGs with similar composition.(Ahmed, Lewis et al. 2004) The percentage of Q^3 species is considerably smaller than Q^1 and Q^2: Q^3 units are approximately 11.1 % of the total PO_4^{3-} tetrahedra in the P45C30N25 glass, and this value reduces to zero in P45C35N20 and to only 5.6 % in P45C40N15. It is interesting to note that the glass with the intermediate composition, P45C35N20, is characterised by the highest concentration of Q^2 species, which appears to occur in particular at the expense of the Q^3 species. Also it is worth to note that all of our models have the composition $(P_2O_5)_{0.45}(MO)_{0.55}$ (M = Ca and Na), which has O:P ratio of 3.11:1.0. According to Hoppe et al., any phosphate glass of this composition will have an average of 78%

Q^2 and 22% Q^1, and coordination numbers of CN(P-BO)=1.78 and CN(P-NBO)=2.22 (Hoppe, Walter et al. 2000). Our results in Table 3-2 are in good agreement with the experimental findings.

Classical MD simulations of the binary $NaPO_3$ glass found a distribution of Q^3 units of 25.4 %, which is considerably larger than those in the ternary $(P_2O_5)_{0.45}(CaO)_x(Na_2O)_{0.55-x}$ glasses (see Table 3-2). This suggests that the calcium ion has a stronger tendency to break P−BO−P bonds and form P−NBO···M species than sodium, and they modify the three-dimensional Q^3 network into a chain-like phosphate network, as illustrated by the snapshot of the CP-MD simulation of the P45C40N15 glass in Figure 3-1.

The population of isolated Q^0 species, also referred to as orthophosphate units, decreases from 5.6 % in P45C30N25 to zero orthophosphate species in the PBGs with 35 or 40 % of CaO (see Table 3-2). It is known from experiment that glasses with higher calcium content show a slower solubility than glasses with higher sodium content (Franks, Abrahams et al. 2000). However, the results from our simulations show that the concentration of isolated PO_4 units in the glass decreases with calcium content, suggesting that the solubility is dependent on the presence of orthophosphate species.

3.4 Structure of the tetrahedral network

The radial distribution functions (RDFs) and angular distribution functions for P and O, reported in Figure 3-2 and Figure 3-3, indicate that the main glass structure is maintained in all three compositions.

The P-O RDFs are all characterised by two quite well-defined peaks, one at 1.52 Å and the other at 1.64 Å, the separation of which increases with the content of calcium in the glass [see Figure 3-2(a)]. The O-O first-neighbour distance, around 2.6 Å, is essentially unaffected by the change of the Na/Ca ratio [see Figure 3-2(b)]. As expected for a network former, a narrow angle distribution from 90° to 130° for O-P-O is observed [see Figure 3-3(a)]. The average value of 109° is in excellent agreement with the theoretical tetrahedral angle of 109.5°. The distribution of the P-O and O-O distances as well as the O-P-O angular distribution functions thus denote structural order within each tetrahedron, which is essentially constant with the change of glass composition.

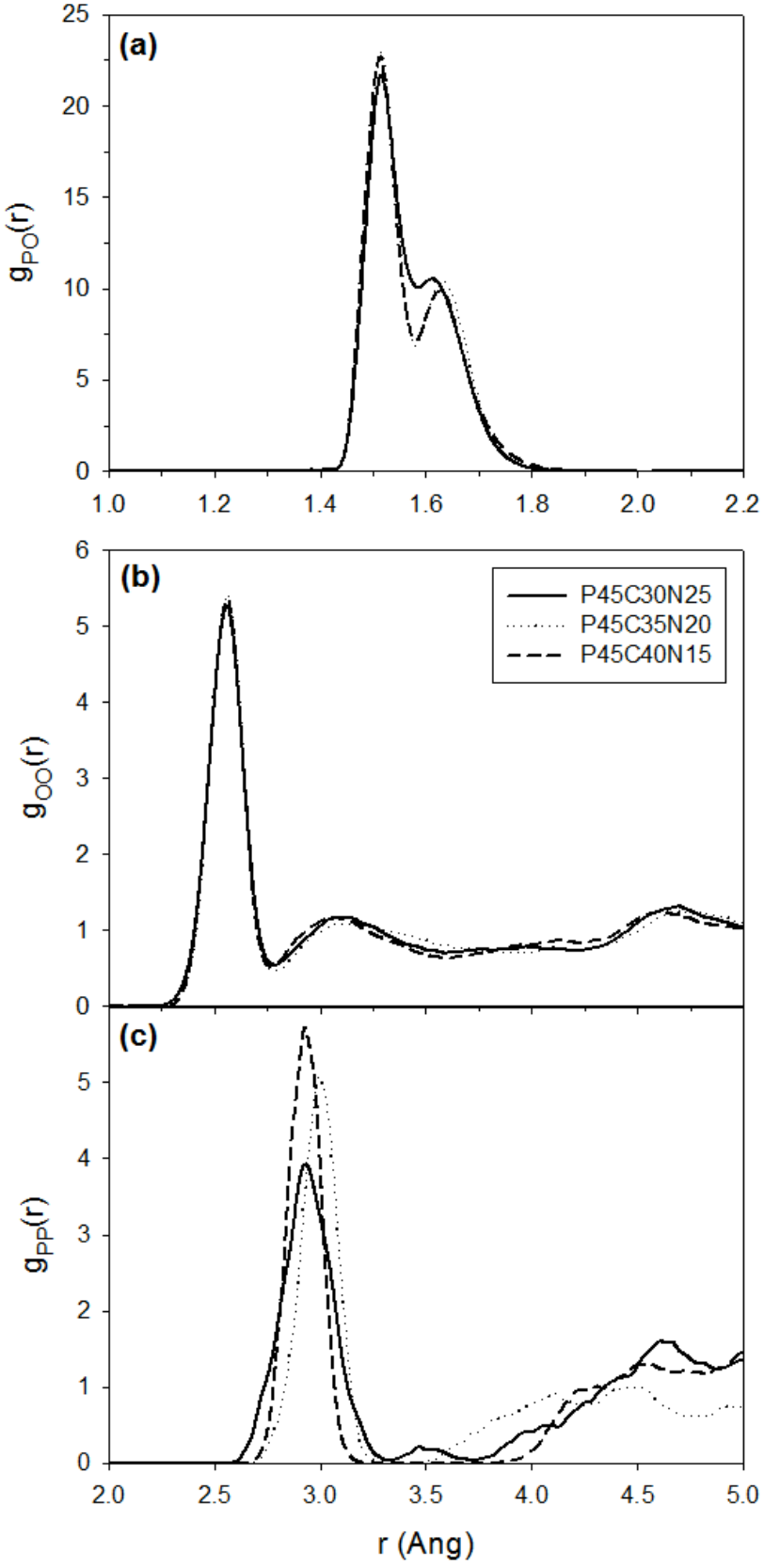

Figure 3-2 Radial distribution functions of the P-O (a), O-O (b) and P-P (c) atomic pairs obtained from the CP-MD simulations of the $(P_2O_5)_{0.45}CaO_xNa_2O_{0.55-x}$ (x = 30, 35 and 40) glasses.

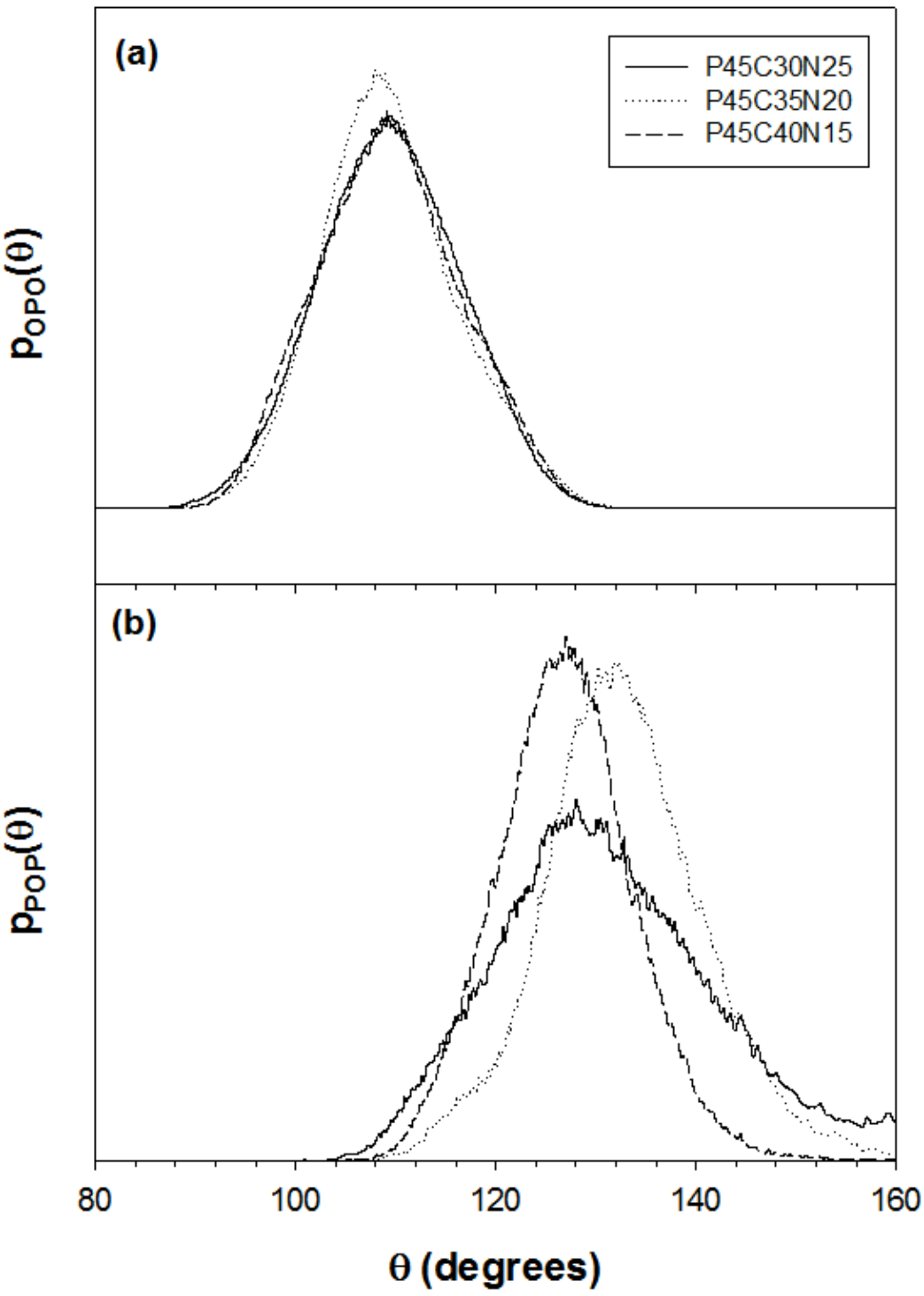

Figure 3-3 Radial distribution functions of the O-P-O (a) and P-O-P (b) angles obtained from the CP-MD simulations of the $(P_2O_5)_{0.45}CaO_xNa_2O_{0.55-x}$ (x = 0.30, 0.35 and 0.40), glasses.

However, the P-P distances [Figure 3-2(c)] and P-O-P angles [Figure 3-3(b)], which reflect the interconnectivity between the phosphate tetrahedra, are affected considerably more by the glass composition. In fact, the full-width-half-maximum (FWHM) of the P-P distances decreases as the concentration of calcium in the glass increase: FWHM is equal to 0.3 Å in P45C30N35, which reduces to 0.12 Å in the glass with 40% CaO content [see Figure 3-2(a)]. Similarly, the FWHM of the P-O-P angles decrease from the value of 24° in the P45C30N25 glass, to 16° in the P45C40N15. The effect of calcium ions on the structure of the glass is therefore to increase the rigidity of the phosphate P-O-P interconnectivity, which could be interpreted by the more rigid coordination shell of calcium(Ikeda, Boero et al. 2007) compared to that of sodium.(White, Schwegler et al. 2000; Ikeda, Boero et al. 2007) This increased rigidity of the phosphate network with the addition of calcium content could be linked to the observed slower solubility of glasses with higher CaO content (Franks, Abrahams et al. 2000).

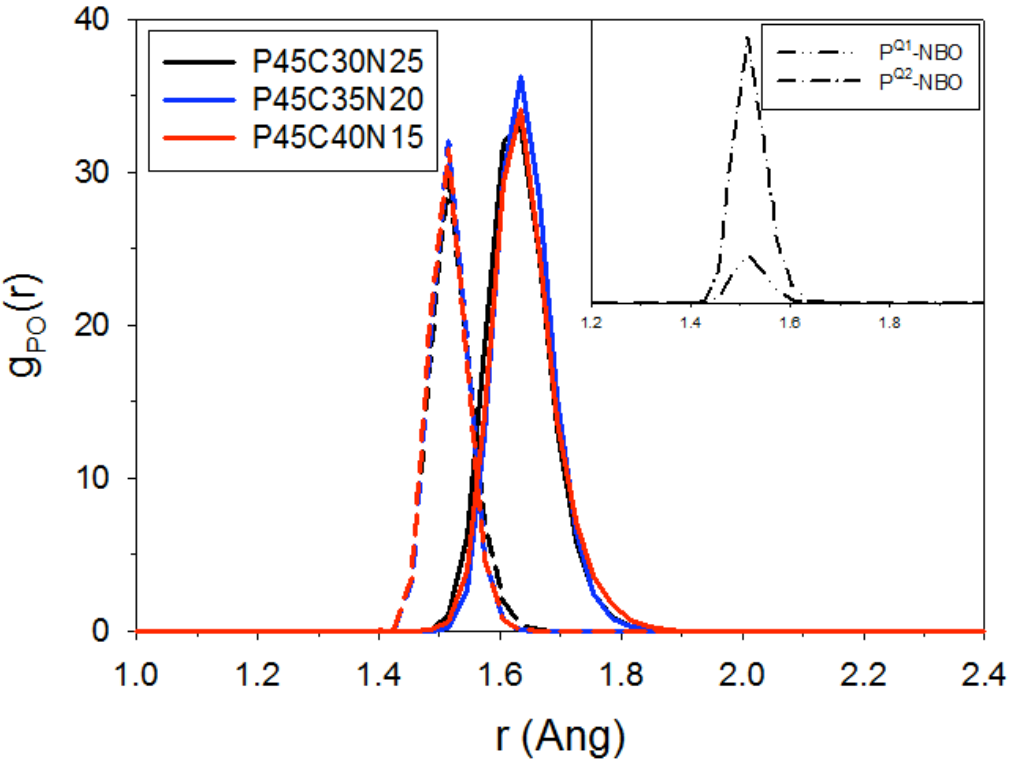

Figure 3-4 Decomposition of the P-O radial distribution functions into their BO (solid line) and NBO (dashed line) components. The inset reports the decomposition of the P-NBO radial distribution function into their P^{Q1}-NBO and P^{Q2}-NBO components of the glass with composition P45C30N25.

Figure 3-4 reports the decomposition of the P-O RDFs into the BO and NBO components. For all three glass compositions, the P-NBO distance is at 1.52 Å, whereas the P-BO RDFs are characterised by a peak at 1.64 Å which are in good agreement with the values of 1.49 Å and 1.63 Å reported by Hoppe et al. for a range of phosphate glasses.(Hoppe, Walter et al. 2000) Neutron diffraction studies of phosphate glasses (Suzuki and Ueno 1985; Hoppe, Walter et al. 2000) showed the occurrence of two well-separated peaks located at approximately 1.5 Å and 1.65 Å, which were attributed by the authors to the different bridging and non-bridging P-O bonds, respectively. Our results clearly support this experimental interpretation.

One of the pending questions on the structure of phosphate bio-glasses regards possible differences between the non-bridging oxygens on individual Q^1 and Q^2 units (Brow 2000). For the glass with composition P45C30N25, the inset in Figure 3-4 shows the decomposition of the P-NBO radial distribution functions into their P^{Q1} and P^{Q2} components, where P^{Q1} is a phosphorus of the Q1 units, and P^{Q2} is a phosphorus of the Q2 units. As both P^{Q1}-NBO and P^{Q2}-NBO peak are at 1.52 Å, our simulations suggest that there is no significant difference between the non-bridging oxygen on the Q^1 and Q^2 units. The other PBGs show a similar behaviour. Table 3-2 also reports the average P-BO and P-NBO coordination numbers, where the overall BO:NBO ratio shows a slightly higher NBO fraction in the PO_4 tetrahedra, which reflects the prevalence of meta-phosphate species.

3.5 Coordination environment of the network modifiers Na and Ca

The radial and angular distribution functions of the calcium and sodium ions with the oxygen, bridging (BO) and non-bridging (NBO) oxygen atoms are reported in Figure 3-5 and Figure 3-6, respectively, and the relevant data of the Na and Ca local environments in the three glasses $(P_2O_5)_{0.45}(CaO)_x(Na_2O)_{0.55-x}$, ($x$ = 0.30, 0.35 and 0.40) are summarised in Table 3-3.

The average Na−O and Ca-O distances range from 2.33 to 2.36 Å, depending on the composition, which are in good agreement with the experimental M-O distances for a series of metaphosphate glasses containing calcium and sodium. (Hoppe, Walter et al. 2000) The coordination shell of Na is composed of approximately six O atoms, whereas the calcium ion is coordinated by 6-7 oxygen atoms, with the average coordination numbers mildly affected by the Ca/Na ratios. The decomposition of the Na-O and Ca-O RDFs into the BO and NBO components in Figure 3-6 further shows very clearly that the sodium and calcium are mostly coordinated to the non-bridging oxygens (see Table 3-3) and that the M-BO and M-NBO distances have two quite distinct values. In fact, the Na-NBO and Ca-NBO RDFs are characterised by well defined peaks at 2.32 Å and 2.35 Å. On the other hand, the Na-NBO RDFs of the glasses P45C30N25 and P45C40N15 have a very broad peak at approximately 2.5 Å. The Ca-BO distance is between 2.6 Å and 2.8 Å, but for the glass with the lowest content of calcium, P45C30N25, the Ca-BO RDFs does not have any first coordination shell peak, indicating the absence of coordination between calcium and bridging oxygens at such composition.

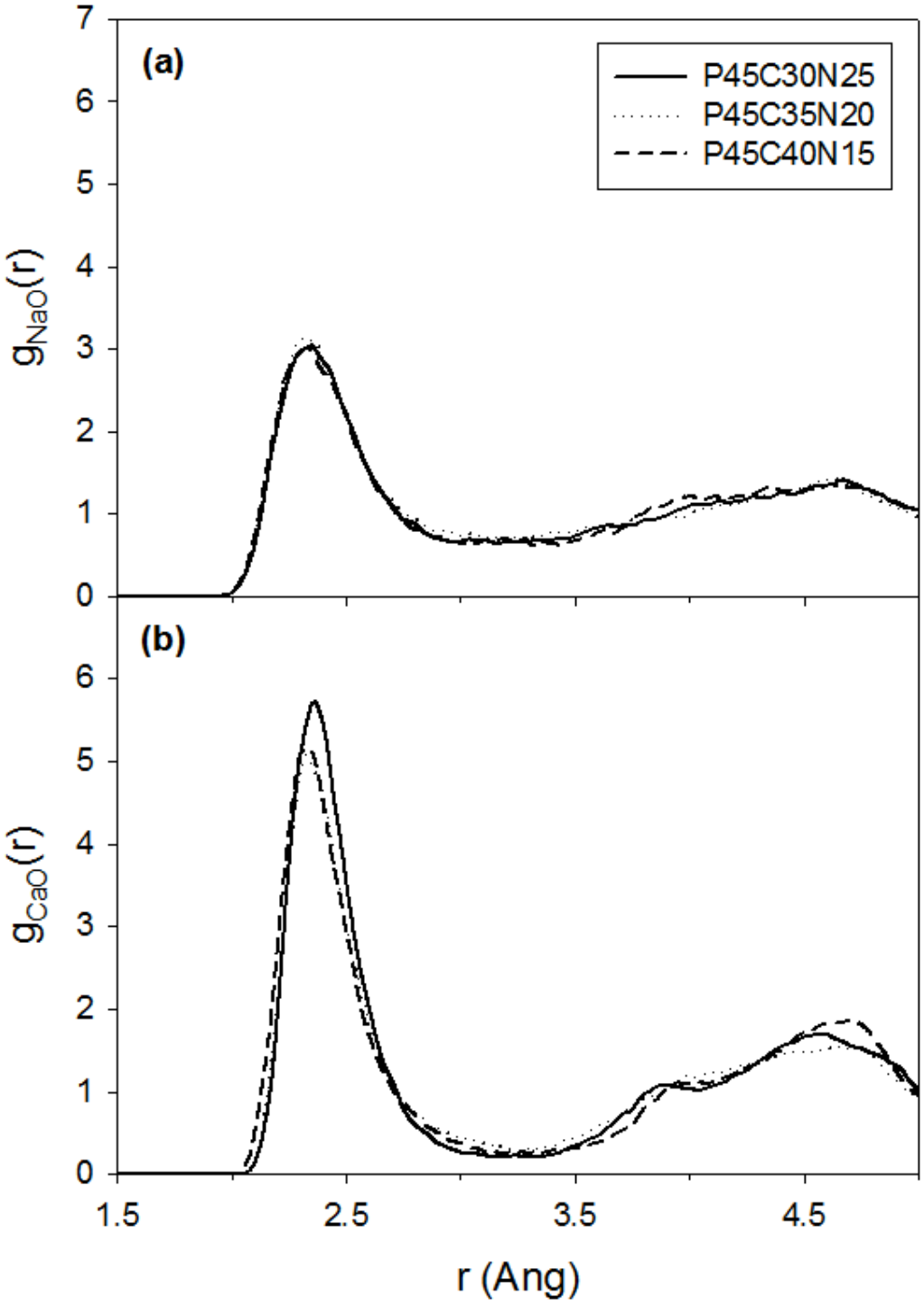

Figure 3-5 Radial distribution function of the Na-O (a) and Ca-O (b) pairs obtained from the CP-MD simulations of the $(P_2O_5)_{0.45}CaO_xNa_2O_{0.55-x}$ (x = 0.30, 0.35 and 0.40) glasses.

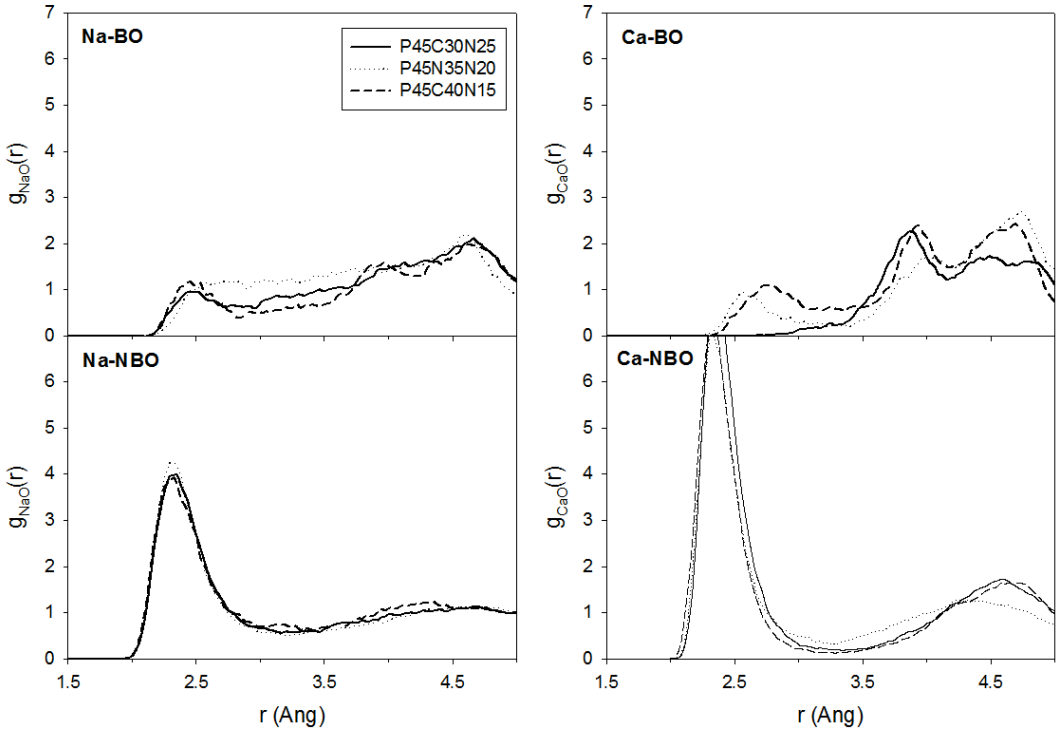

Figure 3-6 Decomposition of the M-O radial distribution functions (M = Na, Ca) into their BO and NBO components.

Table 3-3 Coordination environments of the Na and Ca ions; $r_{\max}^{M-O}$ is the distances are in Å. Coordination numbers are obtained using Na-O and CaO cut-offs of 3.1 Å and 3.2 Å, respectively.

	P45C30N25	**P45C35N20**	**P45C40N15**
Atomic pair	**CN_{av}**	**CN_{av}**	**CN_{av}**
Na-O	5.9	6.1	5.8
Na-BO	0.8	1.1	0.7
Na-NBO	5.1	5.0	5.1
Ca-O	7.1	7.0	7.1
Ca-BO	0	0.5	0.8
Ca-NBO	7.1	6.5	6.3

The arrangements of the oxygens around the sodium and calcium are unveiled in the distribution of O-M-O angles in Figure 3-8. For all three glass compositions, both O-Na-O and O-Ca-O distributions show a peak in the range of 80° to 90°, which represents the sodium and calcium coordination to two NBOs belonging to different PO_4 tetrahedra, as shown in Figure 3-7. The modifier cations thus have the role of connecting and arranging together different chain-like and isolated phosphate fragments, hence controlling their folding and interconnectivity.

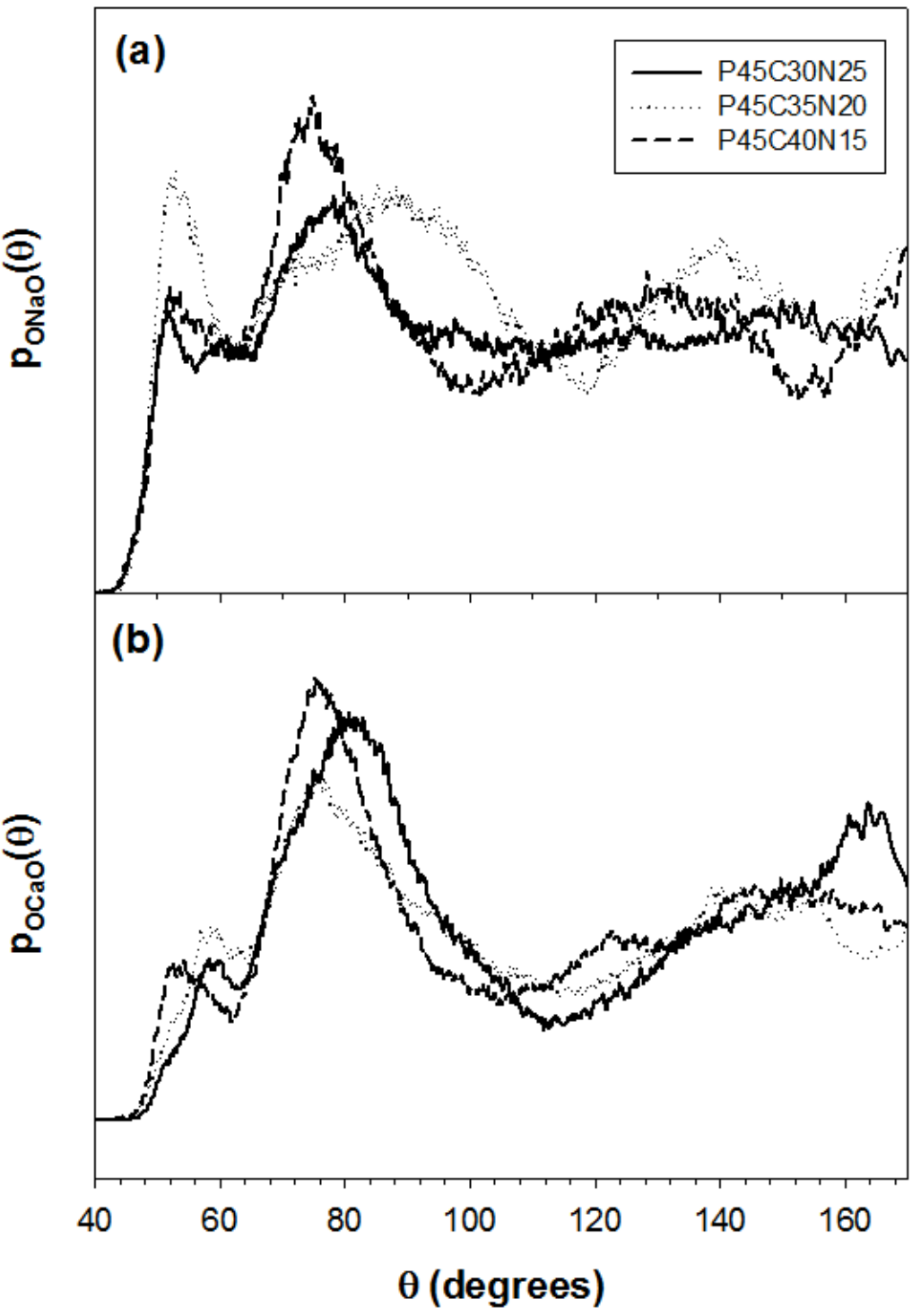

Figure 3-7 Snapshot from the CP-MD trajectory of the P45C30N25 glass showing a typical calcium coordination shell. Ca, Na, O and P are pictured as green, purple, red and pink spheres, respectively.

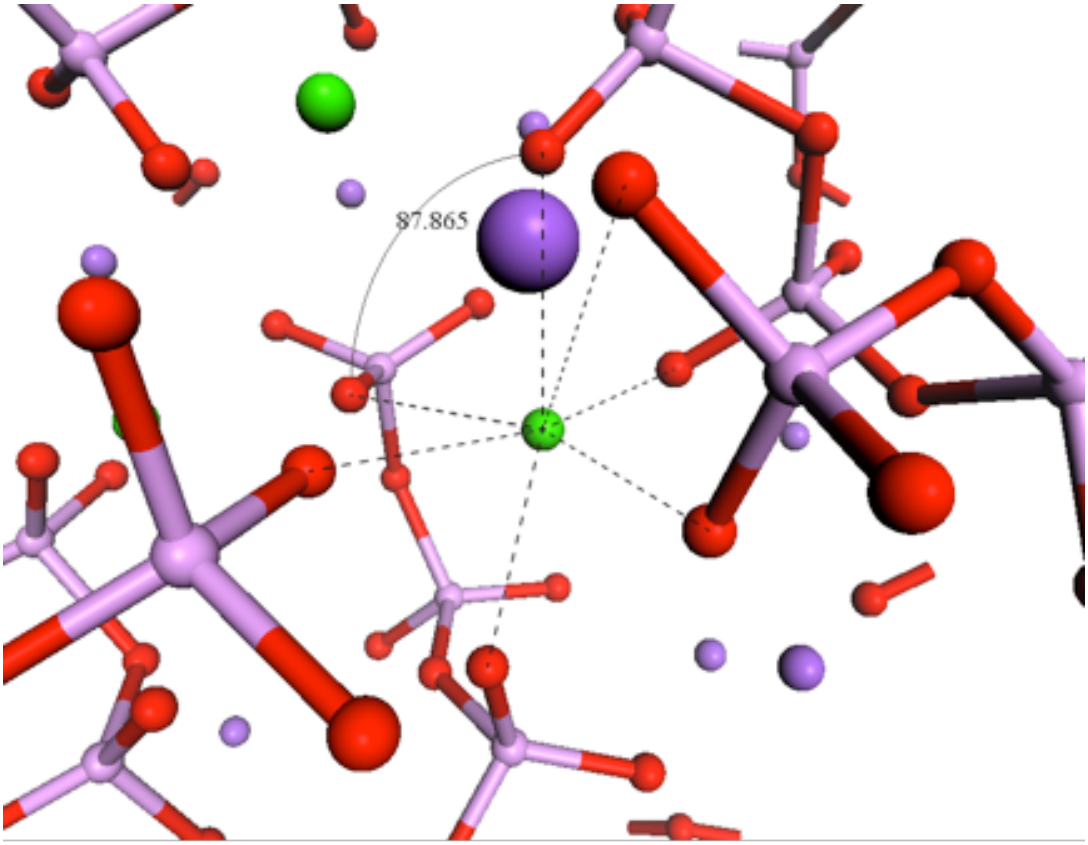

Figure 3-8 The O−Na-O (a) and O-Ca-O (b) angular distribution functions for the simulated $(P_2O_5)_{0.45}CaO_xNa_2O_{0.55-x}$ (x = 0.30, 0.35 and 0.40) glasses.

The influence of glass composition is noticeable on the angular distribution functions of the O-Ca-O in Figure 3-8(b), as the distribution of the angles is more peaked around the value of 80° for the glass with 40% of CaO content. Thus, the increase in calcium content in the PBG decreases the flexibility of the geometries of the coordination shells of Ca, and consequently increases the rigidity of the glass.

3.6 Chapter conclusion

In this chapter, we have reported the first investigation of the local and medium-range structural properties of ternary phosphate based glasses $(P_2O_5)_{0.45}(CaO)_x(Na_2O)_{0.55-x}$, with x = 0.30, 0.35 and 0.40, using *ab initio* molecular dynamics simulations. The structure of these glasses was generated from a full *ab initio* MD melt-and-quench procedure using a nominal cooling rate of 20 K/ps.

The coordination statistics of the phosphate tetrahedral network shows a shift of the Q^n distribution from 100 % Q^3 species in vitreous P_2O_5 to a prevalence of a mixture of metaphosphate Q^2 and pyrophosphate Q^1 species, in agreement with experiment. The analysis of the structure of the tetrahedral network shows that the local arrangement of each PO_4 is essentially constant with change in glass composition. However, the distribution of the P-P distances and P-O-P angles changes significantly with Ca content in the PBGs, suggesting that the effect of calcium on the structure of glasses is to increase the rigidity of the P-O-P interconnectivity.

Regarding the coordination environment of the network modifiers, sodium and calcium, the simulations of the PBGs reveal that Na and Ca are coordinated to approximately 6 and 7 oxygen atoms, respectively. The decomposition of the M-O (M = Na or Ca) RDFs into the BO and NBO contributions show that these metals are preferentially bound to non-bridging oxygens. The distribution of the O-Ca-O angular distribution functions also suggests that the rigidity of the PBGs increases with the concentration of Ca in the glass.

Chapter 4 Hydration Structures of Orthophosphates

In this chapter, extensive Car-Parrinello molecular dynamics simulations of aqueous solutions of orthophosphate species $H_nPO_4^{3-n}$ (n=0-3) were carried out to provide new insights into hydrogen transfer and intermolecular and hydration properties of these important aqueous species. Simulations boxes of the orthophosphate ion PO_4^{3-}, of the hydrogenphosphate anions, HPO_4^{2-} and $H_2PO_4^-$, and of the orthophosphoric acid, H_3PO_4 in 51 explicit water molecules are used. The process of the hydrogen transfer and the structural properties of the orthophosphates in aqueous solution are analysed.

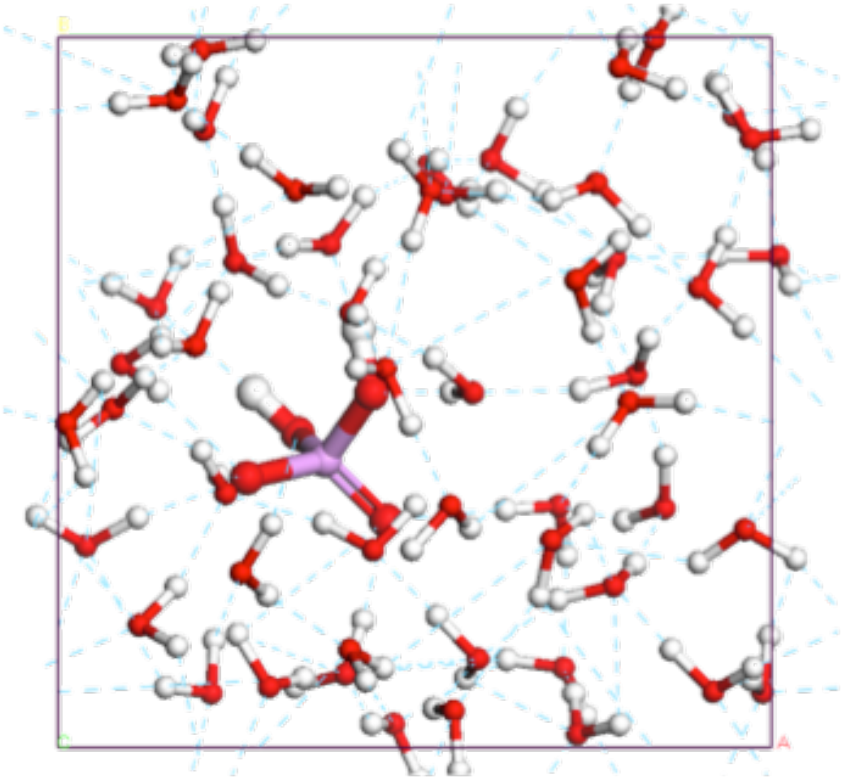

Figure 4-1 Snapshot of simulation box of $H_2PO_4^-$ with 51 water molecules.

4.1 Chapter Introduction

Interest in the chemistry of phosphates is escalating as a result of their importance in biology and technology. Inorganic phosphates play a critical role in diverse cellular functions involving intermediary metabolism and energy-transfer mechanisms, for example, in the production of ATP, (Voet 1995) as well as bone mineralization, (Takeda, Taketani et al. 2004) and they are vital components of RNA and DNA. (Stryer 1988) In the last decade, knowledge of the properties of phosphate ions has also become crucial in the fields of biomaterials and tissue engineering, largely because of the development of phosphate based glasses (PBG) for biomedical applications (Knowles 2003).These glasses, containing phosphorus pentoxide (P_2O_5) as a network former and sodium oxide (Na_2O) and calcium oxide (CaO) as network modifiers, have been classified as 'Third Generation' biomedical materials, i.e. implants which should not only be temporary, but also possess the ability to assist the tissue regeneration process. (Hench and Polak 2002) The PBG are indeed biocompatible (Navarro, Ginebra et al. 2003) and bioactive (Gough, Christian et al. 2002) with the surrounding tissue, chemically similar to the bone tissue, and degradable in aqueous media, and once the hydration of the surface species has proceeded to the actual dissolution of ions and phosphate groups, one of the main issues is determining the nature of the solvated species and whether the ions and phosphate groups chemically interact with the surrounding water to form different species. (Ahmed, Lewis et al. 2004) In this context, in order to identify which phosphate clusters will be observed by experiment, a basic understanding of the solvation properties of the phosphate anions and of the influence of phosphate species on the water structure is essential.

Despite the interest in the properties of phosphates in aqueous solutions, only a few quantum mechanical studies have been conducted on the interaction between phosphates and water, and these studies have mostly relied on static optimization of the $H_nPO_4^{3-n}$, n = 0-3, species interacting with a few explicit water molecules in the gas-phase (Pye and Rudolph 2003) or in a dielectric continuum to simulate the hydrated environment. (Brandan, DÌaz et al. 2007)

Owing to the development of the Car-Parrinello method, (Car and Parrinello 1985) it is now possible to carry out first principle density functional theory molecular dynamics simulations of solvated compounds. (Gaigeot and Sprik 2004; Coskuner 2007; Sadoc, Messaoudi et al. 2007; Kumar, Kalinichev et al. 2008; Spezia, Bresson et al. 2008) In fact, Car-Parrinello molecular dynamics simulations on the electronic and conformational properties of dimethyl phosphate species in aqueous solution have already been reported, (Alber, Folkers et al. 1999; Kuo and Tobias 2001) but, to our knowledge, there is only a single reported molecular dynamics study on the orthophosphate ion PO_4^{3-}, and on the hydrogenphosphate anions, HPO_4^{2-} and $H_2PO_4^{-}$, phosphates anions in water, which is, however, based on empirical inter-atomic force fields. (Ebner, Onthong et al. 2005) Because these methods cannot model processes of proton transfer, which are expected to be rather common in the $H_nPO_4^{3-n}$-water systems, a first principles molecular dynamics investigation of orthophosphate aqueous solutions is clearly justified.

In this study we report Car-Parrinello molecular dynamics (CP-MD) simulations of the orthophosphate ion, PO_4^{3-}, the hydrogenphosphate anions, HPO_4^{2-} and $H_2PO_4^{-}$, and orthophosphoric acid, H_3PO_4 in water in order to obtain detailed information on the mechanism of any proton transfer, the hydration

structure and the hydrogen-bonding network between these important aqueous species and the surrounding water molecules.

4.2 Methodology

Car-Parrinello molecular dynamics (CP-MD) simulations were carried out using the CP public domain code included in the Quantum-ESPRESSO package, version 3.2, which implements Density Functional Theory (DFT) using a plane-wave (PW) basis set and pseudopotentials approach. We have used the Perdew-Burke-Ernzerhof (PBE) generalized gradient approximation (Perdew, Burke et al. 1996) for the exchange and correlation terms, and Vanderbilt ultrasoft pseudopotentials (USPP) (Vanderbilt 1990) to represent core-valence interactions for all atomic species. The USPP for O, H and P were generated using the USPP 7.3 pseudopotential program with a scalar-relativistic calculation , and the accuracy and transferability of these pseudopotentials were tested by comparing the optimized structure and the hydration energies of phosphate species calculated with the USPP-PW approach with the results obtained from an all-electron calculation using the DMol^3 code (Delley 1990; Delley 2000) using the PBE density functional and the double-numeric-polarised basis sets on all atoms. Plane-wave basis set cutoffs for the smooth part of the wavefunctions and the augmented density were set to 40 and 200 Ry, respectively, which ensured convergence in the above test calculations, and *k*-sampling was restricted to the Γ point of the Brillouin zone. In the CP-MD simulations, the hydrogen nuclei were treated as classical particles with the mass of the deuterium isotope, and the fictitious electron mass μ was set equal to 600 a.u. The choice of these parameters is consistent with the ratio $\mu M \leq 0.3$ suggested by Grossman when investigating the structural properties of aqueous solutions. (Grossman, Schwegler et al. 2004) The time step was set equal to 0.121 fs, and all simulations were carried out in the NVT ensemble using a Nosé-Hoover chain

thermostat (Nose 1984; Nosé 1984; Hoover 1985) with a chain length of four and frequency of 60 THz to maintain the average temperature at T = 400 K. Previous CP-MD simulations have shown that the underlying PBE functional yields over-structured water compared to experiment and slow dynamics at T = 300 K, suggesting that the freezing point of water is around 400 K. (Fernandez-Serra and Artacho 2004; Schwegler, Grossman et al. 2004; Sit and Marzari 2005) It was shown by Asthagiri, Pratt and Kresse that at normal conditions the revised PBE (RPBE) functional (Hammer, Hansen et al. 1999) gives a water structure in good agreement with the experimental results. (Asthagiri, Pratt et al. 2003) However, calculation of the water dimer binding energies has shown that while the PBE result differs by only 0.2 kcal mol^{-1} to the energies computed at the *ab initio* CCSD(T) level (CCSD(T): coupled-cluster with single and double excitations and perturbative contribution of connected triple excitations method), the RPBE binding energy is 1.1 kcal mol^{-1} lower than the *ab initio* reference value. (Mattsson and Mattsson 2009) This indicates that RPBE does not describe the hydrogen-bonding between two water molecules as accurately as the PBE functional. One of the main aims of the present study is the hydrogen-bonded interactions between the orthophosphate species and the surrounding water molecules, hence our choice of the PBE approximation for the exchange-correlation term, and of T = 400 K for the MD simulations to obtain a liquid-like water structure and diffusion time scale. A similar simulation set-up has been used successfully in our previous study of the hydration behaviour of $CaCO_3$ and $CaHCO_3^+$ nuclei. (Di Tommaso and de Leeuw 2008)

CP-MD simulations of aqueous solutions of $H_nPO_4^{3-n}$, n = 0 – 3, were carried out on a single $H_nPO_4^{3-n}$ molecule embedded in a box of 51 water molecules. For all phosphate species, the initial configurations were taken from a 20 ps CP-MD simulation of 54 heavy water (D_2O) molecules with a cell length corresponding to the extrapolated experimental density of heavy water at 400 K. The last snapshot of this simulation has been used to generate the initial configurations of $H_nPO_4^{3-n}$, n = 0 – 3, in water by replacing three water molecules with one phosphate species.

4.3 Proton transfer of $H_nPO_4^{3-n}$ (n = 0-3) with water.

Before discussing the structural properties of the orthophosphates in aqueous solution, we consider the process of proton transfer of the $H_nPO_4^{3-n}$ (n=0-3) species with the surrounding water molecules. The pK_a constant for the three protonation states of phosphoric acid are: pK_a^{exp} = 2.2 for the reaction $H_3PO_4 \rightarrow H_2PO_4^- + H^+$; p$K_a^{exp}$ = 7.2 for the reaction $H_2PO_4^- \rightarrow HPO_4^{2-} + H^+$; p$K_a^{exp}$ = 12.3 for the reaction $HPO_4^{2-} \rightarrow PO_4^{3-} + H^+$. (Fasman 1976) Hereafter, oxygen and hydrogen of the water molecules are denoted by O_w and H_w, while oxygen and hydrogen of the phosphate species are denoted by O_p and H_p. Scheme 4-1 gives the convention for the labeling of atoms of the orthophosphates.

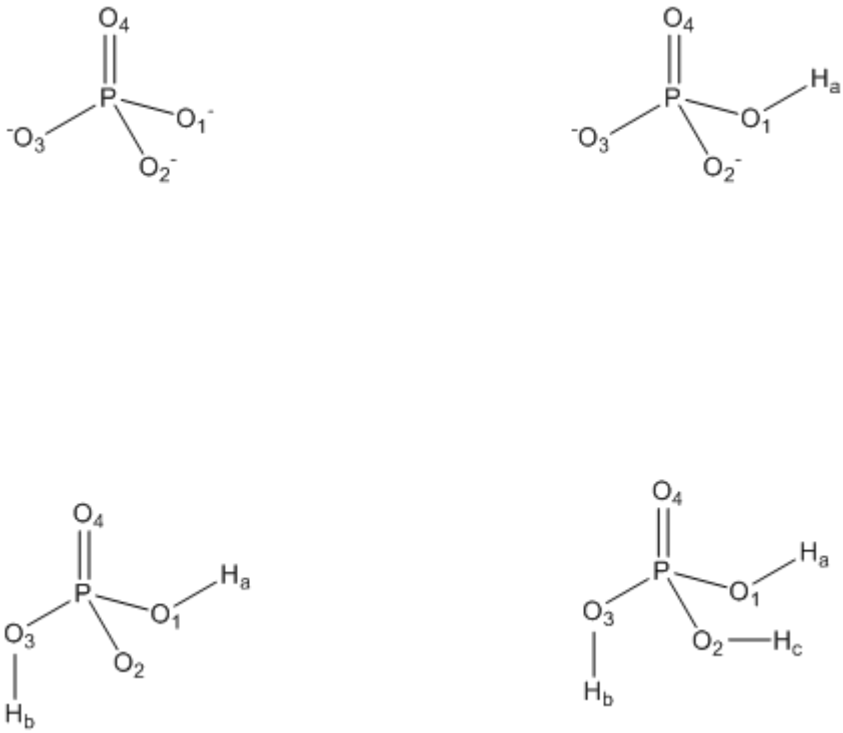

Scheme 4-1

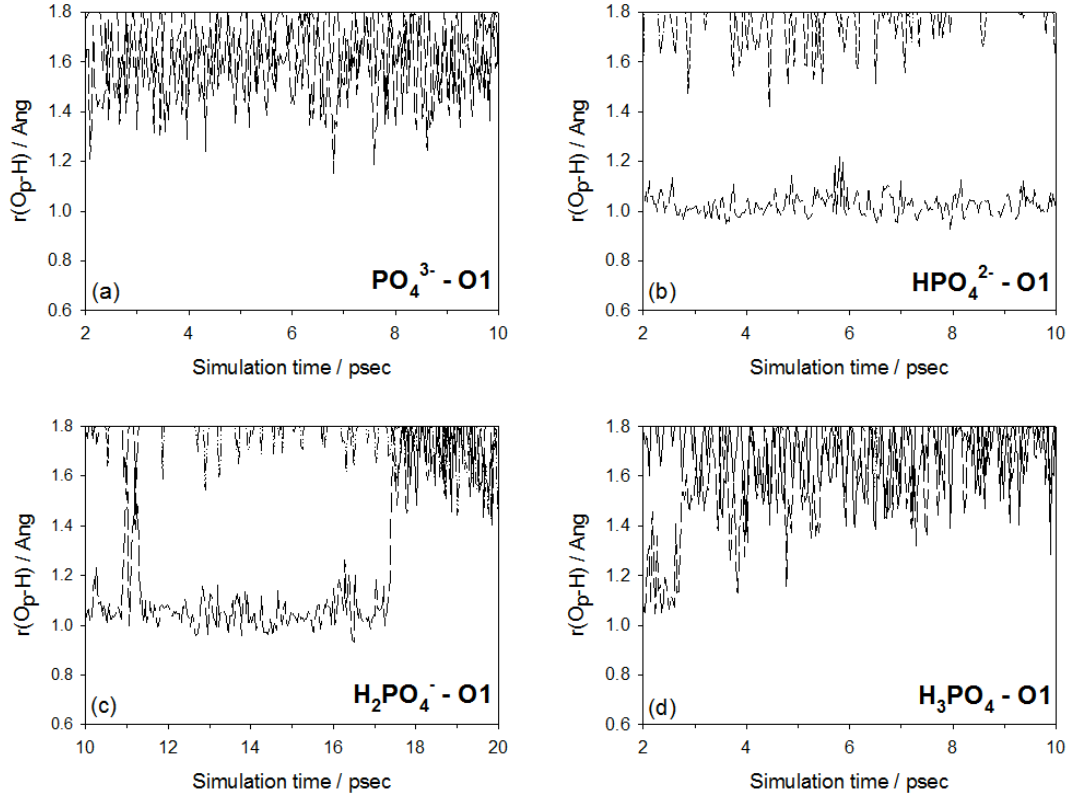

Figure 4-2 Time evolution of the O_p–H distance of the oxygen O1 during the CP-MD simulation of (a) PO_4^{3-}, (b) HPO_4^{2-}, (c) $H_2PO_4^-$ and (d) H_3PO_4 in 51 water molecules (time step: 30.25 fs).

Figure 4-2 reports the time evolution of the distance of the oxygen atoms labeled O1 of the orthophosphate species with the H atoms, r(O_p–H), during the CP-MD simulations of $H_nPO_4^{3-n}$ (n=0-3). Taking 1.0 Å as the average for the intra-molecular O-H bond, we note that throughout the simulation period the oxygen t

atoms of the orthophosphate ion PO_4^{3-} [Figure 4-2 (a)] and the hydrogen-phosphate anion HPO_4^{2-} [Figure 4-2 (b)] are not involved in any proton (H) transfer processes with the water. The number of H-transfer events increases when going to the dihydrogen-phosphate $H_2PO_4^-$ [Figure 4-2 (c)] and the orthophosphoric acid H_3PO_4 [Figure 4-2 (d)]. In the case of the H_3PO_4 species, the oxygen O1 loses its

proton after only 3 ps, and visualization of the trajectory shows that the de-hydrogenated H_3PO_4 remains mostly as $H_2PO_4^-$ throughout the dynamics, suggesting that the orthophosphoric acid is not stable under the simulated conditions. On the other hand, for HPO_4^{2-} and $H_2PO_4^-$ the analysis of the O_p–H distances and the visualization of the molecular movements indicate that both species are stable.

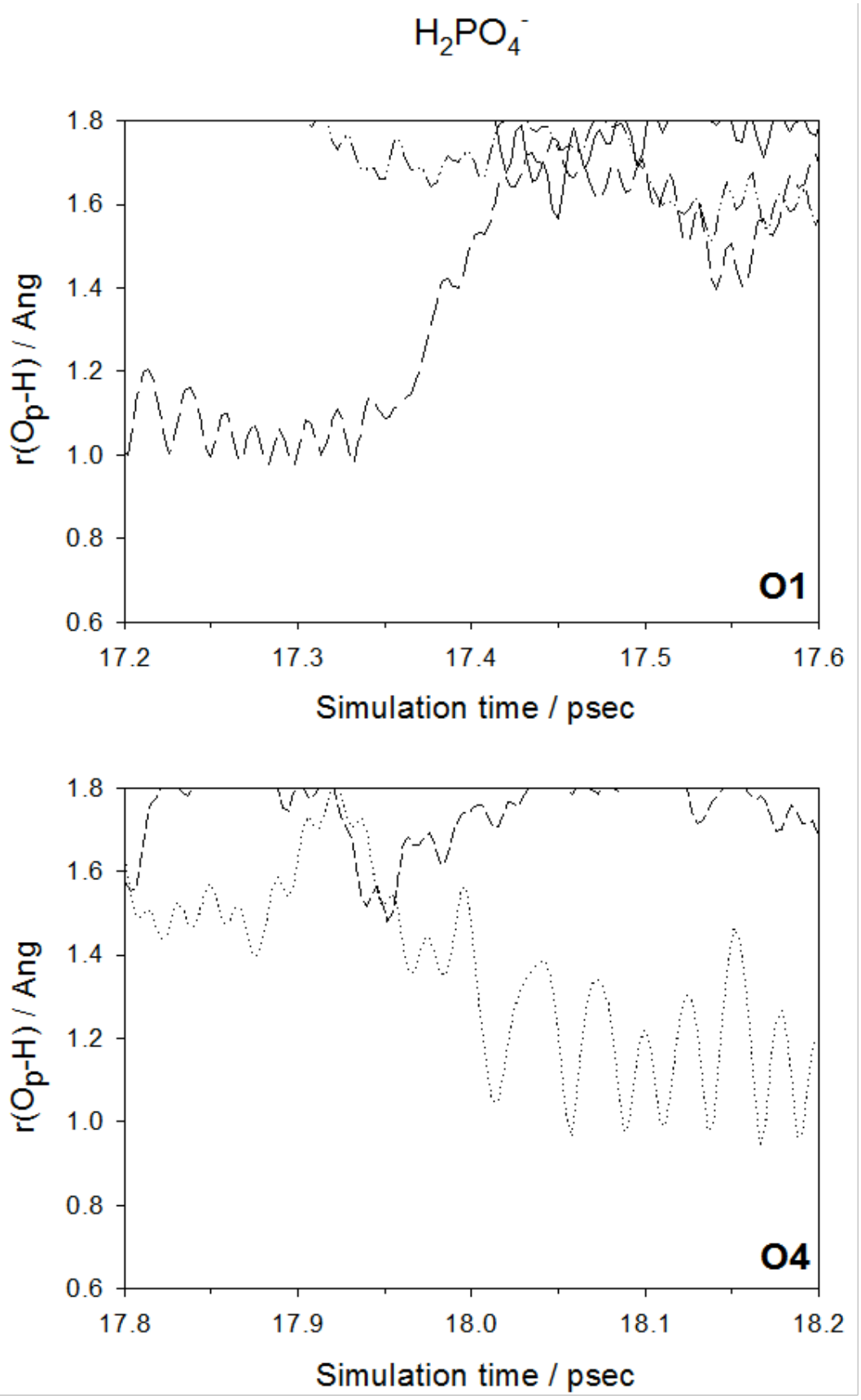

Figure 4-3 Time evolution of the O_p–H distance during the CP-MD simulation of $H_2PO_4^-$ in 51 water molecules (time step:0.60 fs). Above: O1 oxygen; Below: O4 oxygen.

In Figure 4-3, for the $H_2PO_4^-$ water system we have considered a more detailed analysis of the distances O_p−H for the atoms O1 and O4−H using a smaller time step (0.60 fs). This graph shows that between 17 ps and 19 ps the $H_2PO_4^-$ anion undergoes a double H-transfer process, with the dissociation of the O1−H bond and formation of the O4−H bond, and clearly indicates that the H-transfer from $H_2PO_4^-$ to the surrounding water molecules is a very fast process, taking approximately 0.1 ps. Figure 4-4 further reports on the dynamics of the de-hydrogenation process by considering the time evolution of the Kohn-Sham energy in the time frame where the process of H-transfer occurs, together with the configurations corresponding to the minima **1**-**5**. These snapshots indicate that the de-hydrogenation of the $H_2PO_4^-$ species occurs through a concerted proton hopping mechanism: In configuration **3** all reported O−H distances are approximately 1.2 Å, which indicates that three protons are contemporaneously involved in the de-hydrogenation process of the $H_2PO_4^-$ with three other water molecules.

We can thus conclude that both PO_4^{3-} and HPO_4^{2-} are stable throughout the CP-MD simulation, and consequently the analysis of the structural and hydration properties of PO_4^{3-} and HPO_4^{2-} will be based on a production time of 18 ps. For the $H_2PO_4^-$ anion, which shows a double H-transfer process between 17 and 19 ps, after 2 ps of equilibration time, statistics will be collected for the first 17 ps in order to avoid the presence in the simulated solution of HPO_4^{2-} in the time frame mentioned above. Finally, because the orthophosphoric acid de-hydrogenates to HPO_4^{2-} after only 3 ps of CP-MD simulation, no structural analysis will be presented for H_3PO_4.

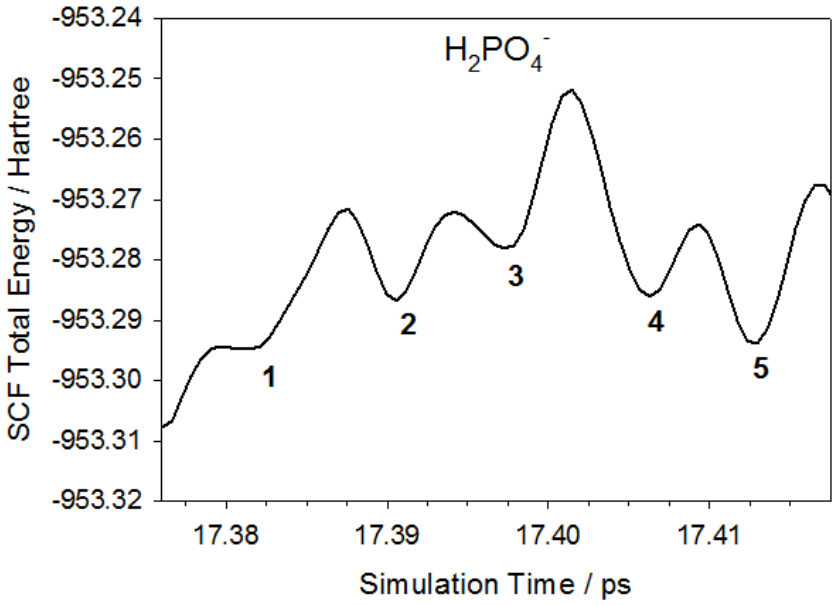
$H_2PO_4^-$
SCF Total Energy / Hartree
-953.24
-953.25
-953.26
-953.27
-953.28
-953.29
-953.30
-953.31
-953.32
17.38
17.39
17.40
17.41
Simulation Time / ps
1
2
3
4
5

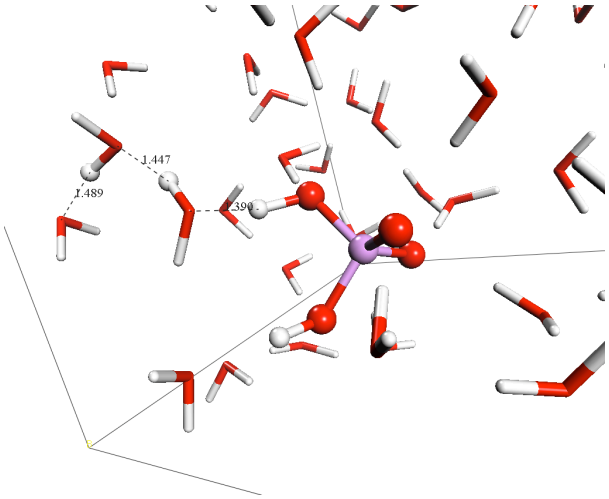
1.447
1.489
1.390

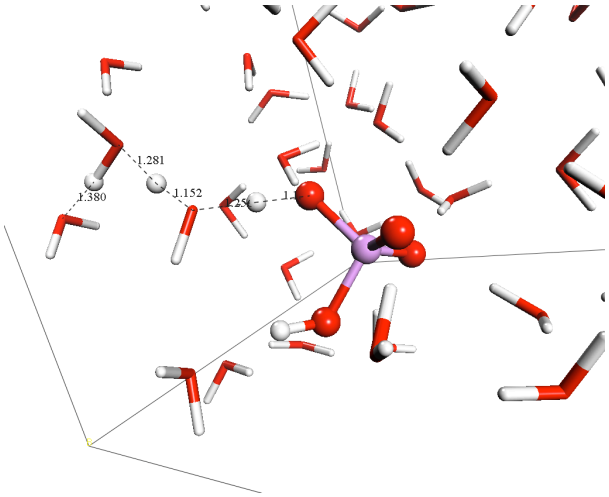
1.281
1.380
1.152

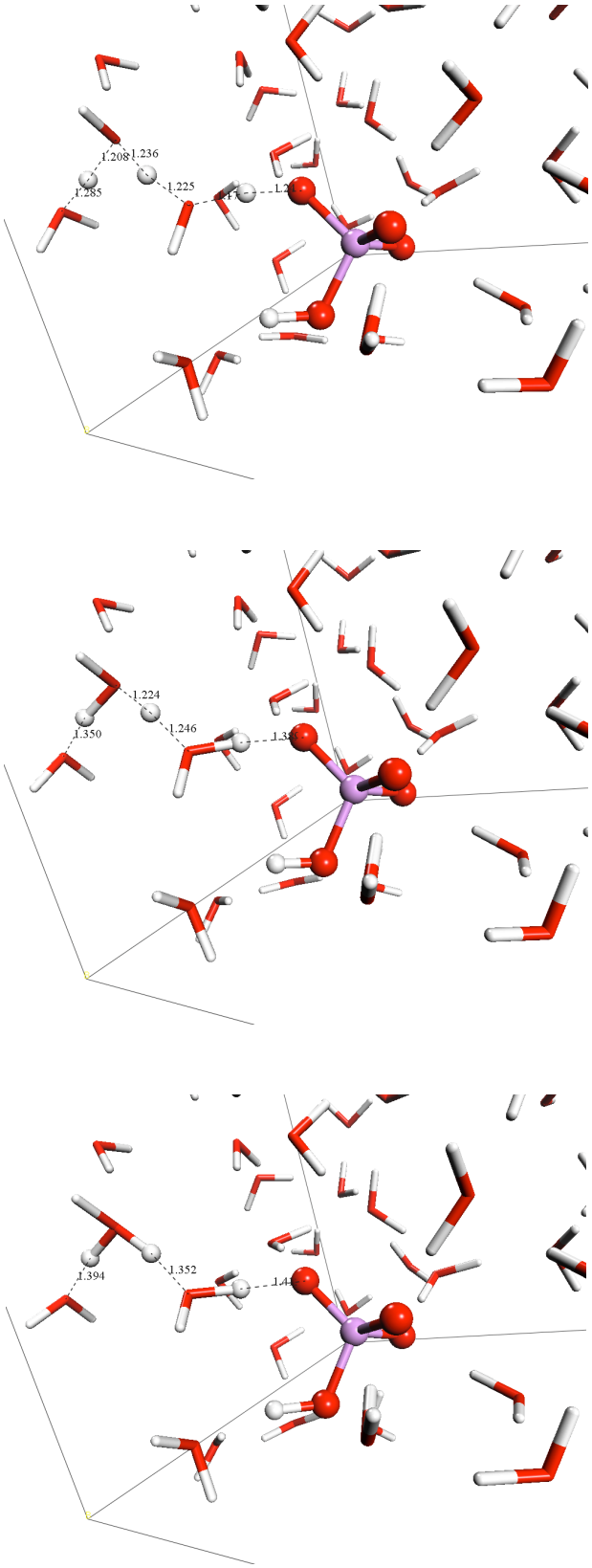

Figure 4-4 Time evolution of the SCF total energy (time step of 0.60 fs) and representative snapshots from the CP-MD simulation of $H_2PO_4^-$ in 51 water molecules (At simulation time 1-5 top down.), showing the proton hopping process involved in the dehydrogenation of $H_2PO_4^-$.

4.4 Inter-molecular properties and hydration structure of $H_nPO_4^{3-n}$ (n = 0-2) in aqueous solution.

Phosphate-water radial and angular distribution functions. Information regarding the structural and hydration properties of the orthophosphate species $H_nPO_4^{3-n}$ (n = 0-2) in water can be obtained from the radial distribution functions (RDFs) $g_{\alpha\beta}(r)$, which represent the probability, relative to a random distribution, of finding an atom of type β at a distance r from an atom of type α. In order to provide additional information, angular distribution functions were also calculated. Before discussing the structural details of the solvated $H_nPO_4^{3-n}$ species, we compare in Figure 4-5 the oxygen–oxygen, hydrogen–hydrogen and oxygen-hydrogen RDFs of the water molecules obtained from the CP-MD simulations of the PO_4^{3-} ion in water with those for pure water obtained from 18 ps simulation of 54 D_2O molecules, and with the experimental partial pair correlation functions for H_2O at 298 K. (Soper 2000) In Figure 4-5(a), the computed O_w–O_w RDF is close to the experimental one: the peak of the O_w–O_w pairs corresponding to the H-bonding interactions, from the PO_4^{3-} aqueous solution and pure water, are both located at 2.72 Å and characterized by a height of 2.81 and 2.93 density units, respectively, in good agreement with the measured values of 2.73 Å and 2.75. This result indicates that the water in our CP-MD simulations, which are based on the DFT-PBE approximation, of $H_nPO_4^{3-n}$ in 51 water molecules at the averaged temperature of 400 K, has a clear liquid-like behaviour. However, the comparison of the O_w–O_w RDF of the PO_4^{3-}-water simulation with that of pure water shows that the inter-molecular peak at 2.72 Å of pure water exhibits a more structured behaviour, suggesting that the PO_4^{3-} ion affects the H-bonding network between the water molecules.

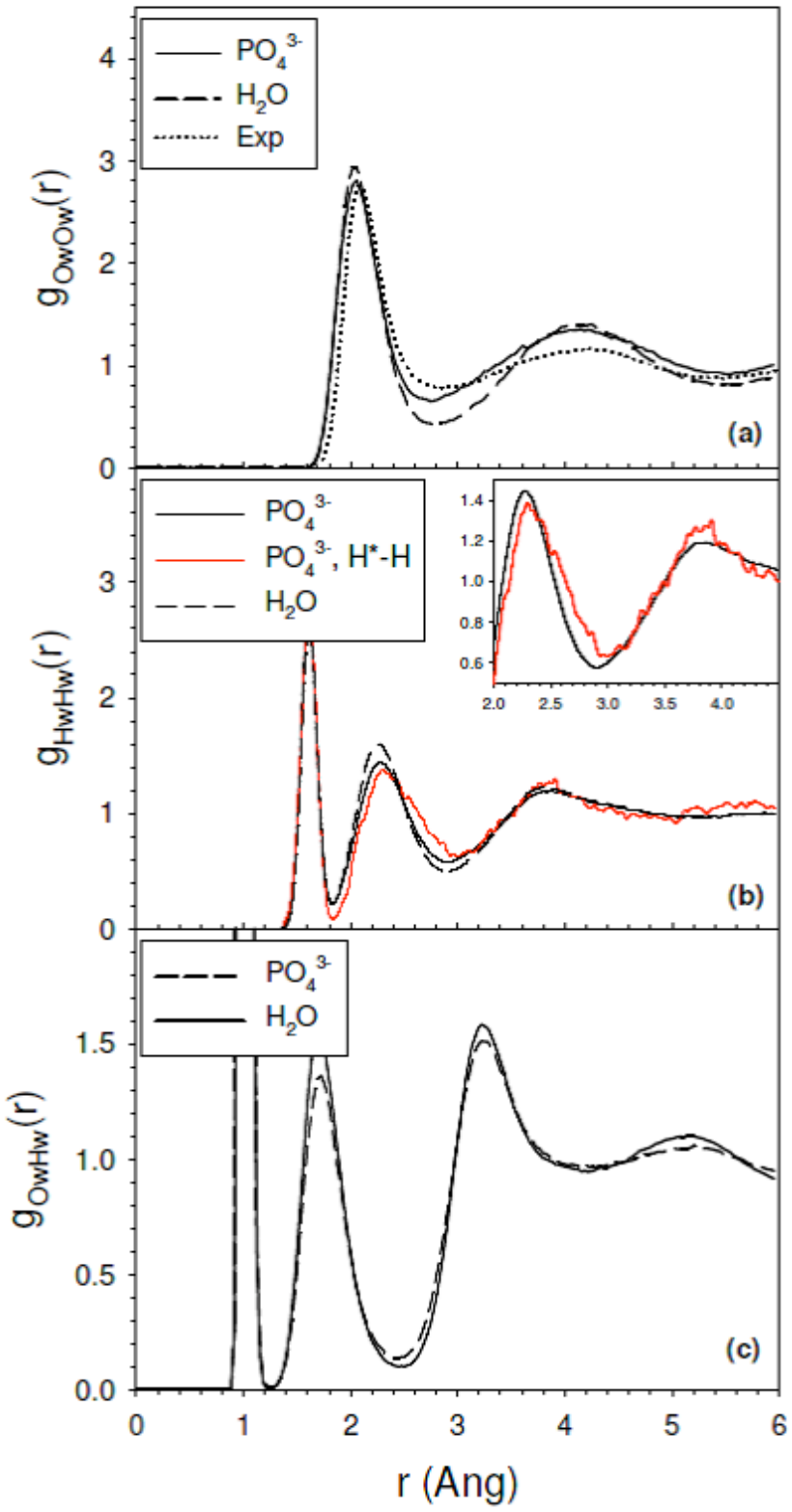

Figure 4-5 The O_w–O_w, H_w–H_w and O_w–H_w radial distribution functions, $g(r)$, of the PO_4^{3-} aqueous solution and of pure water obtained from the CP-MD simulations. The dotted line corresponds to the experimental O_w–O_w partial pair correlation functions for H_2O at 298 K (http://www.isis.rl.ac.uk/disordered/database).

In Figure 4-5(b), the computed H_w–H_w RDF obtained from the simulation on pure water is also more structured than the PO_4^{3-}-water system, particularly in the region of the second feature at 2.3 Å. Within the general water structure where each water molecule H-bonds to two others, the peak at 2.3 Å corresponds to the correlation of the H atom of one water molecule H-bonded to a second molecule, $(O_w–)H---H(–O_w)$. However, using neutron scattering and isotopic substitution experiments, Mason et al. (Mason, Cruickshank et al. 2003) noticed that for K_3PO_4 and K_2HPO_4 aqueous solutions, apart from the peak at 2.3 Å, their H–H RDFs were characterised by two additional peaks at 2.1 Å and 2.9 Å (see Fig. 1 in (Mason, Cruickshank et al. 2003)). The authors propose that, apart from the bulk water $(O_w–)H---H(–O_w)$ correlations, the presence of the highly negatively charged $P–O^–$ moieties induce the formation of new types of H---H interactions around the $PO_4^{3–}$ and $HPO_4^–$ ions. They reason that the interaction $(P–O^–\cdots)H_w---H_w$ is responsible for the peak at 2.1 Å, whereas the peak at 2.9 Å is due to the correlation of two hydrogen atoms H-bonded to the same negatively charged oxygen of the phosphate. In Figure 4-5(b), the computed H–H RDF of the $PO_4^{3–}$ aqueous solution is characterised by a single peak at 2.3 Å, but if we consider the H*-H RDF [red line in Figure 4-5(b)] where H* is the hydrogen of a water molecule that remains H-bonded with the $P–O^–$ moiety throughout the CP-MD simulation, then we notice significant differences between the H*–H and H–H RDFs in the region between 2.5 and 3.0 Å [see the inset in Figure 4-5(b)]. The observed shift in the H*-H RDF could be explained in terms of the correlation between H* and the hydrogen atoms H-bonded to the same $P–O^–$ moiety, as suggested by Mason et al. (Mason, Cruickshank et al. 2003) However, there is no evidence for the peak associated with the $(P–O^–\cdots)H_w---H_w$ interaction also proposed by Mason et al. (Mason,

Cruickshank et al. 2003) Different factors could be responsible for the disagreement between the CP-MD results and the neutron scattering experiments: (i) effects related to the size of the simulation box; (ii) the length of the simulation period, which may have not allowed the formation of a complete hydration structure around the PO_4^{3-} ion; (iii) the possibility that DFT-GGA methods like PBE may not be able to differentiate the three types of H_w---H_w interactions (GGA density functionals have the tendency to give a delocalized description of the electron charge distribution). In this context, first-principles molecular simulations of PO_4^{3-} and HPO_4^{2-} in aqueous solutions using hybrid density functional theory methods (Todorova, Seitsonen et al. 2006) could possibly enable the differentiation between these bonding interactions, which will be the subject of future study.

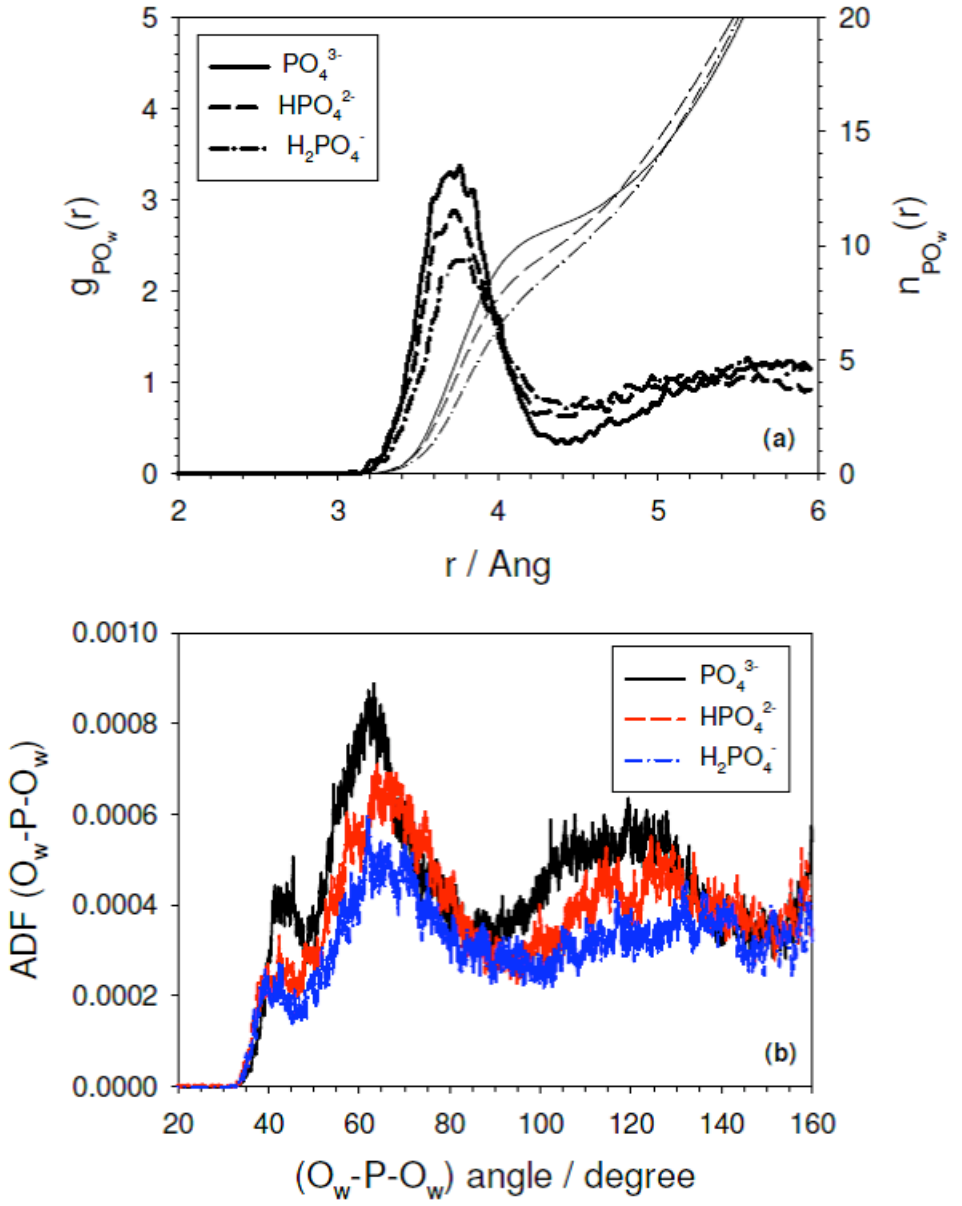

Figure 4-6 (a) The P–O_w radial distribution functions, $g(r)$, and running coordination numbers, $n(r)$, obtained from the CP-MD simulations of PO_4^{3-}, HPO_4^{2-} and $H_2PO_4^{2-}$ in 51 water molecules. (b) The O_w–P–O_w angular distribution functions, ADF, for the water molecules part of the first hydration shell of PO_4^{3-}, HPO_4^{2-} and $H_2PO_4^{2-}$ obtained from the CP-MD simulations of $H_nPO_4^{3-n}$ in 51 water molecules.

Information regarding the geometry of the phosphate anions with the surrounding water molecules is given in Figure 4-6, which reports the P–O_w RDFs

and the O_w–P–O_w angular distribution functions (ADF) of PO_4^{3-}, HPO_4^{2-} and $H_2PO_4^{2-}$ species in aqueous solutions. In Figure 4-6(a) the P–O_w RDFs of the solvated $H_nPO_4^{3-n}$ (n = 0-2) species are displayed together with the running integration number, $n_{PX}(r) = \frac{4\pi N}{V}\int_o^r g_{PX}(r')dr'$, where N is the number of oxygen or hydrogen atoms, V is the volume of the simulation cell and X represents oxygen or hydrogen atoms. Here, the peak of the phosphorus-oxygen RDFs corresponds to the P-O_w correlation for the first hydration shell, and therefore the value of $n_{POw}(r)$ at the position of the minimum of $g_{PO}(r)$ gives the average number of oxygen O_w part of the first hydration shell of each phosphate species, i.e. their hydration number (n_w). Table 4-1 summarizes the relevant data of the first peak of the three P–O RDFs of the $H_nPO_4^{3-n}$ (n = 0-2) species in water. Although a well defined first hydration shell can be located for all phosphate species, the minimum of P-O_w becomes less distinctly separated from the bulk water on going from PO_4^{3-} to the less highly charged anions. In Table 4-1, the ratio between the amplitude of the maximum and the minimum $g_{\max}^{P-O}/g_{\min}^{P-O}$ of PO_4^{3-} is between two and three times the ratio of HPO_4^{2-} and $H_2PO_4^{-}$, which indicates a more tightly structured H-bonding network around the orthophosphate ion.

Figure 4-6(b) reports the ADF of the O_w–P–O_w angles for the water molecules of the first hydration shell of PO_4^{3-}, HPO_4^{2-} and $H_2PO_4^{2-}$, which shows therefore the effect of the different phosphate anions on the ordering of the water molecules: for the PO_4^{3-} anion there are two clear maxima at about 70° and 120°, whereas the angular distribution of O_w–P–O_w becomes less structured for the anions HPO_4^{2-} and $H_2PO_4^{2-}$, where especially for $H_2PO_4^{2-}$ the peak at 120° is drastically reduced, indicating the different structure of the H-bonding network around the

orthophosphate anions. Note that the profile of the ADF of the O_w–P–O_w angles obtained from classical MD simulations of aqueous solution of K_3PO_4 (see Figure 7 in ref (Ebner, Onthong et al. 2005)) shows some differences from the ADF of PO_4^{3-} in Figure 4-6(b), as the angular distribution obtained from the classical MD has two maxima at about 50° and 100°.

Table 4-1 Positions $r_{\max}^{P-O}$, $r_{\min}^{P-O}$ (Å) and amplitudes $g_{\max}^{P-O}$, $g_{\min}^{P-O}$ of the maxima and minima of the second peaks of the P–O_w radial distribution functions, and first shell hydration number n_w obtained from the CP-MD simulations of $H_nPO_4^{3-n}$ (n = 0-2) in 51 water molecules.

	PO_4^{3-}	HPO_4^{2-}	$H_2PO_4^-$
$r_{\max}^{P-O}$	3.73	3.73	3.76
$g_{\max}^{P-O}$	3.26	2.88	2.34
$r_{\min}^{P-O}$	4.42	4.45	4.42
$g_{\min}^{P-O}$	0.34	0.63	0.72
$g_{\max}^{P-O} / g_{\min}^{P-O}$	9.59	4.57	3.25
n_w	11.0	10.4	9.4

In Table 4-1, the average number of water molecules in the first hydration shell n_w decreases from 11 for PO_4^{3-}, to 10.4 for HPO_4^{2-} and 9.4 for $H_2PO_4^-$. In Figure 4-7 we have reported the probability distributions of the number of water molecules surrounding the $H_nPO_4^{3-n}$ (n = 0-2) ions computed up to the minimum of the P-O_w RDFs [Figure 4-6(a)], which show that PO_4^{3-}, HPO_4^{2-} and $H_2PO_4^-$ display multiple coordination numbers and that the flexibility of the first hydration shell increases on going from PO_4^{3-} to $H_2PO_4^-$. Classical molecular dynamics simulations of K_3PO_4 in 508 water molecules computed a first hydration shell consisting of about 16 water molecules molecules (Ebner, Onthong et al. 2005), which agrees

with the coordination number of the PO_4^{3-} ion deduced by Mason et al using neutron scattering techniques (15 ±3) (Mason, Cruickshank et al. 2003). This result is larger than the average first hydration shell determined by our CP-MD simulations (11). It has also been reported that DFT MD simulations using the PBE or BLYP functionals sometimes fail to produce the correct coordination numbers, e.g. 5 instead of 6 for Cu(II) (Pasquarello, Petri et al. 2001). The use of more sophisticated hybrid functionals could improve this feature. Other discrepancies between the CP-MD and the experimental results could be related to the absence of the K^+ counter-ions in the simulation box. Because cation hydration has generally a significant effect on the solvent structure, the presence of K^+ could certainly affect the structure and dynamics of species with a labile first hydration shell like PO_4^{3-}. However, we would like to point out that two other experimental studies, one based on the NMR relaxation method (Chizhik, Egorov et al. 2002) and the other on Raman spectroscopy (Rudolph and Irmer 2007) deduced 12 water molecules of hydration in the first shell of PO_4^{3-}, in good agreement with the hydration number computed by us.

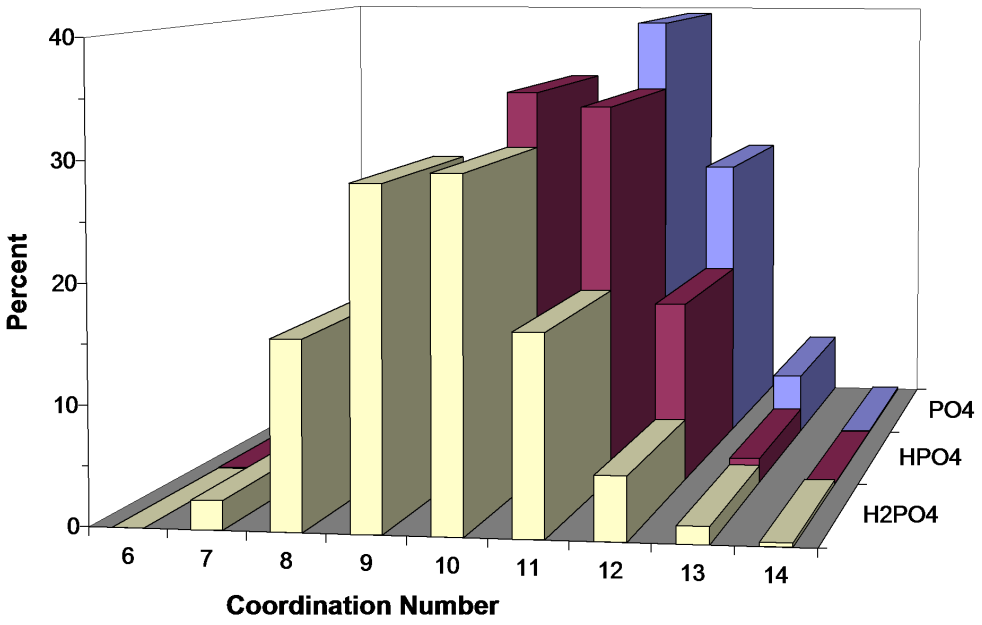

Figure 4-7 Probability distributions of the coordination numbers of the first hydration shell of PO_4^{3-}, HPO_4^{2-} and $H_2PO_4^-$ in water obtained from the CP-MD simulations of $H_nPO_4^{3-n}$ (n = 0-2) in 51 water molecules.

Number and strength of the hydrogen bonds. A more detailed analysis of the hydration structure and the characteristics of the H-bonds between the $H_nPO_4^{3-n}$ (n = 0-2) species and the surrounding water molecules can be obtained from Figure 4-8, which reports the RDFs of the oxygen atoms of the orthophosphate species with the hydrogen atoms of the surrounding water O_p–H_w, and Figure 4-9, which displays the RDFs of the hydrogen atoms of the hydrogenphosphate anions with the oxygen atoms of the water molecules H_p-O_w (Scheme 4-1 gives the convention for the labeling of atoms). The positions of the maxima and minima $r_{\max}^{O-H}$, $r_{\min}^{O-H}$ (Å) and of the amplitudes $g_{\max}^{O-H}$, $g_{\min}^{O-H}$ for the O_p–H and H_p-O_w pairs are reported in Table 4-2 and Table 4-3, respectively. In the O–H RDFs, a peak in the region of 1.5 – 2.0 Å and a minimum at 2.3 – 2.5 Å indicates a hydrogen bond. On this basis, the

RDFs in Figure 4-8 and structural data in Table 4-2 suggest that all oxygen atoms of the PO_4^{3-}, HPO_4^{2-} and $H_2PO_4^-$ species are H-bonded to water molecules. Generally, between 2.5 and 3 hydrogen atoms are bonded to each P–O^- moiety ($2.5 \le n_w^O \le 3$ in Table 4-2) and this number decreases to approximately one H-bonding when this oxygen is hydrogenated to form the P–OH moiety: For the oxygen labelled O1 in Figure 4-9, n_w^{O1} is equal to 2.6 in PO_4^{3-} and 0.9 in HPO_4^{2-}; for O3, n_w^{O3} is equal to 3.0 in PO_4^{3-} and 2.5 in HPO_4^{2-}, but 0.6 in $H_2PO_4^-$. In Table 4-2, the ratio $g_{\max}^{O-H} / g_{\min}^{O-H}$ can be used as a criterion to establish the strength of the H-bonding interactions between the O_p–H_w pairs[29], where the value of $g_{\max}^{Ow-Hw} / g_{\min}^{Ow-Hw}$ = 15.7 obtained from CP-MD simulations of pure water can be used as the reference. The ratios $g_{\max}^{Op-Hw} / g_{\min}^{Op-Hw}$ associated with the (P–)O^- moieties are higher than $g_{\max}^{Ow-Hw} / g_{\min}^{Ow-Hw}$ of the bulk water, which we interpret as evidence that the (P–)O^- ···H_w hydrogen bonds are stronger than the bonds in the bulk liquid. The ratios $g_{\max}^{Op-Hw} / g_{\min}^{Op-Hw}$ become increasingly lower than $g_{\max}^{Ow-Hw} / g_{\min}^{Ow-Hw}$ = 15.7 when the oxygen atoms are hydrogenated. In Table 4-2, for the oxygen O1 the ratio $g_{\max}^{O-H} / g_{\min}^{O-H}$ is equal to 68.75 in PO_4^{3-} and 3.2 in HPO_4^{2-}; for the oxygen O3, the ratio $g_{\max}^{O-H} / g_{\min}^{O-H}$ is equal to 63.3 and 27.5 in PO_4^{3-} and HPO_4^{2-}, respectively, but it becomes 3.43 in $H_2PO_4^-$. The decreasing strength of the H-bond interaction between the oxygen atoms O_p and the surrounding water molecules (decreasing value of the ratio $g_{\max}^{Op-Hw} / g_{\min}^{Op-Hw}$) on going from in PO_4^{3-} to the hydrogenated $H_2PO_4^-$ species explains why the effect of these ions on the structure of water diminishes with the increasing hydrogenation of the orthophosphate anions. Another measure of the hydrogen bond strengths is given by the gas-phase phosphate-water binding energies. The gas phase hydration energies (ΔE_{hyd}) of the

$H_nPO_4^{3-n}(H_2O)_4$ clusters computed at the DFT-PBE level using the double-numeric-polarised basis sets[24,25] are: ΔE_{hyd} (PO_4^{3-}) = -196.3 kcal/mol; ΔE_{hyd} (HPO_4^{2-}) = -135.9 kcal/mol; ΔE_{hyd} ($H_2PO_4^{-}$) = -63.8 kcal/mol. These results support the order of the strength of the O_p–H_w interactions determined from the analysis of the analysis of the $g_{\max}^{Op-Hw} / g_{\min}^{Op-Hw}$ ratios.

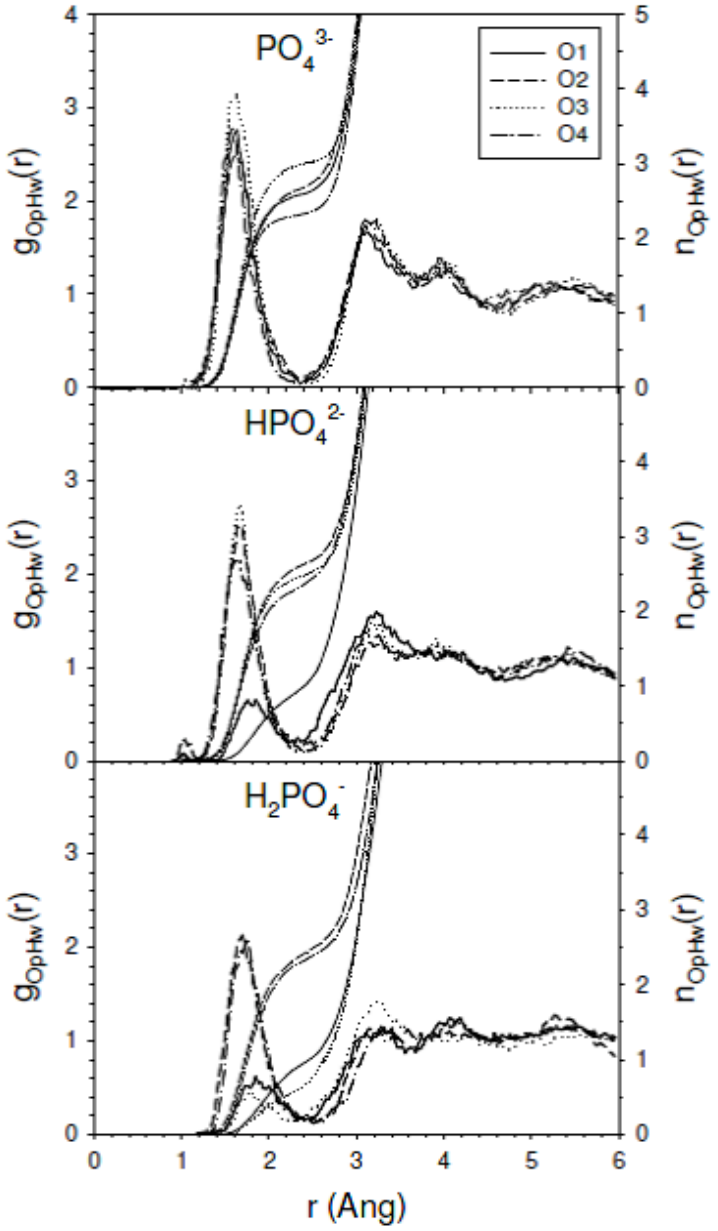

Figure 4-8 The O_p–H_w radial distribution functions, $g(r)$, and running coordination numbers, $n(r)$, of PO_4^{3-}, HPO_4^{2-} and $H_2PO_4^{-}$ in water obtained from the CP-MD simulations of $H_nPO_4^{3-n}$ in 51 water molecules.

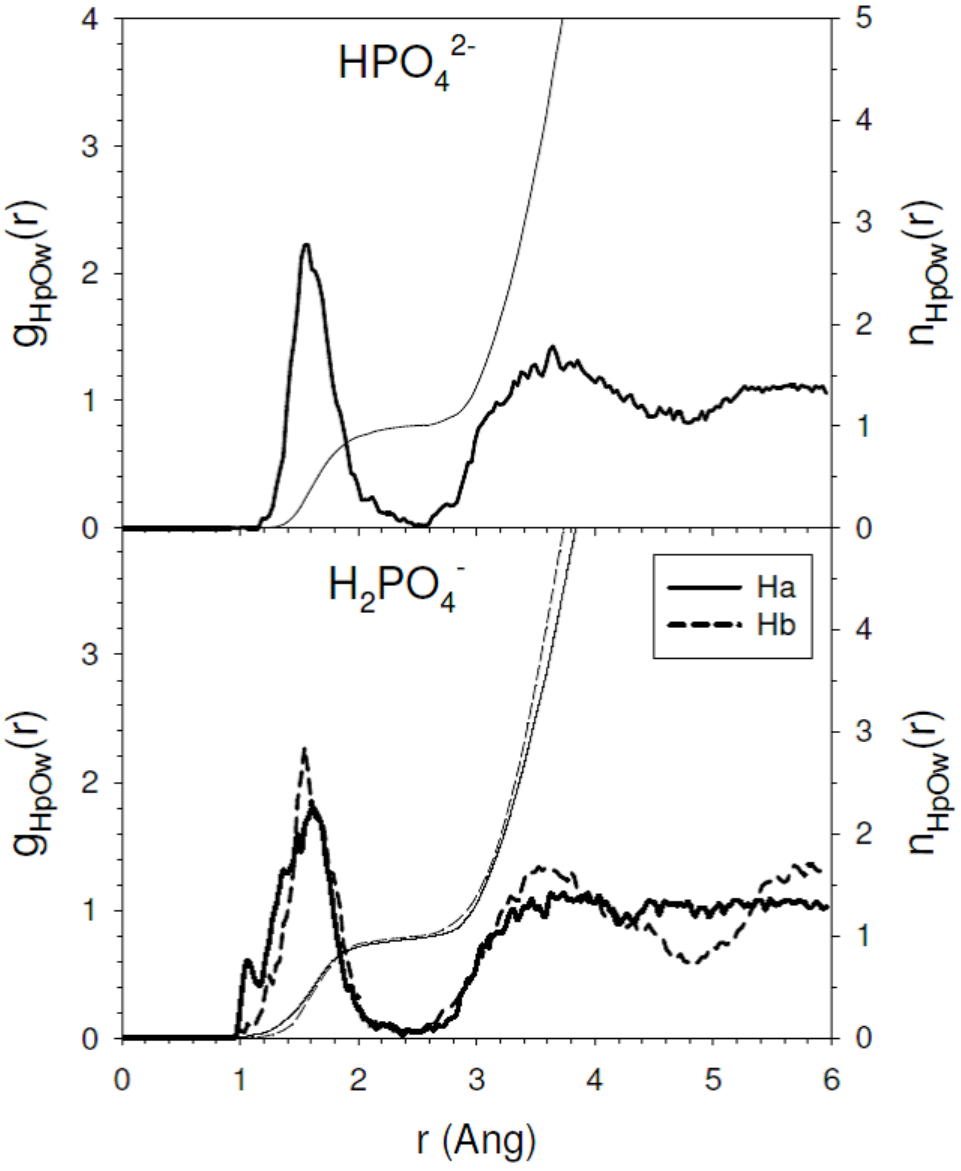

Figure 4-9 The H_p–O_w radial distribution functions, $g(r)$, and running coordination numbers, $n(r)$, for $HPO_4^{2-}$and H_2PO_4 in water obtained from the CP-MD simulations of $H_nPO_4^{3-n}$ in 51 water molecules.

The RDFs for the H_p-O_w pairs of the species HPO_4^{2-} and $H_2PO_4^-$ are reported in Figure 4-9. The running coordination number n_w^{Hp} is characterized by a clear plateau at the first minimum of the H_p-O_w RDF, showing that each H_p atom is

hydrogen-bonded to one water molecule. The values of $g_{\max}^{Hp-Ow} / g_{\min}^{Hp-Ow}$ in Table 4-3 suggest that the $H_p \cdots O_w$ interaction is stronger than the inter-molecular H-bonding in bulk water. This could explain the occurrence of H-transfer processes during the CP-MD simulations of HPO_4^{2-} and $H_2PO_4^-$ (see Figure 4-2), which are not observed for PO_4^{3-}.

Table 4-2 Coordination statistics of the phosphate network from the CP-MD simulations: Q^n distribution, network connectivity (NC), phosphorus (P) coordination and average P-O coordination numbers (CN_{av}).

	PO_4^{3-}	HPO_4^{2-}	$H_2PO_4^-$
$r_{\max}^{O1-H}$	1.64	1.84	1.84
$g_{\max}^{O1-H}$	2.75	0.64	0.61
$r_{\min}^{O1-H}$	2.36	2.29	2.42
$g_{\min}^{O1-H}$	0.04	0.20	0.16
$g_{\max}^{O1-H} / g_{\min}^{O1-H}$	68.75	3.20	3.81
n_w^{O1}	2.6	0.9	1.0
$r_{\max}^{O2-H}$	1.60	1.64	1.70
$g_{\max}^{O2-H}$	2.49	2.50	2.13
$r_{\min}^{O2-H}$	2.36	2.44	2.44
$g_{\min}^{O2-H}$	0.09	0.11	0.14
$g_{\max}^{O2-H} / g_{\min}^{O2-H}$	27.70	22.73	17.43
n_w^{O2}	2.7	2.6	2.4
$r_{\max}^{O3-H}$	1.64	1.66	1.78
$g_{\max}^{O3-H}$	3.16	2.75	0.48
$r_{\min}^{O3-H}$	2.48	2.41	2.30
$g_{\min}^{O3-H}$	0.05	0.10	0.14
$g_{\max}^{O3-H} / g_{\min}^{O3-H}$	63.20	27.50	3.43
n_w^{O3}	3.0	2.5	0.6
$r_{\max}^{O4-H}$	1.58	1.6	1.76
$g_{\max}^{O4-H}$	2.78	2.13	2.10
$r_{\min}^{O4-H}$	2.32	2.26	2.50
$g_{\min}^{O4-H}$	0.04	0.14	0.12
$g_{\max}^{O4-H} / g_{\min}^{O4-H}$	69.5	15.21	17.50
n_w^{O4}	2.3	2.3	2.4

Table 4-3 Positions $r_{\max}^{Hp-Ow}$, $r_{\min}^{Hp-Ow}$ (Å) and amplitudes $g_{\max}^{Hp-Ow}$, $g_{\min}^{Hp-Ow}$ of the maxima and minima of the second peak of the H_p–O_w radial distribution functions, and first shell hydration number n_w obtained from the CP-MD simulations of HPO_4^- and $H_2PO_4^{2-}$ in 51 water molecules.

	HPO_4^{2-}	$H_2PO_4^-$
$r_{\max}^{Ha-Ow}$	1.57	1.60
$g_{\max}^{Ha-Ow}$	2.22	1.80
$r_{\min}^{Ha-Ow}$	2.56	2.35
$g_{\min}^{Ha-Ow}$	0.02	0.03
$g_{\max}^{Ha-Ow} / g_{\min}^{Ha-Ow}$	111.00	78.33
n_w^{Ha}	1.0	1.0
$r_{\max}^{Hb-Ow}$		1.54
$g_{\max}^{Hb-Ow}$		2.27
$r_{\min}^{Hb-Ow}$		2.35
$g_{\min}^{Hb-Ow}$		0.05
$g_{\max}^{Hb-Ow} / g_{\min}^{Hb-Ow}$		45.4
n_w^{Hb}		1.0

In summary, the information obtained from the pair correlation functions of the $H_nPO_4^{3-n}$ species in water are: (i) the P–O^- moieties have between 2.5 – 3 H-bonds; (ii) the P–OH moieties have approximately ~ 1 H-bonds each; (iii) the order of the H-bond strength for the oxygen atoms of the phosphate anions compared with bulk water is: P–O^-···H_w > O_w···H_w > P–O(H)···H_w; (iv) the H-transfer process of the hydrogenated phosphates in water is due to the fact that the H_p···O_w interactions are considerably stronger than the H_w···O_w in bulk water.

4.5 Chapter conclusion

The results of this chapter show that the process of H-transfer from the hydrogenphosphates to the surrounding water molecules is very fast, approximately 0.1 ps, and involves a concerted proton hopping mechanism between the phosphate and three other water molecules.

For the PO_4^{3-} species, comparison of the structural correlation functions of the phosphate aqueous solution and of the pure water shows that the H-bonding network of bulk water is significantly affected by the presence of the anion. Moreover, the CP-MD simulations show a new type of H---H interaction around this orthophosphate compared to the bulk water (O_w–)H---H(–O_w) correlations, a result which is partial agreement with the experimental findings of Mason et al. (Mason, Cruickshank et al. 2003). Analysis of the $H_nPO_4^{3-n}/H_2O$ pair correlation functions indicates that, although a well defined first hydration shell (n_w 1st HS) can be located for all phosphate species (n_w 1st HS = 11 for PO_4^{3-}, 10.4 for HPO_4^{2-}, 9.4 for $H_2PO_4^-$), the probability distributions of the number of water molecules surrounding the $H_nPO_4^{3-n}$ ions show that these phosphate species display a flexible first coordination shell, where the flexibility increases on going from PO_4^{3-} to $H_2PO_4^-$.

A detailed analysis of the number and strength of hydrogen bonds between the $H_nPO_4^{3-n}$ ions and the surrounding water molecules, based on the O_p–H_w RDFs, shows that the P–O^- and the P–OH in the orthophosphate anions have approximately 2.6–3 and 1 H-bonds each, respectively. Moreover, taking the ratio $g_{\max}^{O-H} / g_{\min}^{O-H}$ from the O_p–H_w RDFs as a criterion to establish the strength of the

H···O interaction, with the $g_{\max}^{O-H} / g_{\min}^{O-H}$ for pure water as reference, we have been able to establish the order of the H-bond strength as $P–O^{-}\cdots H_w > O_w\cdots H_w > P–O(H)\cdots H_w$. For the hydrogen atoms of the phosphate species, using similar arguments we have determined that each H_p is firmly hydrogen-bonded to a single water molecule, whereas the values of $g_{\max}^{Hp-Ow} / g_{\min}^{Hp-Ow}$, which are much larger than the in pure water, explain the occurrence of H-transfer processes during the CP-MD simulations of HPO_4^{2-} and $H_2PO_4^{-}$, which are not observed in the simulated PO_4^{3-} aqueous solution.

Chapter 5 Hydration Properties of Phosphates

In this Chapter, first principles density functional theory (Perdew-Burke-Ernzerhof) calculations have been used to compute the hydration properties, aqueous-phase acid dissociation constants (pK_a) and Gibbs free energies of formation of small polyphosphates in aqueous solution. The effect of the hydrated environment has been simulated through a hybrid microsolvation-continuum approach, where the phosphate species are simulated as microsolvated solutes, while the remainder of the bulk solvent is treated as a dielectric continuum using the COSMO solvation model. The solvation free energies of orthophosphates and pyrophosphates have been computed applying *monomer* and *cluster thermodynamic* cycles, and using the geometries optimised in the gas-phase as well as in the COSMO environment.

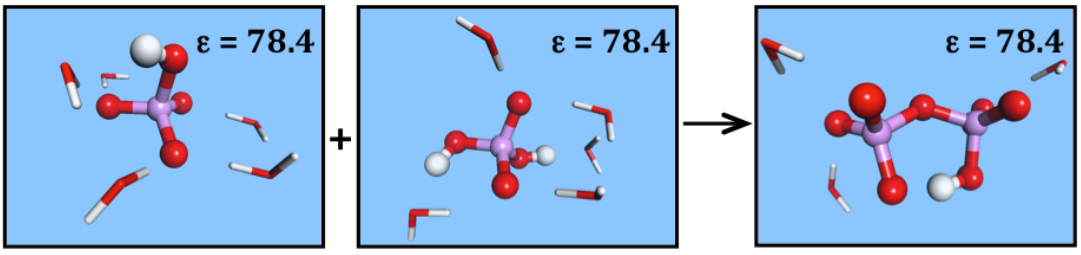

Figure 5-1 The aqueous-phase pK_a and free energies of formation of small polyphosphates in solution are computed using an optimised microsolvation-continuum approach.

5.1 Chapter Introduction

Phosphates play a critical role in a range of cellular functions involving metabolism and mechanisms of energy-transfer, for example in the production of adenosine-5'-triphosphate (ATP). They are also vital components of RNA and DNA and essential constituents in bone mineralization. (Stryer 1988; Voet 1995; Takeda, Taketani et al. 2004) Due to the intrinsic importance of phosphate species in human biology, in the last decade phosphate-based bioactive glasses (PBGs) have become topical materials for scientists and engineers working in the field of biomaterials and tissue engineering (Knowles 2003).These glasses, containing phosphorus pentoxide (P_2O_5) as a network former and sodium oxide (Na_2O) and calcium oxide (CaO) as network modifiers, have been classified as 'Third Generation' biomaterials owing to their ability to assist the process of tissue regeneration. (Hench and Polak 2002) Moreover, PBGs are readily degradable in aqueous media and have the unique advantage that their dissolution rates can be controlled by altering the composition of the phosphate-sodium-calcium glass in order to suit the specific application. (Ahmed, Lewis et al. 2004) To exploit the potentials of PBGs as a bioactive implant material for tissue regeneration, several studies have investigated their compositional dissolution behaviour. (Bitar, Salih et al. 2004; Gao, Tan et al. 2004; Gao, Tan et al. 2004; Ahmed 2005; Ahmed, Lewis et al. 2005; Ahmed, Parsons et al. 2008) In this context, the main issues that have emerged unresolved from these studies were the identification of type of phosphate species released during the dissolution process, and whether the ions and phosphate groups chemically interact with the surrounding water to form different species. (Ahmed 2005; Ahmed, Lewis et al. 2005) Additionally, since it is not clear which ions or

groups of ions are dissolved from the glass into the solution, the aim of this work is also to identify which ion clusters will be most likely to exist as independent hydrated species, and which polyphosphate species could form spontaneously in solution.

Ab initio and Density Functional Theory (DFT) computational methods have already been used successfully to model the condensation reactions in solution of species like silica clusters, (Pereira 1998; Miguel J. Mora-Fonz 2005; Schaffer and Thomson 2008) where the effect of the solvent is considered through a polarisable continuum solvation model (PCM). Here, we therefore report a study on the use of these DFT methods to investigate the formation in solution of small polyphosphate species. In particular, the effect of solution is described through a hybrid microsolvation-continuum approach (Mora-Fonz, Catlow et al. 2007; Zhang l 2007), where the phosphate species are considered as microsolvated solutes, i. e. $H_xPO_4^{3-x}(H_2O)_n$ with x = 0-3 and n = 0-6, while the remainder of the bulk solvent is treated as a dielectric continuum. Within this framework, the hydration free energies of the phosphates have been computed to identify the stability of these species present in solution and to evaluate the free energies of condensation reactions to form polyphosphates.

It is important to recognize that for species like $H_xPO_4^{3-x}$, and polyphosphates in general, the calculation of accurate values of the hydration free energies is a challenging task, because continuum dielectric solvent models are often inadequate when dealing with ionic solutes that have concentrated charge densities with strong local solute-solvent interactions. (Chipman 2003; Chipman and Chen 2006) To overcome this problem, it has become a common practice to

attach some water molecules to the ionic species (Martin, Hay et al. 1998; Pliego and Riveros 2001; Zhan and Dixon 2001; Pliego and Riveros 2002; Mora-Fonz, Catlow et al. 2007; Bryantsev, Diallo et al. 2008). Nevertheless, questions remain on the minimum number of water molecules that should be included in the calculation. For ions with well-defined coordination numbers, like Ca^{2+} and Zn^{2+}, the optimum micro-hydration number n_{H_2O} is usually equal to the number of solvent molecules in the first coordination shell.(Parchment, Vincent et al. 1996; Tommaso and de Leeuw 2008) However, ionic species like $H_xPO_4^{3-x}$ are characterised by multiple and very flexible first hydration shells, (Tang, Di Tommaso et al. 2009) and the hydrated phosphate clusters $H_xPO_4^{3-x}(H_2O)_n$ should probably include a relatively large number of explicit water molecules to achieve a converged value of the solvation free energy. This would consequently introduce the problem of determining the low energy conformers of the hydrated clusters, thus increasing the cost and complexity of the computation. Therefore, when applying the cluster-continuum method to compute free energies of reaction in solution, there is no clear prescription regarding the number of water molecules that should be added to ionic species like $H_xPO_4^{3-x}$.

Under these circumstances, we have investigated the effect of the number of water molecules included in the hydrated orthophosphates $H_xPO_4^{3-x}(H_2O)_n$, pyrophosphates $H_xP_2O_7^{4-x}(H_2O)_n$ and triphosphates $H_xP_3O_4^{5-x}(H_2O)_n$ on the computed values of the solvation free energies, aqueous-phase acid dissociation constants (pK_a) and Gibbs free energies of condensation reactions. In fact, one of the aims of the present study was to assess the performance of polarisable continuum models to compute accurate free energies of condensation reactions

involving charged species like phosphates, and the development of a methodology based on the cluster-continuum approach, which would be able to model the formation of polyphosphate species in an aqueous environment.

In this chapter, having described the details of DFT cluster-continuum calculations in the methodological section, we consider the hydration properties of the ortho- and pyro- phosphates in aqueous solutions by discussing the calculation of the solvation free energies and the aqueous-phase acid dissociation constants. We then present the Gibbs free energies of formation of the pyro- and tri-phosphates species and the dependence of their accuracy on the number of explicit water molecules included in the microsolvation model.

5.2 Methodology

5.2.1 Electronic Structure Calculations

All DFT calculations were performed using the DMol^3 code. (Delley 1990; Delley 2000; Delley 2000) DMol^3 implements DFT using localised atom-centred numerical orbitals. The electronic structure was described using the Perdew-Burke-Ernzerhof (PBE)(Perdew, Burke et al. 1996) approximation and all-electron double-numeric-polarised (DNP) basis sets on all atoms. This basis set is variationally comparable to the 6-31G(d,p) basis set, but the numerical functions are far more complete than the traditional Gaussian functions. Owing to the quality of these orbitals, basis set superposition effects are minimized, (Delley 1990; Delley 2000) and it is possible to obtain an excellent description, even of weak bonds. (Di Tommaso and De Leeuw 2009) Each basis function was restricted to a large cutoff radius of Rcut = 6.2 Å in order to describe properly the diffuse nature of the wave-function of the phosphate anions. The electron density was approximated using a multi-polar expansion up to octupole. The minimum character of all optimised gas-phase structures was verified by evaluation of the harmonic vibrational frequencies. Gas-phase vibrational, rotational and translational contributions to the free energy (G_{VRT}) were computed on the basis of these frequencies and the ideal-gas partition functions $q(p,T)$, applying standard statistical mechanical formulae (McQuarrie D. A. 2000) at the conditions of T = 298 K and p = 1 atm.

To ensure that the initial models of the triphosphate species were not trapped in a local minimum, we have also performed *ab initio* molecular dynamics (AIMD) simulations using the SIESTA 2.0.1 code. (Soler 2002) The electronic structure was described using the Perdew-Zunger local density approximation, (Perdew 1981)

with the Troullier-Martins pseudopotentials (Troullier and Martins 1991) to represent the core-valence interactions, and single numeric basis sets with a cut-off of 30 Ryd were used to describe the valence electrons. The search for the initial structures of triphosphates was conducted by performing the following series of AIMD simulations: i) 2 ps at 300K; ii) 2 ps from 300 K up to 800 K; iii) 2 ps at 800 K; iv) cooling down from 800 K to 300 K for 5 ps with a cooling rate of 100 K/ps. The final configuration from these AIMD simulations were then optimised both in the gas-phase and in the solvation environment.

5.2.2 Solvation Model

The effect of the bulk water was estimated using the Conductor-like Screening Model (COSMO) (Klamt and Schuurmann 1993; Klamt 1995) variation of the self-consistent reaction field model. (Tomasi 2002; Tomasi, Mennucci et al. 2005) To compute the hydration energies of the $H_xPO_4^{3-x}(H_2O)_n$ species at ambient conditions we have used a dielectric constant ε = 78.4, which corresponds to water at 300 K. The value of ΔG^*_{solv}, computed using quantum mechanical continuum solvation models like COSMO, is critically dependent on two factors: (i) the quantum mechanical level used to describe the solute charge distribution; (ii) the choice of the solute cavity. (Takano and Houk 2004) We have therefore tested the effect of these two parameters on the values of the solvation free energy of the orthophosphate species $H_xPO_4^{3-x}$. Table 5-1 reports the values of ΔG^*_{solv}, computed using the COSMO model as implemented in the DMol^3 (COSMO) and Gaussian03 (Frisch, Trucks et al. 2004) (CPCM) codes. The solvation free energies have been obtained on the geometries optimised in the polarisable continuum models.

Table 5-1 Solvation free energies of the orthophosphate $H_nPO_4^{3-n}$ species computed using the COSMO model and at the various levels of theory. Calculations performed on the geometries optimised in the polarisable continuum model. Values in kcal/mol.

	PBE			PBE0			HF		
Species	**DNP - COSMO**	**TNP - COSMO**	**aug-cc-pVTZ - UAKS/CPCM**	**6-31G(d) - UAKS/CPCM**	**aug-cc-pVTZ - UAKS/CPCM [a)]**	**6-31G(d) - UAHF/CPCM**	**aug-cc-pVTZ - UAHF/CPCM [a)]**	**6-31+G(d,p) - UAKS/CPCM**	**Exp.**
PO_4^{3-}	-523.2	-509.0	-491.0	-538.2	-502.9	-521.9	-501.4	-518	-637 [b)]
HPO_4^{2-}	-237.2	-232.6	-226.5	-239.5	-229.9	-233.3	-227.8	-239	-299 [b)]
$H_2PO_4^-$	-67.2	-66.5	-66.4	-69.3	-68.1	-68.0	-66.8	72.8	-68 [c)]
H_3PO_4	-12.7	-12.6	-14.4	-15.5	-15.0	-16.3	-15.6	-18.1	

[a)] The geometries were optimised using the 6-31G(d) basis set. [b)] George et al., *Biochim. Biophys. Acta* 1970, **223**, 1. [c)] Li et al., *Theor. Chem. Acc.* 1999, **103**, 9.

For the DMol^3 calculations, we employed the PBE functional with the double-numeric-polarised (DNP) and triple-numeric polarised (TNP) basis sets for all atoms (cutoff radius of 6.2 Å for both basis sets). In order to build the molecular shape cavity in the COSMO calculations we have used the optimised Klamt atomic radii of 1.30 Å for hydrogen, 1.72 Å for oxygen and 2.12 Å for phosphorus, which were optimised using the DNP basis set. (Andzelm, Kolmel et al. 1995) In this respect, the values in Table 5-1 show that increasing the size of the basis set from DNP to TNP does not improve the values of the solvation free energies compared with experiment, as usually happens in gas-phase calculations.

For the Gaussian03 calculations, we have employed different methods [PBE, PBE0 (Adamo and Barone 1999) and HF] and basis sets [6-31G(d,p), 6-31+G(d,p), aug-cc-pVTZ], whereas the molecular cavities were generated using the united atom topological model applied on radii optimized for the PBE0/6-31G(d) level of theory (UAKS) or applied on radii optimized for the HF/6-31G(d) (UAHF). Takano and Houk (Takano and Houk 2004) have extensively benchmarked the CPCM model, which is the implementation of the conductor-like screening ansatz COSMO in the framework of the PCM model, for the calculation of the aqueous solvation free energies of neutral, cationic and anionic species, and their calculations suggested that the HF/6-31+G(d)//HF/6-31+G(d) level of theory with the UAKS cavities was the method providing best agreement with the experimental data.

The results in Table 5-1 indicate that the computation of the solvation free energies at the PBE/aug-cc-pVTZ level is considerably worse than the one computed at the PBE/DNP level. The difference is probably also related to the

united atom topological model used to build the molecular shape cavity in the COSMO calculations, which was fitted to the PBE0/6-31G(d)method. In fact, the PBE0/6-31G(d) – UAKS/CPCM and the HF/6-31G(d) – UAHF/CPCM models give better agreement with the experiment. Therefore, the use of more extended basis sets (aug-cc-pVTZ) in the calculation of solvation free energies for which, however, the model used to build the cavity has not been optimized, does not guarantee better agreement with the experimental solvation free energies of the phosphate species, especially for the more highly charged species. Therefore, the calculations of the solvation free energies of the bare and hydrated phosphate species have been performed at the PBE/DNP level of theory.

To compute the solvation free energies ΔG^{*}_{solv} of the $H_xPO_4^{3-x}$ species we have used the *monomer* and *cluster* thermodynamic cycles. (Bryantsev, Diallo et al. 2008) (see 2.5.2.2 Solvation Free Energy Scheme)

5.2.3 Condensation Reactions In Aqueous Solution

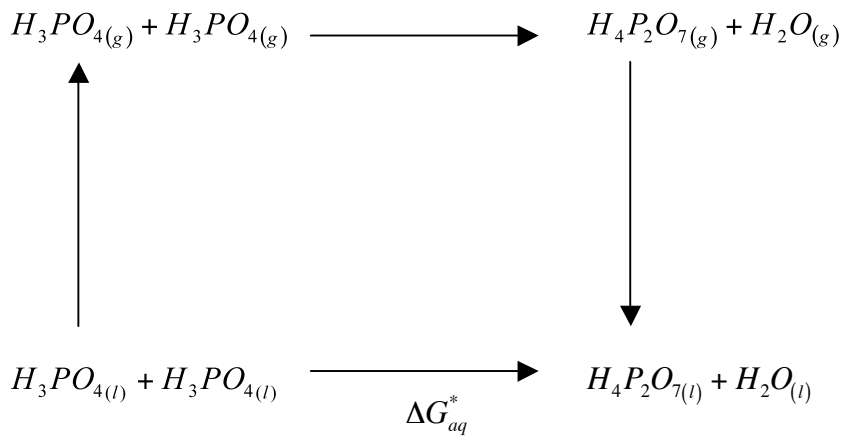

Scheme 5-1

The formation of the pyrophosphate $H_xP_2O_7^{4-x}$, x = 1-4, and the triphosphate $H_xP_3O_{10}^{5-x}$, x = 1-5, species in aqueous solution has been modelled using thermodynamic cycles like the one presented in Scheme 5-1. The free energy change for the condensation reactions in aqueous solution is then given by the following equation:

$$\Delta G^*_{aq} = \Delta E_e + \Delta G^O_{VRT} + \Delta\Delta G^*_{solv} \tag{5-1}$$

where ΔE_e is the gas-phase total electronic energy change at 0 K and ΔG^O_{VRT} is the gas-phase vibrational, rotational and translational contribution to the free energy at a fixed temperature and pressure, whereas the term $\Delta\Delta G^*_{solv}$ in Equation (5-1) is the sum of the solvation free energies of the products minus that for the reactants, i.e. $\Delta\Delta G^*_{solv} = \sum_P \Delta G^*_{solv}(P) - \sum_R \Delta G^*_{solv}(R)$. Note that the solvation energy contributions $\Delta G^*_{solv}\left(H_xPO_4^{3-x}\right)$, $\Delta G^*_{solv}\left(H_xP_2O_7^{4-x}\right)$ and $\Delta G^*_{solv}\left(H_xP_3O_{10}^{5-x}\right)$ have been computed using the microsolvation-continuum approach on the optimized structures in solution. Reliable estimates of ΔG^*_{aq} will depend on the accurate determination of each term in Equation (5-1).

5.3 Hydration Free Energies of Ortho- and Pyro-phosphates

In this section, we will discuss the calculation of the hydration free energies ΔG^*_{solv} of the orthophosphates $H_xPO_4^{3-x}$ and pyrophosphates $H_xP_2O_7^{4-x}$ species. The aim is to investigate the effect of the number of explicit water molecules n_{H_2O} used in the microsolvation-continuum approach, and if it is possible to determine the optimal n_{H_2O} that provides the most accurate value of the solution energy term $\Delta\Delta G^*_{solv}$ (Equation (5-1)). After all, a reliable estimate of the Gibbs free energy of condensation reaction ΔG^*_{aq} depends mostly on the accuracy of the solvation contribution $\Delta\Delta G^*_{solv}$. (Parchment, Vincent et al. 1996; Tommaso and de Leeuw 2008)

The free energies of solvation of the orthophosphate species are calculated using the monomer (Figure 2-2) and cluster (Figure 2-3) thermodynamical cycles. The gas-phase and solvent-phase contributions to $\Delta G^*_{solv}(S)$ calculated using the monomer and cluster thermodynamic cycles are listed in Table 5-2 and Table 5-3, respectively. In order to investigate the effect of re-optimisation in solution, the hydration free energies have been computed on the geometries optimised in the gas phase as well as in the COSMO environment. We note that the values of ΔG^*_{solv} obtained by applying the monomer and cluster cycles on the hydrated clusters $H_nPO_4^{3-n}(H_2O)_w$, $n_{H_2O} \leq 5$, differ by less than 1 kcal/mol. Based on this observation, we have adopted the monomer thermodynamic cycle (Figure 2-2) for all our further solvation free energy discussions.

Table 5-2 Solvation free energies of the orthophosphate $H_nPO_4^{3-n}$ species obtained using the *monomer* thermodynamic cycle. Gas-phase free energy contributions computed at the PBE/DNP level and solvation free energies computed at the COSMO/PBE/DNP level. Values in kcal/mol.

		Gas-Phase Optimised Geometry			COSMO Optimised Geometry			
Species	$\Delta G_{clust}(S(H_2O)_n)$	$n\Delta G_{vap}(H_2O)$ [a]	$\Delta G^*_{solv}(S(H_2O)_n)$	$\Delta G^*_{solv}(S)$	$n\Delta G_{vap}(H_2O)$ [b]	$\Delta G^*_{solv}(S(H_2O)_n)$	$\Delta G^*_{solv}(S)$	**Expt.**
PO_4^{3-}				-531.7			-523.2	-637 [c]
$PO_4^{3-}(H_2O)_2$	-89.8	2.0	-471.1	-558.9	1.2	-448.0	-536.6	
$PO_4^{3-}(H_2O)_3$	-123.2	3.0	-455.8	-576.0	1.8	-418.9	-540.3	
$PO_4^{3-}(H_2O)_4$	-151.0	4.0	-446.5	-593.5	2.4	-396.7	-545.3	
$PO_4^{3-}(H_2O)_5$	-173.2	5.0	-437.0	-605.2	3.0	-375.9	-546.1	
HPO_4^{2-}				-240.1			-237.2	-299 [c]
$HPO_4^{2-}(H_2O)$	-24.4	1.0	-213.5	-236.9	0.6	-217.4	-241.2	
$HPO_4^{2-}(H_2O)_2$	-43.4	2.0	-199.9	-241.3	1.2	-201.0	-243.2	
$HPO_4^{2-}(H_2O)_3$	-58.8	3.0	-187.9	-243.7	1.8	-187.1	-244.1	
$HPO_4^{2-}(H_2O)_4$	-69.3	4.0	-178.0	-243.3	2.4	-179.6	-246.5	
$HPO_4^{2-}(H_2O)_5$	-77.6	5.0	-173.0	-245.6	3.0	-176.7	-251.3	
$H_2PO_4^-$				-69.3			-67.2	-68 [d]
$H_2PO_4^-(H_2O)$	-5.8	1.0	-64.3	-69.1	0.6	-64.3	-69.5	
$H_2PO_4^-(H_2O)_2$	-11.7	2.0	-61.1	-70.8	1.2	-61.1	-71.6	
$H_2PO_4^-(H_2O)_3$	-14.3	3.0	-58.7	-70.0	1.8	-58.1	-70.6	
$H_2PO_4^-(H_2O)_4$	-14.7	4.0	-57.0	-67.7	2.4	-58.6	-70.9	
$H_2PO_4^-(H_2O)_5$	-20.0	5.0	-54.4	-69.4	3.0	-57.7	-74.7	
H_3PO_4				-13.7			-12.7	
$H_3PO_4(H_2O)$	-3.1	1.0	-58.5	-60.6	0.6	-13.5	-16.0	
$H_3PO_4(H_2O)_2$	-5.5	2.0	-53.4	-56.9	1.2	-15.0	-19.3	
$H_3PO_4(H_2O)_3$	-3.8	3.0	-57.5	-58.3	1.8	-16.2	-18.2	
$H_3PO_4(H_2O)_4$	-5.9	4.0	-52.5	-54.4	2.4	-17.1	-20.6	
$H_3PO_4(H_2O)_5$	-3.6	5.0	-54.7	-53.3	3.0	-20.8	-21.4	

[a] The solvation free energy of the water molecule, $\Delta G^*_{solv}(H_2O)$, computed on the gas-phase optimised geometry is -5.2 kcal mol^{-1} and taking [H_2O] = 55.5 mol L^{-1} then eq 2 gives $\Delta G^*_{vap}(H_2O)$ of 1.0 kcal mol^{-1}. [b] The solvation free energy of the water molecule, $\Delta G^*_{solv}(H_2O)$, computed on the COSMO optimised geometry is -4.8 kcal mol^{-1} and taking [H_2O] = 55.5 mol L^{-1} then Eq. 2 gives a vaporization energy $\Delta G^*_{vap}(H_2O)$ of 0.6 kcal mol^{-1}. [c] George et al., *Biochim. Biophys. Acta* 1970, **223**, 1. [c] Li et al., *Theor. Chem. Acc.*, 1999, **103**, 9.

The effect of geometry re-optimisation in solution on the solvation energy term $\Delta G^*_{solv}(S(H_2O)_n)$ increases with the degree of micro-hydration *n* (see Table 5-2 and Table 5-3), but the magnitude of variation of the solvation free energy on going from the optimised gas-phase structure to the optimised aqueous-phase structure depends also on the particular orthophosphate species. The PO_4^{3-} ion displays the largest variations in the solvation free energy: on going from the gas- to the liquid-phase optimised structure the value of $\Delta G^*_{solv}(PO_4^{3-}(H_2O)_n)$ changes by 8.5 kcal/mol for n_{H_2O}= 0, and by 59 kcal/mol for n_{H_2O}= 5. On the other hand, the solvation free energies of the HPO_4^{2-} and $H_2PO_4^-$ ions are much less sensitive to the geometry re-optimisation, as $\Delta G^*_{solv}(S(H_2O)_n)$ changes by only 0-3 kcal/mol (see Table 5-1 and Table 5-2).

Table 5-3 Solvation free energies of the hydrated $H_nPO_4^{3-n}$ species obtained using the *cluster* thermodynamic cycle. Gas-phase free energy contributions computed at the PBE/DNP level and solvation free energies computed at the COSMO/PBE/DNP level. Values in kcal mol^{-1}.

		Gas-Phase Optimised Geometry			COSMO Optimised Geometry			
Species	**$\Delta G_{clust}(S(H_2O)_n)$**	**$\Delta G^*_{solv}(S(H_2O)_n)$**	**$\Delta G^*_{solv}((H_2O)_n)$**	**$\Delta G^*_{solv}(S)$**	**$\Delta G^*_{solv}(S(H_2O)_n)$**	**$\Delta G^*_{solv}((H_2O)_n)$**	**$\Delta G^*_{solv}(S)$**	**Expt.**
PO_4^{3-}				-531.7			-523.2	637[a]
$PO_4^{3-}(H_2O)_2$	-93.2	-471.1	-9.2	-558.2	-448.0	-8.4	-535.9	
$PO_4^{3-}(H_2O)_3$	-126.5	-455.8	-9.7	-575.2	-418.9	-8.6	-539.5	
$PO_4^{3-}(H_2O)_4$	-153.2	-446.5	-9.5	-592.7	-396.7	-7.9	-544.5	
$PO_4^{3-}(H_2O)_5$	-178.1	-437.0	-13.0	-604.5	-375.9	-11.1	-545.3	
HPO_4^{2-}				-240.1			-237.2	299[a]
$HPO_4^{2-}(H_2O)$	-24.4	-213.5	-5.2	-236.9	-217.4	-4.8	-241.3	
$HPO_4^{2-}(H_2O)_2$	-46.8	-199.9	-9.2	-240.6	-201.0	-8.4	-242.5	
$HPO_4^{2-}(H_2O)_3$	-62.0	-187.9	-9.7	-242.9	-187.1	-8.6	-243.2	
$HPO_4^{2-}(H_2O)_4$	-71.6	-178.0	-9.5	-242.6	-179.6	-7.9	-245.8	
$HPO_4^{2-}(H_2O)_5$	-82.5	-173.0	-13.0	-244.9	-176.7	-11.1	-250.5	
$H_2PO_4^-$				-69.3			-67.2	-68[b]
$H_2PO_4^-(H_2O)$	-5.8	-64.3	-5.2	-69.1	-64.3	-4.8	-69.5	
$H_2PO_4^-(H_2O)_2$	-15.2	-61.1	-9.2	-70.2	-61.1	-8.4	-71.0	
$H_2PO_4^-(H_2O)_3$	-17.5	-58.7	-9.7	-69.2	-58.1	-8.6	-69.7	
$H_2PO_4^-(H_2O)_4$	-17.0	-57.0	-9.5	-67.0	-58.6	-7.9	-70.2	
$H_2PO_4^-(H_2O)_5$	-25.0	-54.4	-13.0	-68.7	-57.7	-11.1	-74.0	
H_3PO_4		-13.7		-13.7	-12.7		-12.7	
$H_3PO_4(H_2O)$	-3.1	-58.5	-5.2	-60.7	-13.5	-4.8	-16.1	
$H_3PO_4(H_2O)_2$	-9.0	-53.4	-9.2	-56.2	-15.0	-8.4	-18.7	
$H_3PO_4(H_2O)_3$	-7.0	-57.5	-9.7	-57.5	-16.2	-8.6	-17.3	
$H_3PO_4(H_2O)_4$	-8.1	-52.5	-9.5	-53.6	-17.1	-7.9	-19.8	
$H_3PO_4(H_2O)_5$	-8.5	-54.7	-13.0	-52.6	-20.8	-11.1	-20.6	

[a] George et al., *Biochim. Biophys. Acta* 1970, **223**, 1. [b] Li et al., *Theor. Chem. Acc.*, 1999, **103**, 9.

The observed behaviour could be explained in terms of the strength of the hydrogen bonds between the orthophosphates and the surrounding water molecules, and the flexibility of their first hydration shell structures (Tang, Di Tommaso et al. 2009). Previous Car–Parrinello molecular dynamics (CP-MD) simulations of the orthophosphate $H_nPO_4^{3-n}$ species in explicit water have shown that the strength of the inter-molecular $H_nPO_4^{3-n} - H_2O$ hydrogen bonds decreases on going from PO_4^{3-} to $H_2PO_4^-$ (Tang, Di Tommaso et al. 2009). Consequently, the structural rearrangement of the hydrated orthophosphates $H_xPO_4^{3-x}(H_2O)_n$ from the gas- to the liquid-phase is more important for the PO_4^{3-} hydrated clusters than for the hydrogen-phosphates. The solvation free energy $\Delta G^*_{solv}(S)$ of the species $H_2PO_4^-$ computed on the bare ion, -67.2 kcal/mol, or on the single hydrated cluster, -69.5 kcal/mol, are in good agreement with the experimental value of -68 kcal mol^{-1}. (Li, Zhu et al. 1999) However, the values of the hydration energy of HPO_4^{2-} (-299 kcal/mol) and PO_4^{3-} (-637 kcal/mol) estimated by George et al. (George, Witonsky et al. 1970) suggest that the solvation energies computed by us differ significantly from the experimental estimate.

Table 5-4 Average values of the ratio $g_{\max}^{O_p-H_w} / g_{\min}^{O_p-H_w}$ obtained from CP-MD simulations of the orthophosphate species $H_nPO_4^{3-n}$, and of the molecules H_2O and HCO_3^- in water, together with the solvation free energies of these species computed at the COSMO/PBE/DNP level.

Species	$\left\langle g_{\max}^{O_p-H_w} / g_{\min}^{O_p-H_w} \right\rangle$	**$\Delta G^*_{solv}(S)$ [kcal mol^{-1}]**	**Exp. ΔG^*_{solv} [kcal mol^{-1}]**
H_2O	15.7	-5.2	-6.3 [a]
$H_2PO_4^-$	10.5	-67.2	-68 [b]
HPO_4^{2-}	24.4	-237.2	-299 [c]
PO_4^{3-}	57.3	-523.2	-637 [c]
HCO_3^-	7.6	-70.5	-81.5 [d]

[a] Pliego and Riveros, 2002, **106**, 7434. [b] Li et al., *Theor. Chem. Acc.*, 1999, **103**, 9. [c] George et al., *Biochim. Biophys. Acta*, 1970, **223**, 1. [d] Z. Peng and K. M. Merz, Jr. *J. Am. Chem. Soc.* 1992, **114**, 2733.

In our previous CP-MD study of the hydration properties of $H_nPO_4^{3-n}$, (Tang, Di Tommaso et al. 2009) the ratio $g_{\max}^{O_p-H_w} / g_{\min}^{O_p-H_w}$ between the maxima $g_{\max}^{O_p-H_w}$ and minima $g_{\min}^{O_p-H_w}$ of the radial distribution functions (RDFs) of the oxygens of the orthophosphates with the hydrogens of the surrounding water (O_p–H_w) was used as the criterion to establish the strength of the hydrogen-bonding interactions between the O_p–H_w pairs. We have reported in Table 5-4 the average values of the ratio $\left\langle g_{\max}^{O_p-H_w} / g_{\min}^{O_p-H_w} \right\rangle$ together with the computed and experimental solvation free energies of the species $H_nPO_4^{3-n}$ and, for comparison, of the molecules H_2O and HCO_3^-. Note that the solvation energies of H_2O and $H_2PO_4^-$ computed by the COSMO model are in good agreement with experiment. Moreover, the value of the ratios $\left\langle g_{\max}^{O_p-H_w} / g_{\min}^{O_p-H_w} \right\rangle$ obtained for H_2O (15.7) and $H_2PO_4^-$ (10.5) are similar, which suggest that the strength of the hydrogen bonds between $H_2PO_4^-$ and the surrounding water molecules is comparable to the hydrogen-bonded interactions between the water molecules in the bulk solvent. However, the values of $\left\langle g_{\max}^{O_p-H_w} / g_{\min}^{O_p-H_w} \right\rangle$ for PO_4^{3-} (57.3) and HPO_4^{2-} (24.4) indicate that the hydrogen-bonding interactions between phosphate-water in these species are considerably larger than in the bulk water, and we note that the solvation free energies of PO_4^{3-} and HPO_4^{2-} differ considerably from the estimated experimental results.

We could therefore suggest that the ability of polarisable continuum solvation models to compute accurate solvation energies depends on the degree of perturbation of the hydrogen-bonding interactions between the water molecules and the solute compared to the bulk water. In Table 5-4 we have also reported the value

of $\left\langle g_{\max}^{O_p-H_w} \middle/ g_{\min}^{O_p-H_w} \right\rangle$ and the solvation free energies of HCO_3^-, (Peng and Merz 1992) which partially support our conclusions, in that its $\left\langle g_{\max}^{O_p-H_w} \middle/ g_{\min}^{O_p-H_w} \right\rangle$ value also deviates from that of H_2O and its ΔG_{solv} deviates in a similar way from the experimental value as $H_2PO_4^-$.

Table 5-5 reports the free energies of solvation of the pyrophosphate species and the various gas-phase and solvent phase contributions, calculated using the monomer thermodynamic cycles and the geometries optimised in the COSMO solvation environment. The comparison between the computed and estimated experimental hydration free energies of $P_2O_7^{4-}$, $HP_2O_7^{3-}$, $H_2P_2O_7^{2-}$ and $H_3P_2O_7^-$ again suggests that neither the simple COSMO model nor the cluster-continuum approach are able to compute quantitative solvation free energies for the pyrophosphates. Note, however, that the solvation free energies of the pyrophosphates $H_xP_2O_7^{4-x}$ are less dependent on the number of water molecules n_{H2O} of the microsolvated model $S(H_2O)_n$ than the value of $\Delta G^*_{solv}(S)$ of the orthophosphates: the variation of $\Delta G^*_{solv}(H_xP_2O_7^{4-x})$ with n_{H2O} is in the range of 0.5-4 %, whereas $\Delta G^*_{solv}(H_nPO_4^{3-n})$ change by 4 to 11.2 % on going from $H_nPO_4^{3-n}$ to $H_nPO_4^{3-n}(H_2O)_5$. We also note that both ortho- and pyro-phosphoric acids H_3PO_4 and $H_4P_2O_7$ display significant variations of the solvation free energies with the micro-solvation number n_{H2O}.

Table 5-5 Solvation free energies of the pyrophosphate species obtained using the *monomer* thermodynamic cycle. Gas-phase free energy contributions computed at the PBE/DNP level and solvation free energies computed at the COSMO/PBE/DNP level using the COSMO optimised geometry. Values in kcal/mol.

Species	ΔG_{clust}	$n\Delta G_{vap}(H_2O)$ [a]	$\Delta G^*_{solv}(S(H_2O)_n)$	$\Delta G^*_{solv}(S)$	Expt. [b]
$P_2O_7^{4-}$				-747.0	-584
$P_2O_7^{4-}(H_2O)$	-43.5	0.6	-708.8	-751.7	
$P_2O_7^{4-}(H_2O)_2$	-81.1	1.2	-674.9	-754.9	
$P_2O_7^{4-}(H_2O)_3$	-112.6	1.8	-645.6	-756.5	
$P_2O_7^{4-}(H_2O)_4$	-141.4	2.4	-628.5	-767.7	
$P_2O_7^{4-}(H_2O)_6$	-188.2	3.6	-594.0	-778.9	
$HP_2O_7^{3-}$				-423.9	-358
$HP_2O_7^{3-}(H_2O)$	-26.6	0.6	-399.3	-425.2	
$HP_2O_7^{3-}(H_2O)_2$	-49.2	1.2	-377.7	-425.8	
$HP_2O_7^{3-}(H_2O)_3$	-66.6	1.8	-360.7	-425.6	
$HP_2O_7^{3-}(H_2O)_4$	-78.6	2.4	-354.5	-430.9	
$HP_2O_7^{3-}(H_2O)_5$	-94.6	3.0	-342.6	-434.4	
$HP_2O_7^{3-}(H_2O)_6$	-105.4	3.6	-331.8	-433.8	
$H_2P_2O_7^{2-}$				-189.8	-134
$H_2P_2O_7^{2-}(H_2O)$	-10.8	0.6	-178.7	-188.9	
$H_2P_2O_7^{2-}(H_2O)_2$	-20.7	1.2	-168.8	-188.4	
$H_2P_2O_7^{2-}(H_2O)_3$	-27.4	1.8	-162.1	-187.8	
$H_2P_2O_7^{2-}(H_2O)_4$	-33.0	2.4	-155.8	-186.6	
$H_2P_2O_7^{2-}(H_2O)_5$	-38.0	3.0	-153.9	-189.1	
$H_2P_2O_7^{2-}(H_2O)_6$	-41.8	3.6	-150.4	-188.8	
$H_3P_2O_7^{1-}$				-60.2	-84
$H_3P_2O_7^{1-}(H_2O)$	-0.6	0.6	-65.2	-65.2	
$H_3P_2O_7^{1-}(H_2O)_2$	-4.0	1.2	-56.8	-59.7	
$H_3P_2O_7^{1-}(H_2O)_3$	-9.7	1.8	-58.2	-66.2	
$H_3P_2O_7^{1-}(H_2O)_4$	-9.8	2.4	-55.1	-62.7	
$H_3P_2O_7^{1-}(H_2O)_5$	-10.9	3.0	-54.1	-62.2	
$H_3P_2O_7^{1-}(H_2O)_6$	-8.4	3.6	-57.3	-62.3	
$H_4P_2O_7$				-13.1	
$H_4P_2O_7(H_2O)$	-6.7	0.6	-14.6	-20.8	
$H_4P_2O_7(H_2O)_2$	-4.2	1.2	-16.6	-19.7	
$H_4P_2O_7(H_2O)_3$	1.9	1.8	-21.4	-17.8	
$H_4P_2O_7(H_2O)_4$	-6.4	2.4	-21.0	-25.2	
$H_4P_2O_7(H_2O)_5$	-9.8	3.0	-22.1	-29.1	
$H_4P_2O_7(H_2O)_6$	-7.2	3.6	-29.6	-33.5	

[a] The solvation free energy of the water molecule, $\Delta G^*_{solv}(H_2O)$ computed on the COSMO optimised geometry is -4.8 kcal mol^{-1} and taking $[H_2O]$ = 55.5 mol L^{-1} then Eq. 2 gives a vaporization energy $\Delta G^*_{vap}(H_2O)$ of 0.6 kcal mol^{-1}. [b] George et al., *Biochim. Biophys. Acta* 1970, **223**, 1.

5.4 pK_as of ortho- and pyro-phosphates in water

The discussion in Section 5.3 suggests that for species like ortho- and pyro-phosphates, simple polarisable continuum models and hybrid microsolvation-continuum models are generally unable to compute accurate solvation free energies. However, the solvation free energy contribution to the reaction free energy ΔG^*_{aq}, $\Delta\Delta G^*_{solv} = \sum_P \Delta G^*_{solv}(P) - \sum_R \Delta G^*_{solv}(R)$, could be determined with sufficient accuracy through a "balanced" description of the product $\Delta G^*_{solv}(P)$ and reagent $\Delta G^*_{solv}(R)$ solvation energy terms. In this respect, let us consider the pK_a constants for the three protonation states of phosphoric acid: $H_3PO_4 \rightarrow H_2PO_4^- + H^+$ (pK_a^{exp} = 2.2); $H_2PO_4^- \rightarrow HPO_4^{2-} + H^+$ (pK_a^{exp} = 7.2); $HPO_4^{2-} \rightarrow PO_4^{3-} + H^+$ (pK_a^{exp} = 12.3). (Fasman 1976) For each proton transfer reaction, $HA \rightarrow A^- + H^+$, we have computed the pK_a values using the relation of Pearson: (Pearson 1986)

$$-\Delta G^*_{solv}\left(A^-\right) = PA - 267 + \left(-\Delta G^*_{solv}\left(HA\right)\right) - 1.36\,pK_a \qquad (5\text{-}2)$$

where PA are the gas-phase proton affinities for the proton transfer reaction $HA \rightarrow A^- + H^+$, and $\Delta G^*_{solv}(HA)$ and $\Delta G^*_{solv}(A^-)$ are the solvation free energies of the conjugate species HA/A^-. The values of $\Delta G^*_{solv}(A^-)$ and $\Delta G^*_{solv}(HA)$ have been taken from

Table 5-2, i.e. using the microsolvation-continuum approach, the monomer cycle and a degree of micro-hydration $0 \le n_{H2O} \le 5$, whereas accurate values of the

gas-phase proton affinities PA have been taken from calculations at the MP2/6-311++G(d,p) level. (Colvin, Evleth et al. 2002) The predicted pK_a of the phosphoric acids are reported and compared with experiment in Table 5-6. For the conjugate species HPO_4^{2-}/PO_4^{3-} the values of pK_a associated with $PO_4^{3-}(H_2O)_1$ are missing because this species was not stable in the gas-phase as proton transfer occurred between H_2O and PO_4^{3-} during the geometry optimisation.

Table 5-6 Aqueous-phase acid dissociation constant pK_a for the three protonation states of the phosphoric acid. Solvation free energy contributions computed at the COSMO/PBE/DNP level using the COSMO optimised geometry, the microsolvation-continuum approach and the *monomer* cycle (pK_a units).

		computed pK_a						Expt. [a]
		A^-						
HA	n_{H2O} → ↓	0	1	2	3	4	5	
H_3PO_4	0	3.2	1.5	9.8	0.7	0.4	-2.4	2.1
	1	5.6	3.9	13.4	3.1	2.9	0.1	
	2	8.0	6.3	17.0	5.5	5.3	**2.5**	
	3	7.2	5.5	15.6	4.7	4.5	1.7	
	4	9.0	7.3	17.6	6.5	6.3	3.5	
	5	9.6	7.9	20.2	7.1	6.8	4.0	
$H_2PO_4^-$	0	13.4	10.4	9.0	8.3	6.5	3.0	7.2
	1	15.1	12.1	10.7	10.0	8.2	4.7	
	2	16.6	13.7	12.2	11.5	9.8	6.2	
	3	15.9	12.9	11.5	10.8	9.0	5.5	
	4	16.1	13.2	11.7	11.0	9.3	5.7	
	5	18.9	16.0	14.5	13.8	12.1	**8.5**	
HPO_4^{2-}	0	17.8	−	8.0	5.3	1.6	1.0	12.4
	1	20.8	−	10.9	8.2	4.5	3.9	
	2	22.2	−	12.4	9.7	6.0	5.4	
	3	22.9	−	13.1	10.3	6.7	6.1	
	4	24.7	−	14.8	12.1	8.4	7.8	
	5	28.2	−	18.3	15.6	11.9	**11.4**	

[a] Fasman, G. D. Handbook of Biochemistry and Molecular Biology; CRC Press, Boca Raton, **1976**.

Table 5-6 shows that the stand-alone COSMO model [$n_{H2O}(HA) = 0$ and $n_{H2O}(A^-) = 0$] gives results in quite good agreement with the experimental pK_a only for the conjugate species H_3PO_4/H_2PO_4 (computed pK_a = 3.2; experimental pK_a = 2.1), whereas deviations from the predicted values of pK_a exceeds 5 units for the other conjugate species. Moreover, note that the computed values of pK_a depend significantly on the number of water molecules n_{H_2O} used to evaluate the term $\Delta G^*_{solv} = \Delta G^*_{solv}(A^-) - \Delta G^*_{solv}(HA)$ of eq. 6. For example, when the solvation energies of the conjugate species $H_3PO_4/H_2PO_4^-$ are computed using the combination $H_3PO_4(H_2O)_2 - H_2PO_4^-(H_2O)_5$ then we obtain a pK_a of 2.5, very close to the experimental value of 2.1. However, the pK_a does not converge as n_{H_2O} increases.

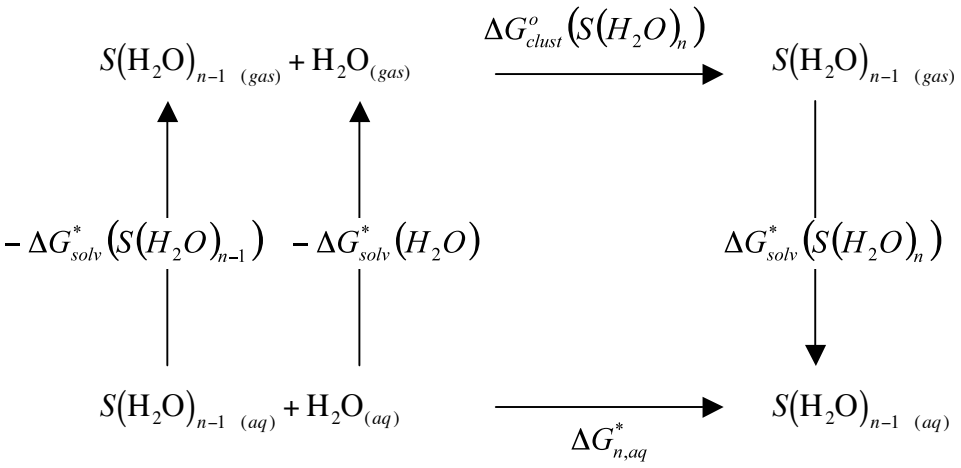

Scheme 5-2

To determine the optimum number of explicit water molecules in the hydrated cluster $S(H_2O)_n$ for the purpose of application of the microsolvation-continuum approach, we have computed the "incremental" water-binding free energy ($\Delta G^*_{n,aq}$) associated with the process of adding a water molecule to a micro-solvated phosphate:

$$S(H_2O)_{n-1} + H_2O \rightarrow S(H_2O)_n \tag{5-3}$$

The value of n which gives the largest negative value of $\Delta G^*_{n,aq}$ is then considered as the optimal number of H_2O to be used in the evaluation of the hydration free energies for the calculation of pK_a (equation (5-2)). Using the thermodynamic cycle in Scheme 5-3, $\Delta G^*_{n,aq}$ can be computed via the following expression:

$$\Delta G^*_{n,aq} = \Delta G^o_{clust}\left(S(H_2O)_n\right) + \Delta G^*_{solv}\left(S(H_2O)_n\right) - \Delta G^*_{solv}\left(S(H_2O)_{n-1}\right) - \Delta G^*_{solv}(H_2O) - \Delta G^{o\rightarrow *} \tag{5-4}$$

where $\Delta G^*_{solv}(X)$ are the hydration free energies of the species X = $S(H_2O)_n$, $S(H_2O)_{n-1}$ and H_2O; $\Delta G^o_{clust}\left(S(H_2O)_n\right)$ is the gas-phase free energy for the reaction $S(H_2O)_{n-1} + H_2O \rightarrow S(H_2O)_n$, and $\Delta G^{o\rightarrow *}$ is the free energy associated with moving a standard state that uses a concentration of 1 atm in the gas-phase and 1 mol L^{-1} in the liquid phase (denoted by "°"), to a standard state that uses a concentration of 1 mol L^{-1} in both the gas- and liquid phases (denoted by "*"). At the conditions of T = 298 K, $\Delta G^{o\rightarrow *}$ is equal to 1.89 kcal mol^{-1}. (Kelly 2006)

Table 5-7 Incremental water binding free energy ($\Delta G^{*}_{n\,aq}$) of the orthophosphate clusters. Gas-phase free energy contributions computed at the PBE/DNP level, and solvation free energies computed at the COSMO/PBE/DNP using the gas-phase geometry, the microsolvation-continuum approach and the *monomer* cycle. In bold the values lowest value of $\Delta G^{*}_{n\,aq}$. Values in kcal mol^{-1}.

n	PO_4^{3-}	HPO_4^{2-}	$H_2PO_4^{-}$	H_3PO_4	$P_2O_7^{4-}$	$HP_2O_7^{3-}$	$H_2P_2O_7^{2-}$	$H_3P_2O_7^{1-}$	$H_4P_2O_7$
1	−	-1.6	-0.0	-1.1	-0.5	2.8	5.1	-0.9	-3.5
2	−	0.4	0.3	-1.1	1.0	3.6	4.7	9.8	5.3
3	-1.4	1.4	3.4	3.4	2.6	4.4	4.8	-2.4	6.0
4	-2.7	-0.2	2.0	-0.1	-7.0	-1.1	5.4	7.7	-3.2
5	1.5	-2.4	-1.5	1.4	-11.1	0.7	1.6	4.7	0.2

In Table 5-7 we have reported the "incremental" water binding free energies $\Delta G^{*}_{n,aq}$ for the orthophosphate and pyrophosphate species. The results suggest the optimal set of micro-hydration numbers n_{H_2O}, which (i) for the orthophosphates is $PO_4^{3-}(H_2O)_4$, $HPO_4^{2-}(H_2O)_5$, $H_2PO_4^{-}(H_2O)_5$, $H_3PO_4(H_2O)$ or $H_3PO_4(H_2O)_2$, and (ii) for the pyrophosphates is $P_2O_7^{4-}(H_2O)_5$, $HP_2O_7^{3-}(H_2O)_4$, $H_2P_2O_7^{2-}(H_2O)_5$, $H_3P_2O_7^{1-}(H_2O)_3$ and $H_4P_2O_7(H_2O)_1$.

Table 5-8 Aqueous-phase acid dissociation constant pKa for the protonation states of the orthophosphoric and pyrophosphoric acids. Solvation free energies contributions computed at the COSMO/PBE/DNP level using the COSMO optimised geometry. The solvation free energies of the conjugate species HA/A- have been determined using the optimal number of water molecules reported in Table 5-6 (pKa units).

Reaction	This study	MP2/6-311++G(d,p) [a)]	AM1-SM2 [a)]	PM3-SM3 [a)]	Exp. [b)]
$H_3PO_4 \rightarrow H_2PO_4^{-} + H^{+}$	0.1	1.3	10.3	31.7	2.1
$H_2PO_4^{-} \rightarrow HPO_4^{2-} + H^{+}$	8.5	7.7	15.6	20.2	7.2
$HPO_4^{2-} \rightarrow PO_4^{3-} + H^{+}$	11.9	11.8	14.7	28.6	12.4
$H_4P_2O_7 \rightarrow H_3P_2O_7^{1-} + H^{+}$	-3.7	-4.9	13.8	34.8	0.8
$H_3P_2O_7^{1-} \rightarrow H_2P_2O_7^{2-} + H^{+}$	6.5	-2.0	13.3	25.3	2.2
$H_2P_2O_7^{2-} \rightarrow HP_2O_7^{3-} + H^{+}$	8.7	5.5	10.6	23.5	6.7
$HP_2O_7^{3-} \rightarrow P_2O_7^{4-} + H^{+}$	13.8	13.9	13.5	32.4	9.4

a) Colvin et al. J. Am. Chem. Soc. 1995, 117, 5357. b) Martell Fasman, G. D. "Handbook of Biochemistry and Molecular Biology" CRC Press, Boca Raton, 1976.

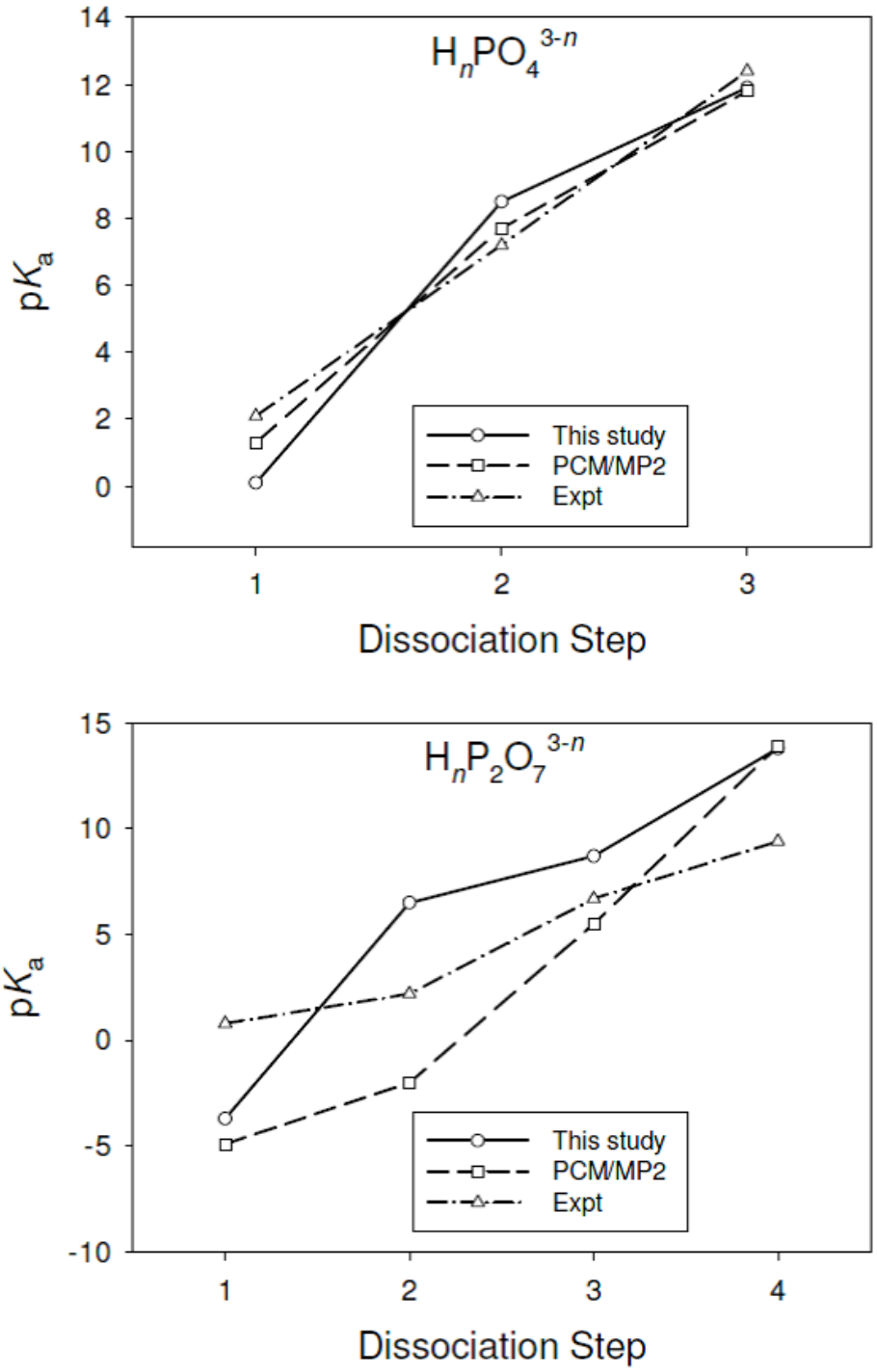

Figure 5-2 Aqueous-phase dissociation steps of the orthophosphates and pyrophosphates.

Table 5-8 reports the calculated pK_a values for the orthophosphoric $H_nPO_4^{3-n}$ and pyrophosphoric $H_nP_2O_7^{4-n}$ acids using the microsolvation-continuum model, where the number of explicit water molecules n_{H_2O} has been determined using the criterion of minimum "incremental" free energy $\Delta G^*_{n,aq}$ and taken from Table 5-7. The results are compared with the pK_a values obtained from *ab initio* PCM/MP2 and semi-empirical AM1-SM2 and PM3-SM3 solvation models.(Cramer and Truhlar 1992; Colvin, Evleth et al. 2002) For the orthophosphate species, the values obtained by us are comparable with the PCM/MP2 and experimental results. For the pyrophosphate species, both the microsolvation-continuum approach and the PCM/MP2 give less quantitative agreement with experiment. However, if we compare in Figure 5-2 the experimental and the computed values of pK_a of the consecutive $H_nP_2O_7^{4-n}$ dissociation constants we note that the trend of the values of pK_a obtained using the microsolvation-continuum method is consistent with the experimental one, whereas the values obtained using the simple PCM/MP2 model deviate from linearity as the charges of the HA/A^- species increases. We explain this in terms of the more balanced description of the product $\Delta G^*_{solv}\left(A^-\right)$ and reagent $\Delta G^*_{solv}(HA)$ solvation energy terms, which is probably due to the fact that the phosphate anions are more "hidden" within the microsolvated cluster.

The results in Table 5-8 indicate that the "incremental" binding free energy method could represent an unbiased approach in the determination of the optimal number of water molecules to be used in the calculation the free solvation energy term $\Delta\Delta G^*_{solv}$ using the microsolvation-continuum approach, as this is the term that

controls the accuracy that we can obtain in the evaluation of the free energy of the condensation reaction ΔG^{*}_{aq} (Equation (5-1)).

5.5 Formation of pyro- and tri-phosphates in aqueous solution

In this section we report the calculation of the Gibbs free energies ΔG^*_{aq} for the formation of the pyrophosphate and triphosphate species. We have shown in Section 5.4 that the accuracy in the calculation of pK_a critically depends on the number of water molecules n_{H_2O} included in the microsolvation-continuum model (Table 5-6). Therefore, we have initially investigated the effect of n_{H_2O} on the free energies of the orthophosphate condensation reactions in Scheme 5-3. The complete list of free energies for the formation of the pyrophosphates $H_xP_2O_7^{4-x}$ computed using the entire combination of the hydrated clusters $H_xPO_4^{3-x}(H_2O)_n$ ($0 \le n \le 5$) and $H_xP_2O_7^{4-x}(H_2O)_n$ ($0 \le n \le 6$) is reported in the Supplementary Information (see Appendix). The results indicate that the values of ΔG^*_{aq} can vary by tens of kcal mol^{-1}, depending on the particular combination $H_xPO_4^{3-x}(H_2O)_n / H_xP_2O_7^{4-x}(H_2O)_n$ used to evaluate the solvation energy term $\Delta\Delta G^*_{solv}$ (Equation (5-1)). This suggests that the number of water molecules used in the application of the microsolvation-continuum approach is a critical choice when modelling the condensation reactions involving charged species like phosphates.

$$H_3PO_4 + H_3PO_4 \rightarrow H_4P_2O_7 + H_2O$$

$$H_3PO_4 + H_2PO_4^- \rightarrow H_3P_2O_7^- + H_2O$$

$$H_2PO_4^- + H_2PO_4^- \rightarrow H_2P_2O_7^{2-} + H_2O$$

$$H_2PO_4^- + HPO_4^{2-} \rightarrow HP_2O_7^{3-} + H_2O$$

$$HPO_4^{2-} + HPO_4^{2-} \rightarrow P_2O_7^{4-} + H_2O$$

Scheme 5-3 The condensation reactions of the orthophosphate species to form pyrophosphate products.

Table 5-9 reports representative values of the free energies of reaction for the formation of the pyrophosphate species. Here, the number of implicit water molecules has been determined using the following schemes:

a. The COSMO stand-alone method (n_{H_2O} A, B, C = 0).

b. The minimum "incremental" free energy $\Delta G^*_{n,aq}$ discussed in section 3.2, which has been applied to the monomers (*b*.1), to the dimer (*b*.2), and to both monomeric and dimeric species (b.3).

c. The addition of number of water molecules simply equal to the effective charge of the phosphate species.

d. The "incremental" binding energy approach (*b*) for the orthophosphate species and the effective charge approach (*c*) for the pyrophosphates.

Table 5-9 Effect of the water molecules n_{H_2O} used to compute the solvation energy term $\Delta\Delta G^*_{solv}$ on the free energies of condensation reaction ΔG^*_{aq} for the formation of the pyrophosphate species. Approaches used to determine the hydration numbers n_{H_2O}: b) "Incremental" binding free energy approach; c) Effective charge approach; d) "Incremental" binding free energy approach for the orthophosphates and Effective charge approach of pyrophosphates. Values in kcal mol^{-1}.

$A + B \rightarrow C + H_2O$	Approach	n_{H_2O} A	n_{H_2O} B	n_{H_2O} C		Exp. [a]
$H_3PO_4 + H_3PO_4 \rightarrow H_4P_2O_7 + H_2O$	*a* (*c*)	0	0	0	10.9	9.5
	b.1	1	1	0	8.2	
	b.1	2	2	0	20.4	
	b.2	0	0	1	3.2	
	b.3	1	1	1	0.5	
	d	**2**	**2**	**1**	**12.7**	
$H_3PO_4 + H_2PO_4^- \rightarrow H_3P_2O_7^- + H_2O$	*a*	0	0	0	-6.0	7.5
	b.1	1	5	0	-2.9	
	b.1	2	5	0	3.2	
	b.2	0	0	3	-12.0	
	b.3	1	5	3	-9.0	
	b.3	2	5	3	-2.8	
	c	0	1	1	-11.6	
	d	**2**	**5**	**1**	**-1.9**	
$H_2PO_4^- + H_2PO_4^- \rightarrow H_2P_2O_7^{2-} + H_2O$	*a*	0	0	0	-3.8	7.7
	b.1	5	5	0	5.0	
	b.2	0	0	5	-3.1	
	b.3	5	5	5	5.7	
	c	1	1	2	-3.4	
	d	**5**	**5**	**2**	**6.4**	
$H_2PO_4^- + HPO_4^{2-} \rightarrow HP_2O_7^{3-} + H_2O$	*a*	0	0	0	-3.2	7.1
	b.1	5	5	0	8.8	
	b.2	0	0	4	-10.2	
	b.3	5	5	4	1.9	
	c	1	2	3	-1.5	
	d	**5**	**5**	**3**	**7.2**	
$HPO_4^{2-} + HPO_4^{2-} \rightarrow P_2O_7^{4-} + H_2O$	*a*	0	0	0	19.7	10.4
	b.1	5	5	0	35.1	
	b.2	0	0	5	-16.2	
	b.3	5	5	5	-0.8	
	c	2	2	4	5.2	
	d	**5**	**5**	**4**	**14.4**	

a) George et al., Biochim. Biophys. Acta, 1970,223,1.

The results in Table 5-9 show that the reaction free energies computed using the COSMO stand-alone method (approach *a*) are in good agreement with experiment in the case of the neutral pyrophosphate $H_4P_2O_7$ species only. For the other condensation reactions, the non-addition of explicit water molecules gives results which strongly disagree with the experiment.

Regarding the "incremental" binding free energy method (approach *b*), results in Table 5-9 show the importance of adding explicit water molecules to the monomeric species. In fact, if we consider the reaction $H_2PO_4^- + H_2PO_4^- \rightarrow H_2P_2O_7^{2-} + H_2O$, the combination $H_2PO_4^-(H_2O)_5$ / $H_2P_2O_7^{2-}(H_2O)_0$ (approach *b*.1) gives a free energy of 5.0 kcal mol^{-1}, which agrees well with the experimental value of 7.7 kcal mol^{-1} determined by George et al., (George, Witonsky et al. 1970) whereas inclusion of explicit water molecules only for the dimer, $H_2PO_4^-(H_2O)_0$/ $H_2P_2O_7^{2-}(H_2O)_5$ (approach *b*.2) gives a calculated value of ΔG^*_{aq} of -3.1 kcal mol^{-1}. The quality of the results therefore seems to be less dependent on the number of water molecules included in the pyrophosphates, which may be explained in terms of the intra-molecular hydrogen-bonding in the hydrogenated pyrophosphates, as shown in Figure 5-3 that causes the effective charges of the dimers to become less influential on the surrounding water molecules. Finally, the inclusion of the optimal number of water molecules according to the "incremental" binding energy method to both the monomeric $H_xPO_4^{3-x}(H_2O)_n$ and dimeric $H_xP_2O_7^{4-x}(H_2O)_n$ species (approach *b*.3) does not give a general and systematic improvement over approach *b*.2.

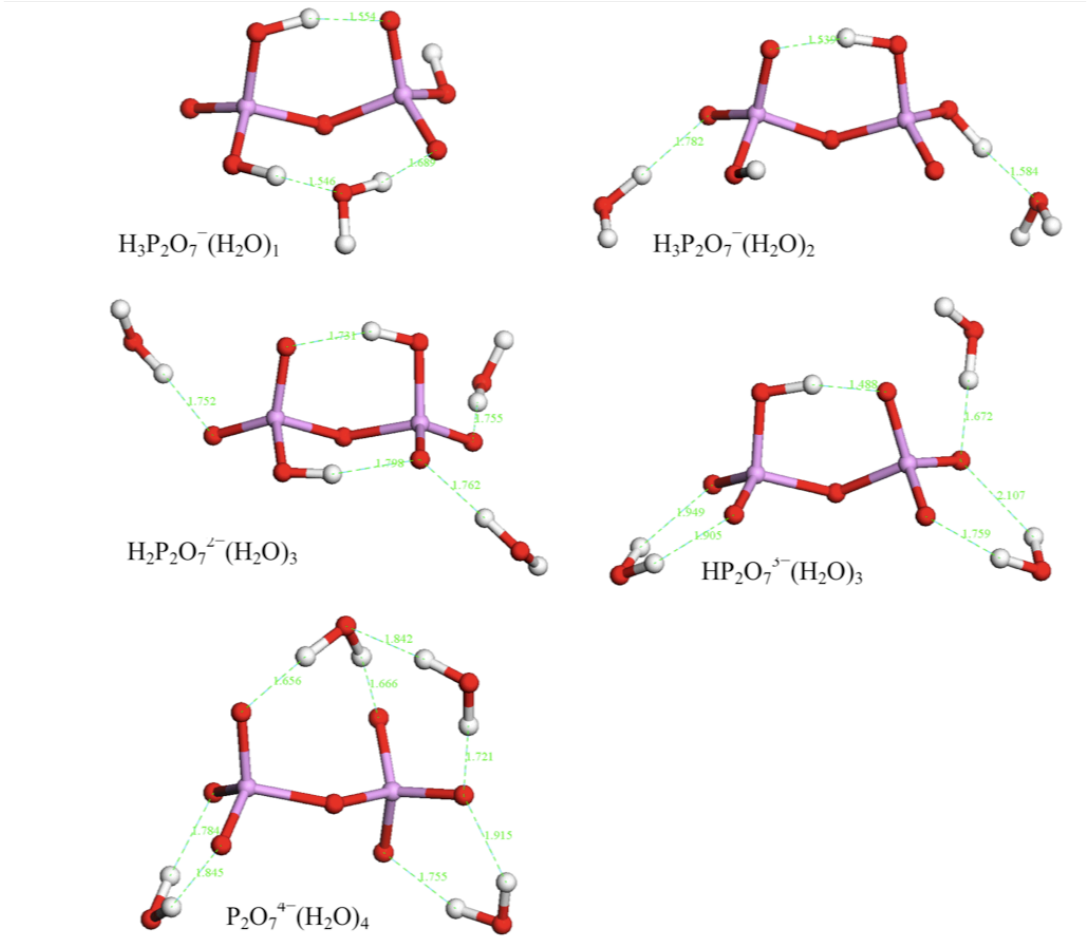

Figure 5-3 Optimised structure of representative hydrated pyrophosphate species obtained at the COSMO/PBE/DNP level. Bond lengths in Å

The approach *c* in Table 5-9, where the number of water molecules added to the species is simply equal to the formal charge of the anion, gives results which are generally not in good agreement with the experiment. However, if we consider method *d*, where for $H_xPO_4^{3-x}(H_2O)_n$ n_{H2O} is the optimal value suggested by the "incremental" binding energy method and for $H_xP_2O_7^{4-x}(H_2O)_n$ n_{H2O} is simply equal to the effective charge of the pyrophosphate, then for all reactions in Scheme 5-3 the computed values of ΔG^*_{aq} agree reasonably well with the experiment.

Table 5-10 reports the free energies of condensation ΔG^{*}_{aq} for the formation of the pyrophosphates $H_nP_2O_7^{4-n}$ and triphosphates $H_nP_3O_{10}^{5-n}$ at the conditions where the HPO_4^{2-} and $H_2PO_4^{-}$ monomers are readily available (pH 7.0). The values of ΔG^{*}_{aq} of the pyrophosphates and triphosphates have been computed using the microsolvation-continuum model, where the number of implicit water molecules has been determined applying the "hybrid" approach (*d*): the "incremental" binding energy method for the orthophosphates, and the effective charge approach for pyro- and tri-phosphates.

Table 5-10 Gibbs free energies of condensation reaction ΔG^{*}_{aq} for the formation of the pyrophosphate and triphosphate species. The hydration number n_{H_2O} has been determined applying approach d (the "incremental" binding free energy approach for the orthophosphates and effective charge approach for pyrophosphates). Values in kcal mol^{-1}.

$A + B \rightarrow C + H_2O$	n_{H_2O} A	n_{H_2O} B	n_{H_2O} C	This study	MP2/6-311++G(d,p) [a]	Exp. [b]
$H_2PO_4^- + H_2PO_4^- \rightarrow H_2P_2O_7^{2-} + H_2O$	5	5	2	6.4	-2.7	7.7
$H_2PO_4^- + HPO_4^{2-} \rightarrow HP_2O_7^{3-} + H_2O$	5	5	3	7.1	-6.6	7.1
$HPO_4^{2-} + HPO_4^{2-} \rightarrow P_2O_7^{4-} + H_2O$	5	5	4	14.4	0.8	10.4
$H_2PO_4^- + H_2P_2O_7^{2-} \rightarrow H_2P_3O_{10}^{3-} + H_2O$	5	2	3	8.2		7.3
$H_2PO_4^- + HP_2O_7^{3-} \rightarrow HP_3O_{10}^{4-} + H_2O$	5	3	4	10.0		7.2
$HPO_4^{2-} + HP_2O_7^{3-} \rightarrow P_3O_{10}^{5-} + H_2O$	5	3	5	20.4		10.5

a) Colvin et al. J. Am. Chem. Soc. 1995, 117, 5357. b) George et al., Biochim. Biophys. Acta, 1970, 223, 1.

For the pyrophosphate species $H_2P_2O_7^{2-}$, $HP_2O_7^{-}$ and $P_2O_7^{3-}$ the application of method (*d*) gives a very good agreement with the experiment, and it also performs considerably better than the PCM/MP2 method.

The free energies of formation of the triphosphates $H_2P_3O_{10}^{3-}$ (ΔG^*_{aq} = 8.2 kcal mol^{-1}) and $HP_3O_{10}^{4-}$ (ΔG^*_{aq} = 10.0 kcal mol^{-1}) computed using method (*d*) differ by only 0.9 kcal mol^{-1} and 2.8 kcal mol^{-1} from the experimental values, respectively. Our prediction is however too high by as much as 10 kcal mol^{-1} for the penta-ionic trimer $P_3O_{10}^{5-}$, although this species is unlikely to exist in biological aqueous environments.

5.6 Chapter conclusion

We have reported results from first principles DFT-PBE calculations of the hydration properties, aqueous-phase acid dissociation constants (pK_a), and Gibbs free energies of formation of small polyphosphates in aqueous solutions. The effect of the hydrated environment has been simulated through a microsolvation-continuum approach, where the phosphate species are represented as a microsolvated solute, while the remainder of the bulk solvent is treated as a dielectric continuum using the COSMO solvation model. One of the main aims of this study was to determine the performance of DFT microsolvation-continuum methods to model the oligomerization of polyphosphate species in aqueous solution. Based on the results of our calculations and comparison with available theoretical and experimental work, we conclude the following:

- Stand-alone polarisable continuum models such as COSMO or microsolvation-continuum approaches are unable to compute accurate solvation free energies of orthophosphates $H_nPO_4^{3-n}$, n = 0-3, and pyrophosphate $H_nP_2O_7^{4-n}$, n = 0-4.
- Using the microsolvation-continuum approach, it is, however possible to compute values of the orthophosphate acid dissociation constants in good agreement with experiment. The values of pK_a calculated using this method depend significantly on the number of water molecules n_{H_2O} used to evaluate the solvation free energy contribution to the reaction free energy ΔG^*_{aq}.

- In the context of the calculation of the pK_a, the optimal number of explicit water molecules in the hydrated cluster $S(H_2O)_n$ for the application of the microsolvation-continuum approach has been determined as the number n that gives the minimum value of the "incremental" water-binding free energy ($\Delta G^*_{n,aq}$) associated with the process of adding a water molecule to a micro-solvated phosphate.

- The free energy of formation of pyro- and tri-phosphates is also critically dependent on the size of the hydrated phosphate clusters. We propose a hybrid approach were in the calculation of free energy condensation reactions of phosphates the number of water molecules attached to the monomeric species n_{H_2O} is given by the "incremental" binding energy approach, and for the polyphosphate species n_{H_2O} is simply equal to the effective charge of the phosphate species.

- The application of this hybrid method to compute the free energy of formation of pyrophosphate and tryphosphate species gives good agreement with experiment, and better performance than the PCM/MP2 method. This hybrid scheme is particularly attractive as the calculation of the incremental binding energies for the phosphates would lead to such large numbers of possible configurations, as to make the method computationally prohibitive.

Chapter 6 Conclusion

In this thesis, we have presented an investigation of phosphate-based bioglasses (PBG) and their dissolution products in water using first principle computer simulation methods. One of the major challenges in the development of PBGs tailored to suit the end application is to understand the relation between the properties of PBGs and their dissolution behaviour. In order to achieve this goal, it is first of all necessary to obtain a molecular level understanding of the structural properties of PBGs, and of the processes of hydration and oligomerisation of the phosphate clusters released during the dissolution process. The investigation carried out during this PhD has, therefore, been logically divided into three themes:

- Structures of phosphate bioglasses
- Hydration phosphate clusters
- Condensation reactions of phosphates in aqueous solution

Firstly, the structures of three bioactive phosphate glasses with compositions $(P_2O_5)_{0.45}(CaO)_x(Na_2O)_{0.55-x}$ (where x = 0.30, 0.35 and 0.40) have been simulated by Car-Parrinello molecular dynamics. Our analysis of the structures shows the prevalence of the metaphosphate Q^2 and pyrophosphate Q^1 species, whereas the number of the Q^3 units, which constitute the three-dimensional network, significantly decreases with the increase of calcium content in the glasses. Calculation of the pair and angular distribution functions also suggests that the rigidity of the phosphate increases with the concentration of calcium, an observation which is interpreted in terms of the tendency of Ca^{2+} to be a stronger coordinator than sodium ion. This finding may explain the lower solubility and dissolution rate

of high calcium content ternary phosphate glasses observed in previous experimental studies. (Franks, Abrahams et al. 2000; Knowles 2003) According to Knowles studies, the pH influences of the ion release mechanism of the glasses during the dissolution process and the cell proliferation result of MTT assay (Salih, Franks et al. 2000), both suggested glasses with $(P_2O_5)_{0.45}(CaO)_{0.40}(Na_2O)_{0.15}$ composition is more suitable for biomedical use in comparison to its counterparts with lower calcium contents. The coordination statistics of the phosphate network of the $(P_2O_5)_{0.45}(CaO)_{0.40}(Na_2O)_{0.15}$ glass demonstrated its structure was mainly dominated by metaphosphates Q^2, with some pyrophosphates Q^1, and small amount of Q^3 constituting the three-dimensional network. No evidence for the presence of orthophosphates was found. Work was also carried out on a $K_2O-CaO-P_2O_5$ system, the results were similar to the $Na_2O-CaO-P_2O_5$ system, however the solubility was found to be too high for biomedical use (Knowles 2003).

Secondly, extensive Car-Parrinello molecular dynamics simulations have been used to investigate the hydration structures of the orthophosphates. Each orthophosphate $H_nPO_4^{3-n}$ (n=0-3) species was simulated in explicit water. The results show that the proton transfer process from the orthophosphate species to the surrounding water is very fast and indicating that the dehydrogenation occurs through a concerted proton hopping mechanism, which involves $H_nPO_4^{3-n}$ and three water molecules. Analysis of the intermolecular $H_nPO_4^{3-n}$-water structure shows that the PO_4^{3-} anions have a significant effect on the H-bonding network of bulk water and the presence of $P-O^-$ moieties induce the formation of new types of $H-H$ interactions around this orthophosphate. The calculated probability distributions of the coordination numbers of the first hydration shell of PO_4^{3-},

HPO_4^{2-} and $H_2PO_4^-$ show that these phosphate species display a flexible first coordination shell (between 7 and 13 water molecules) and that the flexibility increases on going from PO_4^{3-} to $H_2PO_4^-$. The strength and number of hydrogen bonds of PO_4^{3-}, HPO_4^{2-} and $H_2PO_4^-$ were determined through a detailed analysis of the structural correlation functions. The H-bond interactions between the oxygen atoms of the phosphates and the surrounding water molecules were found to decrease from PO_4^{3-} to the hydrogenated $H_2PO_4^-$ species, which explain the diminished effect on the structure of water with the increasing hydrogenation of the orthophosphate anions. These results give us an insight of how orthophosphate interact with the surrounding aqueous environment, which is an important piece of information to determine whether the ions and phosphate groups chemically interact with the surrounding water to form different species (Ahmed, Lewis et al. 2004) and hence have a better understanding of the dissolution process of the phosphate bioglasses.

Thirdly, the hydration properties of the phosphates have been studied by *ab-initio* density functional theory calculations with a hybrid microsolvation-continuuum approach to simulate the effect of the hydrated environment. Aqueous phase acid dissociation constants $\left(pK_a\right)$ and Gibbs free energies of formation of small polyphosphates in aqueous solution were computed. However, our results indicated that the simple polarisable continuum or microsolvation-continuum models were unable to compute accurate free energies of solvation for charged species like phosphates. The calculation of the pK_a showed that the values of acid dissociation constants were critically dependent on the number of water molecules n_{H_2O} included in the hydrated phosphate clusters. The optimal number $n_{\mathrm{H_2O}}$ is

determined from the minimum value of the "incremental" water binding free energy associated with the process of adding a water molecule to a micro-solvated phosphate species. Analysis of the effect of n_{H_2O} on the free energies $\left(\Delta G^*_{aq}\right)$ of orthophosphate condensation reactions show that ΔG^*_{aq} can vary by tenths of kcal mol^{-1}, depending on the particular choice of n_{H_2O} for the monomeric and dimeric species. We discuss a methodology for the determination of n_{H_2O}; for the orthophosphates the "incremental" binding energy approach is used to determine n_{H_2O}, whereas for the polyphosphates the number of explicit water molecules is simply equal to the effective charge of these anions. The application of this method to compute the free energy of formation of pyro- and tri-phosphates gives generally good agreement with the available experimental data, and also outperform calculation conducted using the more computationally expensive MP2 mthods. This hybrid scheme method is particularly attractive to simulate the condensation reaction of phosphate species in water using a simple computationally feasible approach.

As a result, our study gives an overview of the structural and hydration properties of phosphates and phosphate bioglasses, and demonstrates possible ways to study these materials computationally despite the difficulties. As a potential biomaterial, given the experimental study of phosphate bioglasses showing high CaO content glass gives a significant increase in cell proliferation in the biochemical assays and the fact that the cell culture medium used by Knowles et al. for the assays contained Ca^{2+} and Na^+ ions which led to reasonable speculation that the reason of the increase is related to the phosphate released from the glasses. The free energy results of the condensation reaction ΔG^*_{aq} of the phosphates in this study

as shown the orthophosphates remained the most energetic favourable in aqueous condition and the condensations between orthophosphate to form pyrophosphates is unlikely. This gives a hint to the mechanism of the dissolution process of the phosphate bioglasses. Previous ion chromatography experiments of the dissolution products of the $(P_2O_5)_{0.45}(CaO)_x(Na_2O)_{0.55-x}$ glasses have successfully identified some of the forms of the phosphate fragments released from the bulk glasses to the solution, however, not all fragments can be identified and some long chain fragments remain unknown (Ahmed, Lewis et al. 2005). Base on the results of our study, the probability of those long chain fragments are form during the dissolution process becomes very low. The dissolution products of the phosphate bioglasses are more likely to break down from long chain fragments to orthophosphates, which may contribute to the increase in cell proliferation. The suggested mechanism is coherent with the results found by Frank et al. (Franks, Abrahams et al. 2000), where the annealed amorphous precipitate of the phosphate bioglasses is identified as $Ca_2P_2O_7$ that indicates the possibility of the formation of brushite $CaHPO_4 \cdot (2H_2O)$. The possible reactions occurs during the annealing are:

$$CaHPO_4 \cdot 2H_2O(\text{brushite}) \rightarrow CaHPO_4(\text{monetite}) + 2H_2O$$

$$2CaHPO_4 \rightarrow Ca_2P_2O_7 + H_2O$$

According to Videau et al., hydroxyapatite (HA) is the end product for maturing calcium phosphate precipitation (Videau, Portier et al. 1982), which further support our view on high calcium content and orthophosphate dissolution products as the key factors of the bioactive nature of phosphate bioglasses.

In summary, we agree phosphate bioactive glasses have lots of potential as one of the future biomaterials. Their structural and solvation properties are investigated and analysed in this study. We have also investigated and attempted to build a picture of the dissolution process of the glasses, however, due to the difficulty of modelling phosphates at solvation conditions as discussed in previous chapters, further investigation is needed to confirm the dissolution mechanism and the dissolution products of the glasses.

Appendix

Supplementary Information to Chapter 5 Section 5.5

The complete list of free energies for the formation ΔG^{*}_{aq} of the pyrophosphates $H_xP_2O_7^{4-x}$ computed using the entire combination of the hydrated clusters $H_xPO_4^{3-x}(H_2O)_n$ ($0 \le n \le 5$) and $H_xP_2O_7^{4-x}(H_2O)_n$ ($0 \le n \le 6$) is reported as follow.

$H_3PO_4 + H_3PO_4 \rightarrow H_4P_2O_7 + H_2O$ ΔG^*_{aq} Exp.=9.5

ΔG^*_{aq}	$n_w H_3PO_4 \setminus n_w H_3PO_4$					
n_w of $H_4P_2O_7$	0\0	0\1	0\2	0\3	0\4	0\5
0	10.9	9.5	15.7	14.2	15.0	13.0
1	3.2	1.8	8.0	6.5	7.3	5.3
2	4.3	3.0	9.1	7.6	8.4	6.4
3	6.2	4.8	10.9	9.4	10.2	8.3
4	-1.2	-2.5	3.6	2.1	2.9	1.0
5	-5.1	-6.4	-0.3	-1.8	-1.0	-3.0
6	-9.5	-10.8	-4.7	-6.2	-5.4	-7.3
	1\0	1\1	1\2	1\3	1\4	1\5
0	9.5	8.2	14.3	12.8	13.6	11.7
1	1.8	0.5	6.6	5.1	5.9	4.0
2	3.0	1.6	7.7	6.2	7.0	5.1
3	4.8	3.4	9.6	8.1	8.9	6.9
4	-2.5	-3.9	2.3	0.7	1.6	-0.4
5	-6.4	-7.8	-1.7	-3.2	-2.4	-4.3
6	-10.8	-12.2	-6.1	-7.6	-6.8	-8.7
	2\0	2\1	2\2	2\3	2\4	2\5
0	15.7	14.3	20.4	18.9	19.7	17.8
1	8.0	6.6	12.7	11.2	12.1	10.1
2	9.1	7.7	13.8	12.3	13.2	11.2
3	10.9	9.6	15.7	14.2	15.0	13.1
4	3.6	2.3	8.4	6.9	7.7	5.7
5	-0.3	-1.7	4.4	2.9	3.8	1.8
6	-4.7	-6.1	0.1	-1.5	-0.6	-2.6
	3\0	3\1	3\2	3\3	3\4	3\5
0	14.2	12.8	18.9	17.4	18.2	16.3
1	6.5	5.1	11.2	9.7	10.5	8.6
2	7.6	6.2	12.3	10.8	11.6	9.7
3	9.4	8.1	14.2	12.7	13.5	11.5
4	2.1	0.7	6.9	5.4	6.2	4.2
5	-1.8	-3.2	2.9	1.4	2.3	0.3
6	-6.2	-7.6	-1.5	-3.0	-2.1	-4.1
	4\0	4\1	4\2	4\3	4\4	4\5
0	15.0	13.6	19.7	18.2	19.1	17.1
1	7.3	5.9	12.1	10.5	11.4	9.4
2	8.4	7.0	13.2	11.6	12.5	10.5
3	10.2	8.9	15.0	13.5	14.3	12.4
4	2.9	1.6	7.7	6.2	7.0	5.1
5	-1.0	-2.4	3.8	2.3	3.1	1.1
6	-5.4	-6.8	-0.6	-2.1	-1.3	-3.3
	5\0	5\1	5\2	5\3	5\4	5\5
0	13.0	11.7	17.8	16.3	17.1	15.2
1	5.3	4.0	10.1	8.6	9.4	7.5
2	6.4	5.1	11.2	9.7	10.5	8.6
3	8.3	6.9	13.1	11.5	12.4	10.4
4	1.0	-0.4	5.7	4.2	5.1	3.1
5	-3.0	-4.3	1.8	0.3	1.1	-0.8
6	-7.3	-8.7	-2.6	-4.1	-3.3	-5.2

$H_3PO_4 + H_2PO_4^- \rightarrow H_3P_2O_7^- + H_2O$ ΔG^*_{aq} Exp.=7.5

ΔG^*_{aq}	$n_w H_3PO_4 \setminus n_w H_2PO_4^-$					
n_w of $H_3P_2O_7^-$	0\0	0\1	0\2	0\3	0\4	0\5
0	-6.0	-6.5	-4.8	-3.9	-5.4	-1.6
1	-11.0	-11.6	-9.8	-9.0	-10.5	-6.6
2	-5.4	-6.0	-4.2	-3.4	-4.9	-1.1
3	-12.0	-12.5	-10.8	-10.0	-11.4	-7.6
4	-8.5	-9.0	-7.3	-6.5	-7.9	-4.1
5	-8.0	-8.5	-6.8	-6.0	-7.4	-3.6
6	-8.1	-8.6	-6.9	-6.1	-7.6	-3.7
	1\0	1\1	1\2	1\3	1\4	1\5
0	-7.3	-7.9	-6.1	-5.3	-6.8	-2.9
1	-12.4	-12.9	-11.2	-10.4	-11.8	-8.0
2	-6.8	-7.3	-5.6	-4.8	-6.3	-2.4
3	-13.3	-13.9	-12.1	-11.3	-12.8	-9.0
4	-9.8	-10.4	-8.6	-7.8	-9.3	-5.4
5	-9.3	-9.9	-8.1	-7.3	-8.8	-4.9
6	-9.5	-10.0	-8.2	-7.4	-8.9	-5.1
	2\0	2\1	2\2	2\3	2\4	2\5
0	-1.2	-1.7	0.0	0.8	-0.7	3.2
1	-6.3	-6.8	-5.0	-4.2	-5.7	-1.9
2	-0.7	-1.2	0.5	1.3	-0.1	3.7
3	-7.2	-7.8	-6.0	-5.2	-6.7	-2.8
4	-3.7	-4.3	-2.5	-1.7	-3.2	0.7
5	-3.2	-3.8	-2.0	-1.2	-2.7	1.2
6	-3.3	-3.9	-2.1	-1.3	-2.8	1.1
	3\0	3\1	3\2	3\3	3\4	3\5
0	-2.7	-3.3	-1.5	-0.7	-2.2	1.7
1	-7.8	-8.3	-6.6	-5.7	-7.2	-3.4
2	-2.2	-2.7	-1.0	-0.2	-1.7	2.2
3	-8.7	-9.3	-7.5	-6.7	-8.2	-4.3
4	-5.2	-5.8	-4.0	-3.2	-4.7	-0.8
5	-4.7	-5.3	-3.5	-2.7	-4.2	-0.3
6	-4.8	-5.4	-3.6	-2.8	-4.3	-0.5
	4\0	4\1	4\2	4\3	4\4	4\5
0	-1.9	-2.4	-0.7	0.1	-1.3	2.5
1	-6.9	-7.5	-5.7	-4.9	-6.4	-2.6
2	-1.4	-1.9	-0.2	0.7	-0.8	3.0
3	-7.9	-8.5	-6.7	-5.9	-7.4	-3.5
4	-4.4	-4.9	-3.2	-2.4	-3.9	0.0
5	-3.9	-4.4	-2.7	-1.9	-3.4	0.5
6	-4.0	-4.6	-2.8	-2.0	-3.5	0.4
	5\0	5\1	5\2	5\3	5\4	5\5
0	-3.8	-4.4	-2.6	-1.8	-3.3	0.6
1	-8.9	-9.4	-7.7	-6.9	-8.4	-4.5
2	-3.3	-3.9	-2.1	-1.3	-2.8	1.1
3	-9.9	-10.4	-8.7	-7.8	-9.3	-5.5
4	-6.4	-6.9	-5.1	-4.3	-5.8	-2.0
5	-5.9	-6.4	-4.6	-3.8	-5.3	-1.5
6	-6.0	-6.5	-4.8	-3.9	-5.4	-1.6

$H_2PO_4^- + H_2PO_4^- \rightarrow H_2P_2O_7^{2-} + H_2O$ ΔG^*_{aq} Exp.=7.7

ΔG^*_{aq}	$n_w H_2PO_4^- \backslash n_w H_2PO_4^-$					
n_w of $H_2P_2O_7^{2-}$	0\0	0\1	0\2	0\3	0\4	0\5
0	-3.8	-4.3	-2.5	-1.7	-3.2	0.6
1	-2.8	-3.4	-1.6	-0.8	-2.3	1.5
2	-2.4	-2.9	-1.1	-0.3	-1.8	2.0
3	-1.7	-2.3	-0.5	0.3	-1.2	2.7
4	-0.5	-1.1	0.7	1.5	0.0	3.9
5	-3.1	-3.7	-1.9	-1.1	-2.6	1.3
6	-2.8	-3.3	-1.6	-0.8	-2.2	1.6
	1\0	1\1	1\2	1\3	1\4	1\5
0	-4.3	-4.8	-3.1	-2.3	-3.8	0.1
1	-3.4	-3.9	-2.2	-1.4	-2.9	1.0
2	-2.9	-3.4	-1.7	-0.9	-2.4	1.5
3	-2.3	-2.8	-1.1	-0.2	-1.7	2.1
4	-1.1	-1.6	0.1	1.0	-0.5	3.3
5	-3.7	-4.2	-2.4	-1.6	-3.1	0.7
6	-3.3	-3.9	-2.1	-1.3	-2.8	1.1
	2\0	2\1	2\2	2\3	2\4	2\5
0	-2.5	-3.1	-1.3	-0.5	-2.0	1.8
1	-1.6	-2.2	-0.4	0.4	-1.1	2.8
2	-1.1	-1.7	0.1	0.9	-0.6	3.2
3	-0.5	-1.1	0.7	1.5	0.0	3.9
4	0.7	0.1	1.9	2.7	1.2	5.1
5	-1.9	-2.4	-0.7	0.1	-1.4	2.5
6	-1.6	-2.1	-0.4	0.5	-1.0	2.8
	3\0	3\1	3\2	3\3	3\4	3\5
0	-1.7	-2.3	-0.5	0.3	-1.2	2.7
1	-0.8	-1.4	0.4	1.2	-0.3	3.6
2	-0.3	-0.9	0.9	1.7	0.2	4.1
3	0.3	-0.2	1.5	2.3	0.8	4.7
4	1.5	1.0	2.7	3.5	2.0	5.9
5	-1.1	-1.6	0.1	0.9	-0.5	3.3
6	-0.8	-1.3	0.5	1.3	-0.2	3.6
	4\0	4\1	4\2	4\3	4\4	4\5
0	-3.2	-3.8	-2.0	-1.2	-2.7	1.2
1	-2.3	-2.9	-1.1	-0.3	-1.8	2.1
2	-1.8	-2.4	-0.6	0.2	-1.3	2.6
3	-1.2	-1.7	0.0	0.8	-0.7	3.2
4	0.0	-0.5	1.2	2.0	0.5	4.4
5	-2.6	-3.1	-1.4	-0.5	-2.0	1.8
6	-2.2	-2.8	-1.0	-0.2	-1.7	2.1
	5\0	5\1	5\2	5\3	5\4	5\5
0	0.6	0.1	1.8	2.7	1.2	5.0
1	1.5	1.0	2.8	3.6	2.1	5.9
2	2.0	1.5	3.2	4.1	2.6	6.4
3	2.7	2.1	3.9	4.7	3.2	7.1
4	3.9	3.3	5.1	5.9	4.4	8.3
5	1.3	0.7	2.5	3.3	1.8	5.7
6	1.6	1.1	2.8	3.6	2.1	6.0

$H_2PO_4^- + HPO_4^{2-} \rightarrow HP_2O_7^{3-} + H_2O$ ΔG^*_{aq} Exp.=7.1

ΔG^*_{aq}	$n_w HPO_4^{2-} \backslash n_w H_2PO_4^-$					
n_w of $HP_2O_7^{3-}$	0\0	0\1	0\2	0\3	0\4	0\5
0	-3.2	-3.8	-2.0	-1.2	-2.7	1.1
1	-4.6	-5.1	-3.4	-2.6	-4.0	-0.2
2	-5.1	-5.7	-3.9	-3.1	-4.6	-0.7
3	-4.9	-5.5	-3.7	-2.9	-4.4	-0.5
4	-10.2	-10.7	-9.0	-8.2	-9.7	-5.8
5	-13.7	-14.3	-12.5	-11.7	-13.2	-9.3
6	-13.1	-13.7	-11.9	-11.1	-12.6	-8.7
	1\0	1\1	1\2	1\3	1\4	1\5
0	-1.0	-1.6	0.2	1.0	-0.5	3.4
1	-2.3	-2.9	-1.1	-0.3	-1.8	2.0
2	-2.9	-3.4	-1.7	-0.9	-2.3	1.5
3	-2.7	-3.2	-1.5	-0.7	-2.1	1.7
4	-8.0	-8.5	-6.8	-5.9	-7.4	-3.6
5	-11.5	-12.0	-10.3	-9.5	-10.9	-7.1
6	-10.9	-11.4	-9.7	-8.9	-10.3	-6.5
	2\0	2\1	2\2	2\3	2\4	2\5
0	-0.2	-0.7	1.0	1.8	0.4	4.2
1	-1.5	-2.1	-0.3	0.5	-1.0	2.9
2	-2.0	-2.6	-0.8	0.0	-1.5	2.3
3	-1.8	-2.4	-0.6	0.2	-1.3	2.5
4	-7.1	-7.7	-5.9	-5.1	-6.6	-2.7
5	-10.6	-11.2	-9.4	-8.6	-10.1	-6.3
6	-10.0	-10.6	-8.8	-8.0	-9.5	-5.7
	3\0	3\1	3\2	3\3	3\4	3\5
0	1.0	0.5	2.2	3.0	1.5	5.4
1	-0.3	-0.9	0.9	1.7	0.2	4.1
2	-0.9	-1.4	0.3	1.2	-0.3	3.5
3	-0.7	-1.2	0.5	1.4	-0.1	3.7
4	-6.0	-6.5	-4.7	-3.9	-5.4	-1.6
5	-9.5	-10.0	-8.3	-7.4	-8.9	-5.1
6	-8.9	-9.4	-7.7	-6.8	-8.3	-4.5
	4\0	4\1	4\2	4\3	4\4	4\5
0	-0.5	-1.1	0.7	1.5	0.0	3.9
1	-1.9	-2.4	-0.7	0.2	-1.3	2.5
2	-2.4	-2.9	-1.2	-0.4	-1.9	2.0
3	-2.2	-2.7	-1.0	-0.2	-1.7	2.2
4	-7.5	-8.0	-6.3	-5.5	-6.9	-3.1
5	-11.0	-11.5	-9.8	-9.0	-10.5	-6.6
6	-10.4	-10.9	-9.2	-8.4	-9.9	-6.0
	5\0	5\1	5\2	5\3	5\4	5\5
0	4.4	3.9	5.6	6.5	5.0	8.8
1	3.1	2.6	4.3	5.1	3.6	7.5
2	2.6	2.0	3.8	4.6	3.1	7.0
3	2.8	2.2	4.0	4.8	3.3	7.2
4	-2.5	-3.1	-1.3	-0.5	-2.0	1.9
5	-6.0	-6.6	-4.8	-4.0	-5.5	-1.6
6	-5.4	-6.0	-4.2	-3.4	-4.9	-1.0

$HPO_4^{2-} + HPO_4^{2-} \rightarrow P_2O_7^{4-} + H_2O$ ΔG^*_{aq} Exp.=10.4

ΔG^*_{aq}	$n_w HPO_4^{2-}$ \ $n_w HPO_4^{2-}$					
n_w of $P_2O_7^{4-}$	0\0	0\1	0\2	0\3	0\4	0\5
0	19.7	22.0	22.8	24.0	22.5	27.4
1	15.1	17.3	18.1	19.3	17.8	22.7
2	11.9	14.1	14.9	16.1	14.6	19.5
3	10.3	12.5	13.4	14.5	13.0	18.0
4	-0.9	1.3	2.2	3.3	1.8	6.8
5	-16.2	-13.9	-13.1	-11.9	-13.4	-8.5
6	-12.1	-9.9	-9.1	-7.9	-9.4	-4.5
	1\0	1\1	1\2	1\3	1\4	1\5
0	22.0	24.2	25.0	26.2	24.7	29.6
1	17.3	19.5	20.4	21.5	20.0	25.0
2	14.1	16.3	17.2	18.3	16.8	21.8
3	12.5	14.8	15.6	16.8	15.2	20.2
4	1.3	3.6	4.4	5.6	4.0	9.0
5	-13.9	-11.7	-10.9	-9.7	-11.2	-6.3
6	-9.9	-7.7	-6.8	-5.7	-7.2	-2.2
	2\0	2\1	2\2	2\3	2\4	2\5
0	22.8	25.0	25.9	27.1	25.5	30.5
1	18.1	20.4	21.2	22.4	20.8	25.8
2	14.9	17.2	18.0	19.2	17.7	22.6
3	13.4	15.6	16.4	17.6	16.1	21.0
4	2.2	4.4	5.2	6.4	4.9	9.8
5	-13.1	-10.9	-10.0	-8.9	-10.4	-5.4
6	-9.1	-6.8	-6.0	-4.8	-6.4	-1.4
	3\0	3\1	3\2	3\3	3\4	3\5
0	24.0	26.2	27.1	28.2	26.7	31.7
1	19.3	21.5	22.4	23.6	22.0	27.0
2	16.1	18.3	19.2	20.4	18.8	23.8
3	14.5	16.8	17.6	18.8	17.3	22.2
4	3.3	5.6	6.4	7.6	6.1	11.0
5	-11.9	-9.7	-8.9	-7.7	-9.2	-4.2
6	-7.9	-5.7	-4.8	-3.6	-5.2	-0.2
	4\0	4\1	4\2	4\3	4\4	4\5
0	22.5	24.7	25.5	26.7	25.2	30.1
1	17.8	20.0	20.8	22.0	20.5	25.5
2	14.6	16.8	17.7	18.8	17.3	22.3
3	13.0	15.2	16.1	17.3	15.7	20.7
4	1.8	4.0	4.9	6.1	4.5	9.5
5	-13.4	-11.2	-10.4	-9.2	-10.7	-5.8
6	-9.4	-7.2	-6.4	-5.2	-6.7	-1.7
	5\0	5\1	5\2	5\3	5\4	5\5
0	27.4	29.6	30.5	31.7	30.1	35.1
1	22.7	25.0	25.8	27.0	25.5	30.4
2	19.5	21.8	22.6	23.8	22.3	27.2
3	18.0	20.2	21.0	22.2	20.7	25.7
4	6.8	9.0	9.8	11.0	9.5	14.4
5	-8.5	-6.3	-5.4	-4.2	-5.8	-0.8
6	-4.5	-2.2	-1.4	-0.2	-1.7	3.2

Reference

. "http://www.physics.rutgers.edu/~dhv/uspp/.".

. "http://www.pwscf.org."

. "http://www.quantum-espresso.org."

(Materials Studio versions 4.0 and 4.1, Accelrys). "DMol^3." from http://www.accelrys.com/products/mstudio.

Abou Neel, E. A., D. M. Pickup, et al. (2009). "Bioactive functional materials: a perspective on phosphate-based glasses." Journal of Materials Chemistry **19**(6): 690-701.

Abrahams, I., G. E. Hawkes, et al. (1997). "Phosphorus speciation in sodium-calcium-phosphate ceramics." Journal of the Chemical Society, Dalton Transactions(9): 1483-1484.

Adamo, C. and V. Barone (1999). "Toward reliable density functional methods without adjustable parameters: The PBE0 model." The Journal of Chemical Physics **110**(13): 6158-6170.

Ahmed, I. (2005). "Quantification of Anion and Cation Release from a Range of Ternary Phosphate-based Glasses with Fixed 45 mol% P_2O_5." Journal of Biomaterials Applications **20**(1): 65.

Ahmed, I., C. A. Collins, et al. (2004). "Processing, characterisation and biocompatibility of iron-phosphate glass fibres for tissue engineering." Biomaterials **25**(16): 3223-3232.

Ahmed, I., M. Lewis, et al. (2004). "Phosphate glasses for tissue engineering: Part 1. Processing and characterisation of a ternary-based P_2O_5-CaO-Na_2O glass system." Biomaterials **25**(3): 491-499.

Ahmed, I., M. Lewis, et al. (2004). "Phosphate glasses for tissue engineering: Part 2. Processing and characterisation of a ternary-based P_2O_5-CaO-Na_2O glass fibre system." Biomaterials **25**(3): 501-507.

Ahmed, I., M. P. Lewis, et al. (2005). "Quantification of anions and cations from ternary phosphate based glasses with fixed 50 and 55 mol% P_2O_5 using ion chromatography." Physics and Chemistry of Glasses - European Journal of Glass Science and Technology Part B **46**: 547-552.

Ahmed, I., M. P. Lewis, et al. (2005). "Quantification of anion and cation release from a range of ternary phosphate-based glasses with fixed 45 mol% P_2O_5." Journal of Biomaterials Applications **20**(1): 65-80.

Ahmed, I., A. J. Parsons, et al. (2008). "Weight loss, ion release and initial mechanical properties of a binary calcium phosphate glass fibre/PCL composite." Acta Biomaterialia **4**(5): 1307-1314.

Alam, T. M., J. J. Liang, et al. (2000). "Molecular dynamics simulations of the lithium coordination environment in phosphate glasses." Physical Chemistry Chemical Physics **2**(19): 4427.

Alam, T. M., J. McLaughlin, et al. (2000). "Investigation of Sodium Distribution in Phosphate Glasses Using Spin−Echo 23Na NMR." The Journal of Physical Chemistry B **104**(7): 1464-1472.

Alber, F., G. Folkers, et al. (1999). "Conformational analysis of dimethyl phosphate in aqueous solution: a density functional theory-based molecular dynamics study." Journal of Molecular Structure: THEOCHEM **489**(2-3): 237-245.

Allan, I., H. Newman, et al. (2001). "Antibacterial activity of particulate BioglassÆ against supra- and subgingival bacteria." Biomaterials **22**(12): 1683-1687.

Andzelm, J., C. Kolmel, et al. (1995). "Incorporation of solvent effects into density functional calculations of molecular energies and geometries." The Journal of Chemical Physics **103**(21): 9312-9320.

Asthagiri, D., L. R. Pratt, et al. (2003). "Free energy of liquid water on the basis of quasichemical theory and ab initio molecular dynamics." Physical Review E **68**(4): 041505.

Becke, A. D. (1988). "Density-functional exchange-energy approximation with correct asymptotic behavior." Physical Review A **38**(6): 3098.

Becke, A. D. (1993). "A new mixing of Hartree--Fock and local density-functional theories." The Journal of Chemical Physics **98**(2): 1372-1377.

Belashchenko, D. K. and O. I. Ostrovskii (2002). "Computer Simulation of Noncrystalline Ionic–Covalent Oxides $CaO–P_2O_5$." Inorganic Materials **38**(2): 146-153.

Benedek, N. A., I. K. Snook, et al. (2005). "Application of numerical basis sets to hydrogen bonded systems: A density functional theory study." The Journal of Chemical Physics **122**(14): 144102-8.

Benoit, M., S. Ispas, et al. (2001). "Structural properties of molten silicates from ab initio molecular-dynamics simulations: Comparison between CaO-Al_2O_3-SiO_2 and SiO_2." Physical Review B **64**(22).

Benoit, M. K., W. (2002). "The vibrational dynamics of vitreous silica: Classical force fields vs. first principles." EPL (Europhysics Letters) **60**(2): 269.

Bernasconi, M., G. L. Chiarotti, et al. "First-principle-constant pressure molecular dynamics." Journal of Physics and Chemistry of Solids **56**(3-4): 501-505.

Bitar, M., V. Salih, et al. (2004). "Soluble phosphate glasses: in vitro studies using human cells of hard and soft tissue origin." Biomaterials **25**(12): 2283-2292.

Blakemore, J. S. (1985). Solid State Physics Cambridge, Cambridge University Press.

Blöchl, P. E. (1994). "Projector augmented-wave method." Physical Review B **50**(24): 17953.

Born, M. and R. Oppenheimer (1927). "Zur Quantentheorie der Moleküln." Annalen der Physik **84**: 457-484.

Boys, S. F. (1950). "Electron wave functions I. A general method for calculation for the stationary states of any molecular system." Proceedings of the Royal Society of London. Series A, Mathematical and Physical Sciences, **200**(1063): 542-554.

Boys, S. F. and F. Bernardi (1970). "The calculation of small molecular interactions by the differences of separate total energies. Some procedures with reduced errors." Molecular Physics **19**(4): 553-556.

Brandan, S. A., S. B. DÌaz, et al. (2007). "Hydration of inorganic phosphates in crystal lattices and in aqueous solution: An experimental and theoretical study." Spectrochimica Acta Part A: Molecular and Biomolecular Spectroscopy **66**(4-5): 1152-1164.

Brow, R. K. (2000). "Review: the structure of simple phosphate glasses." Journal of Non-Crystalline Solids **263-264**: 1-28.

Brow, R. K., R. J. Kirkpatrick, et al. (1990). "The short range structure of sodium phosphate glasses I. MAS NMR studies." Journal of Non-Crystalline Solids **116**(1): 39-45.

Bryantsev, V. S., M. S. Diallo, et al. (2008). "Hydration of Copper(II): New Insights from Density Functional Theory and the COSMO Solvation Model." The Journal of Physical Chemistry A **112**(38): 9104.

Cammi, R. and J. Tomasi (1995). "Remarks on the use of the apparent surface charges (ASC) methods in solvation problems: Iterative versus matrix-inversion procedures and the renormalization of the apparent charges." Journal of Computational Chemistry **16**(12): 1449-1458.

Car, R. and M. Parrinello (1985). "Unified Approach for Molecular Dynamics and Density-Functional Theory." Physical Review Letters **55**(22): 2471.

Carta, D., D. M. Pickup, et al. (2007). "A structural study of sol-gel and melt-quenched phosphate-based glasses." Journal of Non-Crystalline Solids **353**(18-21): 1759-1765.

Cheol Y. Kim, A. E. C. L. L. H. (1992). "Compositional dependence of calcium phosphate layer formation in fluoride bioglasses?" Journal of Biomedical Materials Research **26**(9): 1147-1161.

Chipman, D. M. (2003). "Anion electric field is related to hydration energy." The Journal of Chemical Physics **118**(22): 9937-9942.

Chipman, D. M. and F. Chen (2006). "Cation electric field is related to hydration energy." The Journal of Chemical Physics **124**(14): 144507.

Chizhik, V. I., A. V. Egorov, et al. (2002). "Microstructure and dynamics of electrolyte solutions containing polyatomic ions by NMR relaxation and molecular dynamics simulation." Journal of Molecular Liquids **98-99**: 173-182.

Colvin, M. E., E. Evleth, et al. (2002). "Quantum chemical studies of pyrophosphate hydrolysis." Journal of the American Chemical Society **117**(15): 4357-4362.

Coskuner, O. (2007). "Preferred conformation of the glycosidic linkage of methyl-beta-mannose." The Journal of Chemical Physics **127**(1): 015101-7.

Cossi, M., N. Rega, et al. (2003). "Energies, structures, and electronic properties of molecules in solution with the C-PCM solvation model." Journal of Computational Chemistry **24**(6): 669-681.

Cramer, C. J. and D. G. Truhlar (1992). "AM1-SM2 and PM3-SM3 parameterized SCF solvation models for free energies in aqueous solution." Journal of Computer-Aided Molecular Design **6**(6): 629-666.

Day, R. M. and A. R. Boccaccini (2005). "Effect of particulate bioactive glasses on human macrophages and monocytes in vitro." Journal of Biomedical Materials Research Part A **73A**(1): 73-79.

Delley, B. (1990). "An all-electron numerical method for solving the local density functional for polyatomic molecules." The Journal of Chemical Physics **92**(1): 508-517.

Delley, B. (2000). "DMol^3 DFT studies: from molecules and molecular environments to surfaces and solids." Computational Materials Science **17**(2-4): 122-126.

Delley, B. (2000). "From molecules to solids with the DMol^3 approach." The Journal of Chemical Physics **113**(18): 7756-7764.

Di Tommaso, D. and N. H. de Leeuw (2008). "The Onset of Calcium Carbonate Nucleation: A Density Functional Theory Molecular Dynamics and Hybrid Microsolvation/Continuum Study." The Journal of Physical Chemistry B **112**(23): 6965-6975.

Di Tommaso, D. and N. H. De Leeuw (2009). "Theoretical study of the dimerization of calcium carbonate in aqueous solution under natural water conditions." Geochimica Et Cosmochimica Acta **17**(18): 5394-5405.

Donadio, D., M. Bernasconi, et al. (2004). "Photoelasticity of sodium silicate glass from first principles." Physical Review B **70**(21).

Dreyfus, M. and A. Pullman (1970). "A non-empirical study of the hydrogen bond between peptide units." Theoretical Chemistry Accounts: Theory, Computation, and Modeling (Theoretica Chimica Acta) **19**(1): 20-37.

Driessens, F. C. M., M. M. A. Ramselaar, et al. (1992). "Chemical reactions of calcium phosphate implants after implantation in vivo." Journal of Materials Science: Materials in Medicine **V3**(6): 413-417.

Du, J. and L. R. Corrales (2006). "Compositional Dependence of the First Sharp Diffraction Peaks in Alkali Silicate Glasses: a Molecular Dynamics Study." Journal Name: Journal of Non-crystalline Solids, 352(30-31):3255-3269: Medium: X.

Duben, A. J. and S. Miertus (1981). "The effect of solvent on the internal rotation of formamide: A CNDO/2-solvaton method study." Theoretical Chemistry Accounts: Theory, Computation, and Modeling (Theoretica Chimica Acta) **60**(4): 327-337.

Ebner, C., U. Onthong, et al. (2005). "Computational study of hydrated phosphate anions." Journal of Molecular Liquids **118**(1-3): 15-25.

Fasman, G. D. (1976). Handbook of Biochemistry and Molecular Biology, CRC Press, Boca Raton.

Fermi, E. (1934). "Sopra lo Spostamento per Pressione delle Righe Elevate delle Serie Spettrali." Il Nuovo Cimento (1924-1942) **11**(3): 157-166.

Fernandez-Serra, M. V. and E. Artacho (2004). "Network equilibration and first-principles liquid water." The Journal of Chemical Physics **121**(22): 11136-11144.

Feynman, R. P. (1939). "Forces in Molecules." Physical Review **56**(4): 340.

Fock, V. (1930). "Näherungsmethode zur Lösung des quantenmechanischen Mehrkörperproblems." Zeitschrift für Physik A Hadrons and Nuclei **61**(1): 126-148.

Franks, K., I. Abrahams, et al. (2001). "Investigation of thermal parameters and crystallisation in a ternary CaO-Na_2O-P_2O_5-based glass system." Biomaterials **22**(5): 497-501.

Franks, K., I. Abrahams, et al. (2000). "Development of soluble glasses for biomedical use Part I: In vitro solubility measurement." Journal of Materials Science: Materials in Medicine **11**(10): 609-614.

Franks, K., V. Salih, et al. (2002). "The effect of MgO on the solubility behavior and cell proliferation in a quaternary soluble phosphate based glass system." Journal of Materials Science-Materials in Medicine **13**(6): 549-556.

Frisch, M. J., G. W. Trucks, et al. (2004). Gaussian 03. Wallingford CT, Gaussian, Inc.

Gaigeot, M.-P. and M. Sprik (2004). "Ab Initio Molecular Dynamics Study of Uracil in Aqueous Solution." The Journal of Physical Chemistry B **108**(22): 7458-7467.

Gao, H., T. Tan, et al. (2004). "Dissolution mechanism and release kinetics of phosphate controlled release glasses in aqueous medium." Journal of Controlled Release **96**(1): 29-36.

Gao, H., T. Tan, et al. (2004). "Effect of composition on the release kinetics of phosphate controlled release glasses in aqueous medium." Journal of Controlled Release **96**(1): 21-28.

George, P., R. J. Witonsky, et al. (1970). ""Squiggle-H_2O". An enquiry into the importance of solvation effects in phosphate ester and anhydride reactions." Biochimica et Biophysica Acta (BBA) - Bioenergetics **223**(1): 1-15.

Giacomazzi, L., C. Massobrio, et al. (2007). "First-principles investigation of the structural and vibrational properties of vitreous Ge Se_2." Physical Review B **75**(17): 174207.

Giannozzi, P., S. Baroni, et al. (2009). "QUANTUM ESPRESSO: a modular and open-source software project for quantum simulations of materials." Journal of Physics-Condensed Matter **21**(39): -.

Gough, J. E., P. Christian, et al. (2002). "Synthesis, degradation, and in vitro cell responses of sodium phosphate glasses for craniofacial bone repair." Journal of Biomedical Materials Research **59**(3): 481-489.

Grossman, J. C., E. Schwegler, et al. (2004). "Towards an assessment of the accuracy of density functional theory for first principles simulations of water." The Journal of Chemical Physics **120**(1): 300-311.

Hamann, D. R., Schl, et al. (1979). "Norm-Conserving Pseudopotentials." Physical Review Letters **43**(20): 1494.

Hammer, B., L. B. Hansen, et al. (1999). "Improved adsorption energetics within density-functional theory using revised Perdew-Burke-Ernzerhof functionals." Physical Review B **59**(11): 7413.

Hayem, G. (2001). "Tenology: a new frontier." Joint Bone Spine **68**(1): 19-25.

Hellmann, H. (1937). "Einführung in die Quantenchemie." Leipzig: Franz Deuticke: p. 285.

Hench, L. L. (1980). "Biomaterials." Science **208**(4446, Advanced Technology): 826-831.

Hench, L. L. (1998). "Bioceramics." Journal of the American Ceramic Society **81**(7): 1705-1728.

Hench, L. L. and J. M. Polak (2002). "Third-Generation Biomedical Materials." Science **295**(5557): 1014-1017.

Hench, L. L. and J. Wilson (1984). "Surface-Active Biomaterials." Science **226**(4675): 630-636.

Henry, D. J., A. Varano, et al. (2008). "Performance of Numerical Basis Set DFT for Aluminum Clusters." The Journal of Physical Chemistry A **112**(40): 9835-9844.

Hohenberg, P. and W. Kohn (1964). "Inhomogeneous Electron Gas." Physical Review **136**(3B): B864.

Hoover, W. G. (1985). "Canonical dynamics: Equilibrium phase-space distributions." Physical Review A **31**(3): 1695.

Hoppe, U. (1996). "A structural model for phosphate glasses." Journal of Non-Crystalline Solids **195**(1-2): 138-147.

Hoppe, U. (2005). "Structure of rare-earth phosphate glasses by X-ray and neutron diffraction." Journal of non-crystalline solids **351**(40-42): 3179-3190.

Hoppe, U., G. Walter, et al. (2000). "Structural specifics of phosphate glasses probed by diffraction methods: a review." Journal of Non-Crystalline Solids **263-264**: 29-47.

Hudgens, J. J., R. K. Brow, et al. (1998). "Raman spectroscopy study of the structure of lithium and sodium ultraphosphate glasses." Journal of Non-Crystalline Solids **223**(1-2): 21-31.

Ikeda, T., M. Boero, et al. (2007). "Hydration of alkali ions from first principles molecular dynamics revisited." Journal of Chemical Physics **126**(3).

Ikeda, T., M. Boero, et al. (2007). "Hydration properties of magnesium and calcium ions from constrained first principles molecular dynamics." Journal of Chemical Physics **127**(7).

Inada, Y. and H. Orita (2008). "Efficiency of numerical basis sets for predicting the binding energies of hydrogen bonded complexes: Evidence of small basis set superposition error compared to Gaussian basis sets." Journal of Computational Chemistry **29**(2): 225-232.

Ispas, S., M. Benoit, et al. (2001). "Structural and electronic properties of the sodium tetrasilicate glass $Na_2Si_4O_9$ from classical and ab initio molecular dynamics simulations." Physical Review B **6421**(21).

Karthikeyan, A., P. Vinatier, et al. (1999). "The Molecular Dynamics Study of Lithium Ion Conduction in Phosphate Glasses and the Role of Non-Bridging Oxygen." The Journal of Physical Chemistry B **103**(30): 6185-6192.

Kelly, C. P. (2006). "Aqueous solvation free energies of ions and ion-water clusters based on an accurate value for the absolute aqueous solvation free energy of the proton." The journal of physical chemistry. A **110**(32): 16066.

Kieninger, M., S. n. Suhai, et al. (1994). "The chemical Hamiltonian approach in density functional theory." Chemical Physics Letters **230**(6): 485-490.

Kim, B.-S. and D. J. Mooney (1998). "Development of biocompatible synthetic extracellular matrices for tissue engineering." Trends in Biotechnology **16**(5): 224-230.

Kirkpatrick, R. J. and R. K. Brow (1995). "Nuclear magnetic resonance investigation of the structures of phosphate and phosphate-containing glasses: a review." Solid State Nuclear Magnetic Resonance **5**(1): 9-21.

Klamt, A. (1995). "Conductor-like Screening Model for Real Solvents: A New Approach to the Quantitative Calculation of Solvation Phenomena." The Journal of Physical Chemistry **99**(7): 2224.

Klamt, A. and G. Schuurmann (1993). "Cosmo - a New Approach to Dielectric Screening in Solvents with Explicit Expressions for the Screening Energy and Its Gradient." Journal of the Chemical Society, Perkin Transactions 2(5): 799-805.

Knowles, J. C. (2003). "Phosphate based glasses for biomedical applications." Journal of Materials Chemistry, **13**(10): 2395-2401.

Kohn, W. and L. J. Sham (1965). "Self-Consistent Equations Including Exchange and Correlation Effects." Physical Review **140**(4A): A1133.

Kollman, P. A. and L. C. Allen (1970). "An SCF partitioning scheme for the hydrogen bond." Theoretical Chemistry Accounts: Theory, Computation, and Modeling (Theoretica Chimica Acta) **18**(4): 399-403.

Kreidl, N. J. and W. A. Weyl (1941). "Phosphates in ceramic ware: IV, Phosphate Glasses." Journal of the American Ceramic Society **24**(11): 372-378.

Kumar, P. P., A. G. Kalinichev, et al. (2008). "Hydrogen-Bonding Structure and Dynamics of Aqueous Carbonate Species from Car-Parrinello Molecular Dynamics Simulations." The Journal of Physical Chemistry B **113**(3): 794-802.

Kuo, I. à. and D. J. Tobias (2001). "Electronic Polarization and Hydration of the Dimethyl phosphate Anion: An ab Initio Molecular Dynamics Study." The Journal of Physical Chemistry B **105**(24): 5827-5832.

Laasonen, K., R. Car, et al. (1991). "Implementation of Ultrasoft Pseudopotentials in Abinitio Molecular-Dynamics." Physical Review B **43**(8): 6796-6799.

Lammert, H. and A. Heuer (2005). "Contributions to the mixed-alkali effect in molecular dynamics simulations of alkali silicate glasses." Physical Review B **72**(21): 214202.

Langer, R. (2000). "Tissue Engineering." Molecular Therapy **1**(1): 12-15.

Lee, C., W. Yang, et al. (1988). "Development of the Colle-Salvetti correlation-energy formula into a functional of the electron density." Physical Review B **37**(2): 785.

Li, J., T. Zhu, et al. (1999). "Extension of the platform of applicability of the SM5.42R universal solvation model." Theoretical Chemistry Accounts: Theory, Computation, and Modeling (Theoretica Chimica Acta) **103**(1): 9-63.

Liang, J. J., R. T. Cygan, et al. (2000). "Molecular dynamics simulation of the structure and properties of lithium phosphate glasses." Journal of Non-Crystalline Solids **263-264**: 167-179.

Liang, Y. F., C. R. Miranda, et al. (2007). "Mechanical strength and coordination defects in compressed silica glass: Molecular dynamics simulations." Physical Review B **75**(2): -.

Lozzi, M. F., M. Cossi, et al. (2006). "A polarizable continuum approach for the study of heterogeneous dielectric environments." The Journal of Chemical Physics **124**(18): 184103-9.

Martin, R. A., G. Mountjoy, et al. (2009). "A molecular dynamics model of the atomic structure of dysprosium alumino-phosphate glass." Journal of Physics-Condensed Matter **21**(7): 075102.

Martin, R. L., P. J. Hay, et al. (1998). "Hydrolysis of Ferric Ion in Water and Conformational Equilibrium." The Journal of Physical Chemistry A **102**(20): 3565-3573.

Martyna, G. J., M. L. Klein, et al. (1992). "Nose-Hoover Chains - the Canonical Ensemble Via Continuous Dynamics." Journal of Chemical Physics **97**(4): 2635-2643.

Marx, D. and J. Hutter (2000). "Ab initio molecular dynamics: Theory and Implementation." Modern Methods and Algorithms of Quantum Chemistry (FZ Julich: John von Neumann Institute for Computing) 301-449.

Mason, P. E., J. M. Cruickshank, et al. (2003). "Neutron scattering studies on the hydration of phosphate ions in aqueous solutions of K_3PO_4, K_2HPO_4 and KH_2PO_4." Physical chemistry chemical physics **5**(20): 4686.

Mattsson, A. E., R. Armiento, et al. (2008). "The AM05 density functional applied to solids." The Journal of Chemical Physics **128**(8): 084714-11.

Mattsson, A. E. and T. R. Mattsson (2009). "AM05 Density Functional Applied to the Water Molecule, Dimer, and Bulk Liquid,Ä†." Journal of Chemical Theory and Computation **5**(4): 887-894.

Mayer, I. and VibÛk (1988). "SCF equations in the chemical Hamiltonian approach." Chemical Physics Letters **148**(1): 68-72.

McQuarrie D. A. (2000). Statistical Mechanics. . New York, University Science Books.

Mora-Fonz, M. J., C. R. A. Catlow, et al. (2005). "Oligomerization and Cyclization Processes in the Nucleation of Microporous Silicas." Angewandte Chemie **117**(20): 3142-3146.

Mora-Fonz, M. J., C. R. A. Catlow, et al. (2007). "Modeling Aqueous Silica Chemistry in Alkali Media." The Journal of Physical Chemistry C **111**(49): 18155-18158.

Navarro, M., M.-P. Ginebra, et al. (2003). "Cellular response to calcium phosphate glasses with controlled solubility." Journal of Biomedical Materials Research Part A **67A**(3): 1009-1015.

Nose, S. (1984). "A unified formulation of the constant temperature molecular dynamics methods." The Journal of Chemical Physics **81**(1): 511-519.

Nosé, S. (1984). "A Molecular Dynamics method for simulations in the canonical ensemble." Molecular Physics **52**: 255.

Ordejon, P., E. Artacho, et al. (1996). "Self-consistent order-N density-functional calculations for very large systems." Physical Review B **53**(16): R10441.

Parchment, O. G., M. A. Vincent, et al. (1996). "Speciation in Aqueous Zinc Chloride. An ab Initio Hybrid Microsolvation/Continuum Approach." The Journal of Physical Chemistry **100**(23): 9689-9693.

Pasquarello, A., I. Petri, et al. (2001). "First Solvation Shell of the Cu(II) Aqua Ion: Evidence for Fivefold Coordination." Science **291**(5505): 856-859.

Payne, M. C., M. P. Teter, et al. (1992). "Iterative minimization techniques for ab initio total-energy calculations: molecular dynamics and conjugate gradients." Reviews of Modern Physics **64**(4): 1045.

Pearson, R. G. (1986). "Ionization potentials and electron affinities in aqueous solution." Journal of the American Chemical Society **108**(20): 6109-6114.

Peng, Z. and K. M. Merz (1992). "The gas-phase and solution-phase free energy surfaces for carbon dioxide reaction with hydroxide ($CO_2 + OH^- \rightarrow HCO_3^-$)." Journal of the American Chemical Society **114**(7): 2733-2734.

Perdew, C. P. (1981). "Self-interaction correction to density-functional approximations for many-electron systems." Physical review. B Condensed matter and materials physics **23**(10): 5048.

Perdew, J. P., K. Burke, et al. (1996). "Generalized Gradient Approximation Made Simple." Physical Review Letters **77**(18): 3865.

Perdew, J. P., J. A. Chevary, et al. (1992). "Atoms, molecules, solids, and surfaces: Applications of the generalized gradient approximation for exchange and correlation." Physical Review B **46**(11): 6671.

Perdew, J. P., M. Ernzerhof, et al. (1996). "Rationale for mixing exact exchange with density functional approximations." The Journal of Chemical Physics **105**(22): 9982-9985.

Pereira, C. C. G. (1998). "Silica condensation reaction: an ab initio study." Chemical communications **1998**(13): 1387.

Pliego, J. R. and J. M. Riveros (2001). "The Cluster-Continuum Model for the Calculation of the Solvation Free Energy of Ionic Species." J. Phys. Chem. A **105**(30): 7241-7247.

Pliego, J. R. and J. M. Riveros (2002). "Theoretical Calculation of pKa Using the Cluster-Continuum Model." The Journal of Physical Chemistry A **106**(32): 7434-7439.

Pye, C. C. and W. W. Rudolph (2003). "An ab Initio, Infrared, and Raman Investigation of Phosphate Ion Hydration." J. Phys. Chem. A **107**(41): 8746-8755.

Rudolph, W. W. and G. Irmer (2007). "Raman and Infrared Spectroscopic Investigations on Aqueous Alkali Metal Phosphate Solutions and Density Functional Theory Calculations of Phosphate?Water Clusters." Appl. Spectrosc. **61**(12): 1312-1327.

Sadoc, A., S. Messaoudi, et al. (2007). "Structure and Stability of VO_2^+ in Aqueous Solution: A Car-Parrinello and Static ab Initio Study." Inorganic Chemistry **46**(12): 4835-4843.

Salih, V., K. Franks, et al. (2000). "Development of soluble glasses for biomedical use Part II: The biological response of human osteoblast cell lines to phosphate-based soluble glasses." Journal of Materials Science: Materials in Medicine **11**(10): 615-620.

Saravanapavan, P., J. R. Jones, et al. (2003). "Bioactivity of gel-glass powders in the CaO-SiO_2 system: A comparison with ternary (CaO-P_2O_5-SiO_2) and quaternary glasses (SiO_2-CaO-P_2O_5-Na_2O)." Journal of Biomedical Materials Research Part A **66A**(1): 110-119.

Sarnthein, J., A. Pasquarello, et al. (1997). "Origin of the high-frequency doublet in the vibrational spectrum of vitreous SiO_2." Science **275**(5308): 1925-1927.

Schaffer, C. L. and K. T. Thomson (2008). "Density Functional Theory Investigation into Structure and Reactivity of Prenucleation Silica Species." The Journal of Physical Chemistry C **112**(33): 12653-12662.

Schwegler, E., J. C. Grossman, et al. (2004). "Towards an assessment of the accuracy of density functional theory for first principles simulations of water. II." The Journal of Chemical Physics **121**(11): 5400-5409.

Sit, P. H. L. and N. Marzari (2005). "Static and dynamical properties of heavy water at ambient conditions from first-principles molecular dynamics." The Journal of Chemical Physics **122**(20): 204510-9.

Slater, J. C. (1930). "Atomic Shielding Constants." Phys. Rev. **36**: p.57.

Soler, C. M. (2002). "The SIESTA method for ab initio order-N materials simulation." Journal of physics. Condensed matter **14**(11): 2745.

Soler, J. M., E. Artacho, et al. (2002). "The SIESTA method for ab initio order- N materials simulation." Journal of Physics: Condensed Matter **14**(11): 2745.

Soper, A. K. (2000). "The radial distribution functions of water and ice from 220 to 673 K and at pressures up to 400 MPa." Chemical Physics **258**(2-3): 121.

Sourial, E., T. Peres, et al. (1999). "A structural investigation of $Mg(PO_3)_2$, $Zn(PO_3)_2$ and $Pb(PO_3)_2$ glasses using molecular dynamics simulation." Physical Chemistry Chemical Physics **1**(8): 2013-2018.

Speghini, A., E. Sourial, et al. (1999). "Structural investigation of $NaPO_3$ glass using molecular dynamics simulation." Physical chemistry chemical physics **1**(1): 173.

Spezia, R., C. Bresson, et al. (2008). "Solvation of Co(III)-Cysteinato Complexes in Water: A DFT-based Molecular Dynamics Study." The Journal of Physical Chemistry B **112**(20): 6490-6499.

Stephens, P. J., F. J. Devlin, et al. (1994). "Ab Initio Calculation of Vibrational Absorption and Circular Dichroism Spectra Using Density Functional Force Fields." The Journal of Physical Chemistry **98**(45): 11623-11627.

Stryer, L. (1988). Biochemistry, 3rd ed. New York, W. H. Freeman and Co.

Suzuki, K. and M. Ueno (1985). "Experimental discrimination between bridging and nonbridging oxygen phosphorus bonds in P_2O_5, Na_2O glass by pulsed neutron total scattering." Journal De Physique **46**(C-8): 261-265.

Suzuki, Y., K. Takase, et al. (2001). "Short-range structure of vitreous P_2O_5 by MD simulation." Materials Transactions **42**(11): 2242-2246.

Tadjoedin, E. S., G. L. de Lange, et al. (2000). "Histological observations on biopsies harvested following sinus floor elevation using a bioactive glass material of narrow size range." Clinical Oral Implants Research **11**(4): 334-344.

Takano, Y. and K. N. Houk (2004). "Benchmarking the Conductor-like Polarizable Continuum Model (CPCM) for Aqueous Solvation Free Energies of Neutral and Ionic Organic Molecules." Journal of Chemical Theory and Computation **1**(1): 70-77.

Takeda, E., Y. Taketani, et al. (2004). "The regulation and function of phosphate in the human body." BioFactors **21**(1): 345-355.

Tang, E., D. Di Tommaso, et al. (2009). "Hydrogen transfer and hydration properties of $H_nPO_4^{3-n}$ (n = 0–3) in water studied by first principles molecular dynamics simulations " The Journal of Chemical Physics **130**(23): 234502.

Tilocca, A. (2007). "Structure and dynamics of bioactive phosphosilicate glasses and melts from ab initio molecular dynamics simulations." Physical Review B **76**(22): -.

Tilocca, A. (2007). "Structure and dynamics of bioactive phosphosilicate glasses and melts from ab initio molecular dynamics simulations." Physical Review B **76**(22): 224202.

Tilocca, A. (2009). "Structural models of bioactive glasses from molecular dynamics simulations." Proceedings of the Royal Society a-Mathematical Physical and Engineering Sciences **465**(2104): 1003-1027.

Tilocca, A. and N. H. de Leeuw (2006). "Ab initio molecular dynamics study of 45S5 bioactive silicate glass." Journal of Physical Chemistry B **110**(51): 25810-25816.

Tilocca, A. and N. H. de Leeuw (2006). "Structural and electronic properties of modified sodium and soda-lime silicate glasses by Car-Parrinello molecular dynamics." Journal of Materials Chemistry **16**(20): 1950-1955.

Tischendorf, B. C., T. M. Alam, et al. (2003). "The structure and properties of binary zinc phosphate glasses studied by molecular dynamics simulations." Journal of Non-Crystalline Solids **316**(2-3): 261-272.

Tobias, D. J., G. J. Martyna, et al. (1993). "Molecular dynamics simulations of a protein in the canonical ensemble." The Journal of Physical Chemistry **97**(49): 12959-12966.

Todorova, T., A. P. Seitsonen, et al. (2006). "Molecular Dynamics Simulation of Liquid Water:, Äâ Hybrid Density Functionals,Ä†." The Journal of Physical Chemistry B **110**(8): 3685-3691.

Tomasi, J. (2002). "Molecular properties in solution described with a continuum solvation model." Physical chemistry chemical physics **4**(23): 5697.

Tomasi, J., B. Mennucci, et al. (2005). "Quantum Mechanical Continuum Solvation Models." Chemical Reviews **105**(8): 2999.

Tommaso, D. D. and N. H. de Leeuw (2008). "The Onset of Calcium Carbonate Nucleation: A Density Functional Theory Molecular Dynamics and Hybrid Microsolvation/Continuum Study." The Journal of Physical Chemistry B **112**(23): 6965-6975.

Troullier, N. and J. L. Martins (1991). "Efficient pseudopotentials for plane-wave calculations." Physical Review B **43**(3): 1993.

Van Ginhoven, R. M., H. Jonsson, et al. (2005). "Silica glass structure generation for ab initio calculations using small samples of amorphous silica." Physical Review B **71**(2): -.

Vanderbilt, D. (1990). "Soft self-consistent pseudopotentials in a generalized eigenvalue formalism." Physical Review B **41**(11): 7892.

Videau, J.-J., J. Portier, et al. (1982). "Raman spectroscopic studies of fluorophosphate glasses." Journal of Non-Crystalline Solids **48**(2-3): 385-392.

Voet, D., Voet, J (1995). Biochemistry, 2nd ed. New York J. Wiley & Sons Inc.

Walter, G., J. Vogel, et al. (2001). "The structure of $CaO\text{-}Na_2O\text{-}MgO\text{-}P_2O_5$ invert glass." Journal of Non-Crystalline Solids **296**(3): 212-223.

Wesolowski, T. A. and A. Warshel (1993). "Frozen density functional approach for ab initio calculations of solvated molecules." The Journal of Physical Chemistry **97**(30): 8050-8053.

White, J. A., E. Schwegler, et al. (2000). "The solvation of Na^+ in water: First-principles simulations." Journal of Chemical Physics **113**(11): 4668-4673.

Zachariasen, W. H. (1932). "THE Atomic Arrangement in Glass." Journal of the American Chemical Society **54**(10): 3841-3851.

Zhan, C.-G. and D. A. Dixon (2001). "Absolute Hydration Free Energy of the Proton from First-Principles Electronic Structure Calculations." The Journal of Physical Chemistry A **105**(51): 11534.

Zhang l (2007). "Supermolecule density functional calculations suggest a key role for solvent in alkaline hydrolysis of p-nitrophenyl phosphate." Chemical communications **2007**(16): 1638.

Zhang, Y. and W. Yang (1998). "Comment on "Generalized Gradient Approximation Made Simple"." Physical Review Letters **80**(4): 890.